Antarctic Meteorites XXXVI

Papers presented to the Thirty-sixth Symposium on Antarctic Meteorites

November 14-15, 2013

NATIONAL INSTITUTE OF POLAR RESEARCH **国立極地研究所**

TOKYO

Thursday, November 14, 2013

1200 – 1500 **Registration -**
National Institute for Japanese Language and Linguistics (2nd Floor)

Oral sessions will be held in the auditorium, 2nd floor of the National Institute for Japanese Language and Linguistics
** denotes speaker*

1355 – 1400 Opening Address

Chairs: Hidaka H. and Ozawa S.

1500 - 1515 – Coffee break –

Special Talk

Chair: Yamaguchi A.

1800 - 2000 **Welcome Party**
NIPR (6th floor)

Friday, November 15, 2013

Chairs: Arai T. and Komatsu M.

Chairs: Debaille V. and Amari S.

Special Talk

Chair: Shirai N.

Poster Session

ABSTRACTS

Noble Gas Study of the Hamlet Meteorite (LL4). Sachiko Amari[1], Yukie Sabe[2], Tomokazu Shiraishi[2] and Jun-ichi Matsuda[2], [1]McDonnell Center for the Space Sciences and the Physics Department, Washington University, St. Louis, MO 63130, USA, [2]Department of Earth and Space Science, Osaka University, Osaka, 560-0043, Japan.

Introduction:

Heavy noble gases in primitive meteorites are contained in a very small portion (< 1 %) of meteorites [1]. This phase was dubbed Q for quintessence [1]. It is most likely carbonaceous matter [2, 3] but the exact nature of Q remains enigmatic.

In a continued effort to better understand Q [4-7], we separated an HF-HCl residue from Hamlet (LL4) and analyzed noble gases in the residue and the bulk meteorite. It has been shown that the more thermal metamorphism meteorites experienced, the more SiC, diamond, and Q were destroyed, and that Q is most resistant among the three phases [8]. Thus, Hamlet may still contain Q, but not SiC and diamond. Since Q and diamond are hard to separate from each other, a sole presence of Q would help us study characteristics of Q in Hamlet.

Experimental:

The separation was carried out at Washington University in St. Louis, USA. Fragments that weighed 3.47 g were treated alternately with HF-HCl and HCl to dissolve silicates. Elemental sulfur was removed with CS_2. The residue comprised 1.11 % of the starting material.

Noble gases in the bulk meteorites and the HF-HCl residue were analyzed by step-wise heating at Osaka University, Japan. The temperature steps were 600, 800, 1000, 1200, 1400 and 1600°C for both samples. Since the noble gas concentrations in the 1600°C fraction in the HF-HCl residue were so low, only element abundances were determined.

Results and Discussion:

The ^{84}Kr and ^{132}Xe concentrations in our bulk sample are 1.24×10^{-9} and 1.40×10^{-9} cm^3STP/g, respectively. They are 2.2 and 2.8 times higher than those of the same meteorite by Alaerts et al. [9]. However, ^{4}He, ^{22}Ne and ^{36}Ar concentrations are comparable in the two studies, indicating Q is more abundant in our bulk sample. We concluded that the difference was due to heterogeneity in the meteorites. Such substantial differences in samples from the same meteorite are not uncommon: the ^{132}Xe concentration of an HF-HCl residue from the Ornans meteorite (CO3.3) was 1.18×10^{-6} cm^3STP/g by Srinivasan et al. [10], but that by Alaerts et al. [11] was 4.62×10^{-7} cm^3STP/g, significantly lower than the former.

The ^{132}Xe concentration of the HF-HCl residue is 9.24×10^{-8} cm^3STP/g, indicating that Q was enriched 66 times from the bulk sample. The mass balance calculation indicates that 73 percent of the Xe in the bulk sample remains in the HF-HCl residue.

In a $^{134}Xe/^{132}Xe$ – $^{136}Xe/^{132}Xe$ plot, the Xe in the residue were shown with that of Q (=P1) [8, 12] and air (Fig. 1). All data points except that of the 1400°C fraction plot around Q. Diamond carries Xe-HL, which has high $^{134}Xe/^{132}Xe$ and $^{136}Xe/^{132}Xe$ ratios (0.6361 and 0.7, respectively) [13] and plots outside of the figure. Thus, the HF-HCl residue contains only Q but not diamond.

The Ne in both bulk sample and HF-HCl residue show an overwhelming presence of cosmogenic Ne (Fig. 2). The total Ne in the bulk sample plots very close to a typical cosmogenic Ne [14]. Even after removing silicates, the HF-HCl residue still contains a significant amount of cosmogenic Ne. The Ne data points lie on a straight line, which is explained by a two-component mixture, Hamlet Ne-Q and cosmogenic Ne. Interestingly, the mixing line does not go through the typical cosmogenic Ne: the cosmogenic component in the HF-HCl residue contains less ^{21}Ne than the typical cosmogenic Ne. This may be due to the difference of mineral compositions in the bulk sample and the HF-HCl residue. In the former, silicates are dominant, thus Mg and Si are target elements. In the latter, where all silicates are removed, oxides must be a significant component.

In order to determine the $^{20}Ne/^{22}Ne$ ratio of the other end member, Hamlet Ne-Q, we needed to assume what the $^{21}Ne/^{22}Ne$ ratio of Hamlet Ne-Q would be. We took 0.029 as the ratio. It was because $^{21}Ne/^{22}Ne$ ratios of Ne-Q from many meteorites are ~ 0.029 [7, 12]. The $^{20}Ne/^{22}Ne$ of Hamlet Ne-Q was determined to be 11.0 ± 0.5.

It has been known that $^{20}Ne/^{22}Ne$ ratios of Ne-Q vary in different meteorites and that they can be divided into two groups [8, 12]. The first group has $^{20}Ne/^{22}Ne$ ratios of 10.11 ± 0.04 and the second group has those of 10.57 ± 0.19 [12]. The meteorites of the first group include Lnacé (CO3.4), and Cold Bokkeveld (CM2), and those of the second group include Allende (CV3), Chainpur (LL3.4), Grosnaja (CV3) and Murchison (CM2). Hamlet Ne-Q obviously falls into the second group.

References:

[1] Lewis R. S. et al. (1975) *Science*, 190, 1251-1262. [2] Reynolds J. H. et al. (1978) *Geochim. Cosmochim. Acta*, 42, 1775-1797. [3] Ott U. et al. (1981) *Geochim. Cosmochim. Acta*, 45, 1751-1788. [4] Amari S. et al. (2003) *Geochim. Cosmochim. Acta*, 67, 4665-4677. [5] Matsuda J. et al. (2009) *Geochemical J.*, 43, 323-329. [6] Matsuda J. et al.

(2010) *Geochem. Cosmochim. Acta*, 74, 5398-5409. [7] Matsuda J. et al. (2010) *Meteorit. Planet. Sci.*, 45, 361-372. [8] Huss G. R. et al. (1996) *Geochim. Cosmochim. Acta*, 60, 3311-3340. [9] Alaerts L. et al. (1979) *Geochim. Cosmochim. Acta*, 43, 1399-1415. [10] Srinivasan B. et al. (1977) *J. Geophys. Res.*, 82, 762-778. [11] Alaerts L. et al. (1979) *Geochim. Cosmochim. Acta*, 43, 1421-1432. [12] Busemann H. et al. (2000) *Meteorit. Planet. Sci.*, 35, 949-973. [13] Huss G. R. and Lewis R. S. (1994) *Meteoritics*, 29, 791-810. [14] Ozima M. and Podosek F. A. (1983) Noble Gas Geochemistry, Cambridge University Press, pp. 357.

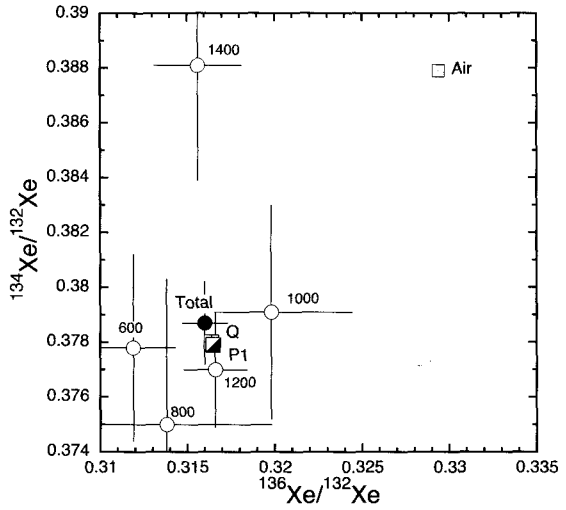

Fig. 1. $^{134}Xe/^{132}Xe$ vs. $^{136}Xe/^{132}Xe$ plot for the HF-HCl residue. The numbers indicate temperatures of the steps.

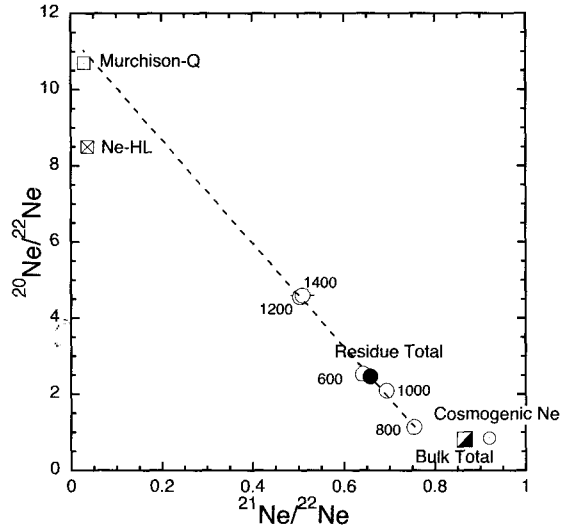

Fig. 2. Ne three-isotope plot for the HF-HCl residue. The data points form all temperature steps lie on a straight line, indicating the Ne in the residue is a two-component mixture.

Iron metal and its compounds in the Almahata Sitta and Antarctic ureilites. Y. Aoyagi[1], T. Mikouchi[1], C. A. Goodrich[2], and M. E. Zolensky[3], [1]Dept. of Earth&Planet. Sci., University of Tokyo. Hongo, Bunkyo-ku, Tokyo 113-0033, Japan, aoyagi@eps.s.u-tokyo.ac.jp, [2]Planet. Sci. Inst., Tucson, AZ 85719, USA, [3]NASA-JSC, Houston, TX 77058, USA.

Introduction:

Ureilites are ultramafic achondrites whose origin and history are still controversial. Ureilites are mainly composed of olivine, low-Ca pyroxene (pigeonite), Fe-Ni metal, Fe sulfides and carbon phases. Almahata Sitta (AS), having fallen on the earth in October 2008, was classified as a polymict ureilite and consists of cm-to-mm fragments of many different ureilitic lithologies with various chondritic lithologies [1,2].

Fe-Ni metal is one of the major components of ureilites. Metal in most AS ureilite fragments, as in other ureilites, exists as primary grain boundary metal, and also as secondary reduction metal at silicate rims. Some grain boundary metals in AS ureilites show unique textures, not found in main group ureilites [3,4]. In particular, metals in AS #44 show complex assemblages with various combinations of α-iron (*bcc*), γ-iron (*fcc*), cohenite ($[Fe,Ni]_3C$) and schreibersite ($[Fe,Ni]_3P$).

We continued to observe grain boundary metals in more AS fragments in order to look for features resembling those in #44. Consequently, we discovered metal grains in other AS samples, showing complex assemblages similar to #44 [5,6].

Because those mineral assemblages have not been reported in other ureilites [3-7], it is of great interest whether such assemblages are really absent in other ureilites. If it is the case, the formation event of such assemblages only occurred in the AS parent body. In order to better understand the formation and thermal history of AS metal together with the formation of ureilite parent body (UPB) in general, we observed several Japanese Antarctic ureilites to search similar assemblages composed of Fe metal and its compounds.

Samples and Analytical Methods:

We studied five thin sections of Japanese Antarctic ureilites (MET78008, Y-792663, Y-82100, Y980851, Y981810) because their degrees of terrestrial weathering are weaker than other samples and metal grains are fresh and unoxidized. Y-792663 is fine-grained, and the others are coarse-grained samples. Their metal grains were analyzed by FEG-SEM (Hitachi S-4500) with EDS and electron backscattered diffraction (EBSD) detectors. To identify mineral phase in metal assemblages, we used EBSD to obtain Kikuchi patterns and analyzed them by using a software developed by [8]. We also performed quantitative analysis and elemental mapping of the metal grains by using EPMA (JEOL JXA-8900L and JXA-8530F).

Results:

A survey of the grain boundary metals in AS ureilites by SEM and elemental mapping revealed that some metals in these samples contain mixtures of various phases similar to those in #44. Especially, in AS #44, #S138 and H1, complex textures and clear contrast variations in BEI and remarkable compositional differences in elemental mapping were observed within some metal grains (Fig. 1).

Based on identification by EBSD, the brighter areas in BEI correspond to α-iron while the darker areas correspond to γ-iron (Fig. 2) although both phases have low-Ni compositions corresponding to "kamacite". In H1, intergrowths of lathy α-iron and interstitial γ-iron areas are obviously seen (Fig. 3). The compositional difference between the two iron phases can hardly be seen as those in other samples. In addition, EBSD analysis in the darkest areas within metal grain revealed that they had patterns different from those of γ-iron and they are either cohenite or schreibersite (Fig. 2). The BEI contrast among γ-iron, cohenite and schreibersite is not strong, but each area is easily distinguished in carbon and phosphorus elemental maps (Fig. 1). Besides, cohenite is present as euhedral crystal while schreibersite is intergrown with other unknown phases.

In AS #27, #49 and MS#154, we also confirmed similar metal textures as well as in #44, #S138 and H1. However, iron and iron compound textures were not pronounced in these samples. Although there are varying degrees in this way, it is suggested that characteristic iron phase assemblages can be seen generally in all AS ureilites.

In Japanese Antarctic ureilites, such unusual metal textures were not common as they are rare in AS #27, #49 and MS#154. Fe carbide was discovered only in a few grains in MET78008, Y82100 and Y980851 (Fig. 4). Also, based on chemical mapping, we found metals surrounded by Fe phosphide. The grains showing contrast in BEI despite homogeneity of Fe composition with low-Ni compositions were observed. This contrast may be derived from coexistence of α-iron and γ-iron, which we are going to characterize in future analysis.

Discussions and Conclusions:

Most metal grains in main group ureilites appear to be pure kamacite, and do not usually show coexisting α-iron and γ-iron as they are remarkable in some AS ureilites [9]. The coexistence of these two iron phases in AS metals suggests a more complex history that did not occur in other ureilites, involving shock-reheating. By shock, metal grains were

reheated till stable temperature of γ-iron and then they were quenched to crystallize lathy α-iron upon cooling. Because cooling was rapid and the presence of C enhanced the γ-iron stability [7], a part of γ-iron areas remained in interstitial areas. Rapid cooling is consistent with the ureilite thermal history.

In AS ureilites, the assemblage of α-iron, γ-iron, cohenite and schreibersite was observed in metal grains. In #44, the assemblage of α-iron and γ-iron (without cohenite and with/without schreibersite) was also found [3,4]. As for other AS samples, the proportions and combinations of iron and iron compound were variable. In a few Japanese Antarctic ureilites, we found Fe carbide existing within the metal grain or Fe-phosphide enclosing around the metal grain. Further, iron compounds are distributed throughout the grain, or distributed to only a portion of the grain. Therefore, we consider that local shock re-melting of different amounts of primary metal and surrounding materials (graphite, Fe phosphide and other Fe compounds) is responsible for the variation of mineral assemblages seen in those ureilites.

These mineral assemblages tend to be less found in elongated metal grains and more in large rounded metal grains. This is probably because elongated metal has no gap between silicates, namely, there is no material which could be mixed with metal. On the other hand, there was enough space for rounded metal to be mixed with materials existing around them.

As already mentioned, the iron carbides and phosphides were found in a small part of the Japanese Antarctic ureilites. That is, more or less, it is indicated that distinct metal textures are seen in all ureilites as well as AS ureilites. Consequently, local remelting of metal which produced iron compounds may have happened on the UPB.

Fine-grained ureilites are believed to be highly shocked and their silicates show mosaicized textures. From the fact that these metal textures are seen in both coarse-grained and fine-grained ureilites, the event that shocked the silicates and the event that shocked the metal may be separate.

References:

[1] Bischoff A. et al. (2010) *MAPS, 45*, 1638-1656. [2] Zolensky M. et al. (2010) *MAPS, 45*, 1618-1637. [3] Goodrich C. A. et al. (2010) *73rd Ann. Met. Soc. Mtg*, #5319. [4] Mikouchi T. et al. (2011) *Antarct. Met., 34*, 49-50. [5] Aoyagi Y. et al. (2013) *LPS 44*, #1448. [6] Aoyagi Y. et al. (2013) *76th Ann. Met. Soc. Mtg*, #5231. [7] Mikouchi T. et al. (2013) *76th Ann. Met. Soc. Mtg*, #5205. [8] Kogure T. (2003) *J. Crystal. Soc. Japan, 45*, 391-395. [9] Goodrich C. A. et al. (2013) *Geochimica et Cosmochimica Acta, 112*, 340-373.

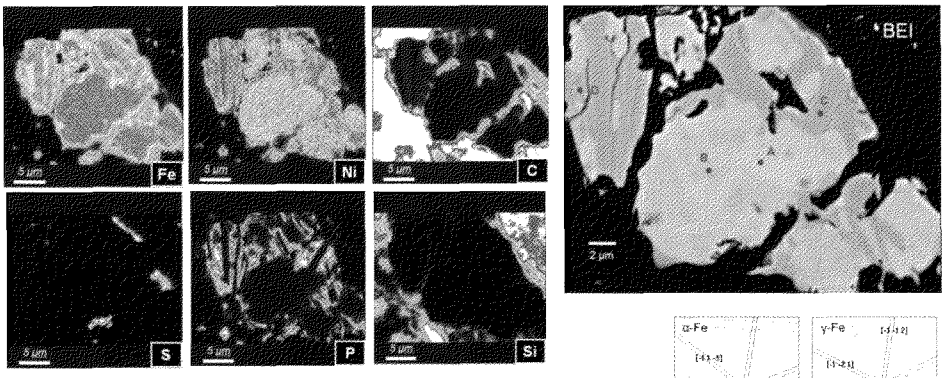

Fig. 1. X-ray mappings (Fe, Ni, C, S, P, Si) and BEI of one of the metals in AS #S138. BEI shows clear contrast. High C and high P areas are cohenite and schreibersite, respectively.

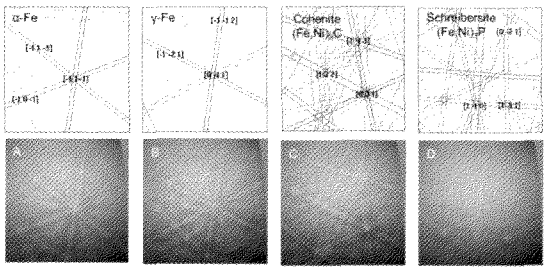

Fig. 2. The Kikuchi bands obtained from four spots (A,B,C and D in BEI of Fig. 1). The calculated patterns (below of each obtained Kikuchi bands) indicate that A is α-iron, B is γ-iron, C is cohenite and D is schreibersite, respectively.

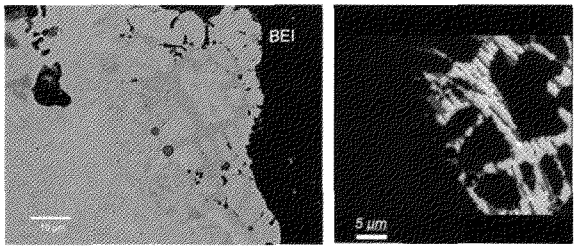

Fig. 3. BEI and combined three elements X-ray map (Red=C, Green=P, Blue=Fe, Right blue=Fe+P, Violet=Fe+C) of AS H1. Intergrowths of lathy α-iron and interstitial γ-iron are obvious. Schreibersite exists among cohenite.

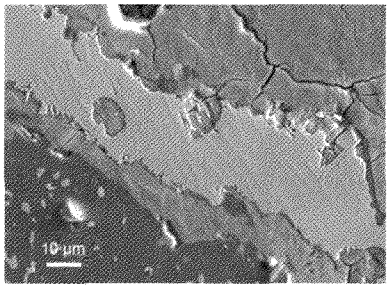

Fig. 4. SEI of Y980851. The relief areas correspond to Fe carbides (probably cohenite).

SODIUM DISTRIBUTION OF PARTIALLY MOLTEN PLANETESIMALS INFERRED FROM METEORS AND METEORITES. T. Arai[1], M. Komatsu[2], K. Otsuka[3], T. Kasuga[4], [1]Planetary Exploration Research Center (PERC), Chiba Institute of Technology, 2-17-1 Tsudanuma, Chiba 275-0016, Japan, (tomoko.arai@it-chiba.ac.jp), [2]Waseda University, Tokyo, Japan 169-8050, [3]Tokyo Meteor Network, 1-27-5 Daisawa, Tokyo 155-0032, Japan, [4]National Astronomical Observatory of Japan, 2-21-1 Osawa, Tokyo 181-8588, Japan.

Introduction: Primitive achondrites have bulk chemical compositions relatively close to those of chondrites, but affected by incipient partial melting proccese to some extent. They record chemical and physical state of the earliest melting on planetesimals. We studied chemical effect of partial melting of planetesimals by mineralogical study of primitive achondrites and astronomical observation of meteor showers whose parent bodies are asteroids.

Samples & methods: LL-type ordinary chondrites of different equilibration degree, Yamato(Y) 792772 (LL4), Y75258 (LL6), and Y82067 (LL7) were provided by National Institute of Polar Research of Japan (NIPR). Uusual primitive achondrite, LEW 86220 [1] was provided by the Antarctic Meteorite Working Group, and Caddo County with silicate inclusions [2] by Prof. H. Takeda of Chiba Institute of Technology (Chitech). Mineralogical analyses were conducted with a JEOL JSM-6510 analytical SEM of PERC/Chitech, a JEOL JXA-8200 EPMA of NIPR, and JEOL JXA-8900 EPMA of Waseda University.

Results:

LEW 86220 consists of fine-grained acapulcoitic lithology and coarse-grained gabbroic lithology with smooth embayed boundaries in between. The former lithology includes olivine, orthopyroxene, plagioclase ($An_{14.7\text{-}16.8}Or_{3.4\text{-}4.5}$) of 100-250 μm, troilite and FeNi metal. The modal abundance is broadly chondritic with <10% plagioclase. The latter has coarse-grained (up to 7 mm across) plagioclase ($An_{9.5\text{-}18.8}Or_{3.1\text{-}6.5}$) (64%), chromian diopside (up to 2.5 mm across) (15 vol.%), with minor FeNi metal, troilite, phosphate.

Silicate inclusion in Caddo County consists of coarse-grained gabbroic lithology, fine-grained mafic-rich lithology, and metal-rich lithology. Mineral compositions are constant among the lithologies. The gabbroic lithology has coarse-grained (up to 9 mm across) plagioclases ($An_{16.5\text{-}18.2}Or_{2.9\text{-}3.3}$) (59%), enclosing chromian diopsides (28%) with smaller (<1 mm across) orthopyroxene (5%) and olivine (7%). The metal-rich lithology in direct contact with the gabbroic lithology includes rounded isolated grains of plagioclase and diopside. The mafic-rich lithology contains finer-grained ($\leqq$1 mm across) olivine, orthopyroxene and diopside with less amount of plagioclase (~10%).

Y792772 contains abundant chondrules with coarse-grained olivine and pyroxene of up to a few mm across. Anorthite plagioclase mostly occurs within chondrules. Y75258 includes relict chondrules and coarse-grained (a few hundreds μm across) equigranular olivines in fine-grained recrystallized matrices of olivines with FeS and FeNi in the grain boundary. Y82067 shows granoblastic texture including fine-grained polygonal grains of olivine and pyroxene with plagioclase, chromite, and metal. Chondrules are rarely found. FeS-FeNi metal are locally segregated.

Figure 1 indicates color composite elemental maps of Fe, Mg, and Na. Among the three chondrites with different equilibration degree, the distribution of the three elements are generally homogeneous within the scale of thin section. In contrast, the elemental distribution is inhomogeneous in LEW 86220 and Caddo County, especially Na and Fe within the thin sections. Na-rich phases and Fe-rich phases are much coarser-grained than Mg-rich phase. Mg-rich phases are recrystallized chondritic materials and/or residual phases, while Fe-rich phase and Na-rich phases are metallic and silicate partial melts. The elemental maps indicate that parital melting cause inhomogeneous distribution of Na and Fe in the millimeter and centimeter scale.

Discussions:

Among the LL chondrites, not much difference in modal abundance and elemental distribution is observed, despite the textural differences. In contrast, the both primitive achondrites show remarkable modal and elemental difference among the distinct lithologies. Gabbroic lithologies represent silicate partial melts generated by an incipient melting of chondrites. Low-degree partial melting of chondrites generate nearly peritectic composition of Fo-An-Qz system with ~ 55% plagioclase, which is broadly consistent with the modal abundance of plagioclase in the gabbroic lithologies. Plagioclase-rich silicate partial melts co-exist with FeNi-FeS melts and residues within the scale of 1 cm. Chondrites with <10 vol% plagioclase has NaO<1 wt% (0.2-0.6 wt%). A silicate partial with 60 vol% plagioclase has 5.4 wt% NaO, while the residues likely show NaO$\ll$1 wt%, probably <0.1 wt%. Partial melting causes local Na variation of one or two order of magnitude.

An extreme Na depletion relative to the solar abundance is reported for the Geminid meteor shower [3-5], whose parent is a B-type [6], active asteroid [7-8], 3200 Phaethon. As the dust grain size is 1-10 mm [9], the Na depletion occurs in the mm-cm scale, which is consistent with the above mineralogical observation. Na

depletion observed for meteor showers with a perihelion distance of < 0.1 AU, is likely caused by solar heating [4]. Since that of the Geminid meteor shower (0.14 AU) exceeds 0.1 AU, the Na depletion could be due to the chemical signature of the parent Phaethon, which may represent a partially-molten planetesimal.

References: [1] McCoy T. J. et al. (1997) *GCA 61*, 639. [2] Takeda H. et al. (2000) *GCA 64*, 1311. [3] Kasuga T. et al. (2005) *A&A 438*, L17. [4] Kasuga T. et al. (2006) *A&A 453*, L17. [5] Torigo-Rodriguez J. M et al. (1993) *MPS 38*, 1283. [6] Whipple F. L. (1983) *IAU Circular* 3881. [7] Jewitt D. & Li, J. (2010), AJ, 140, 1519 [8] Jewitt D. et al. (2013) *ApJL*, 771, L36. [9] Borovicka J. B. et al (2010) *Proc. IAU Symp.263*, 218.

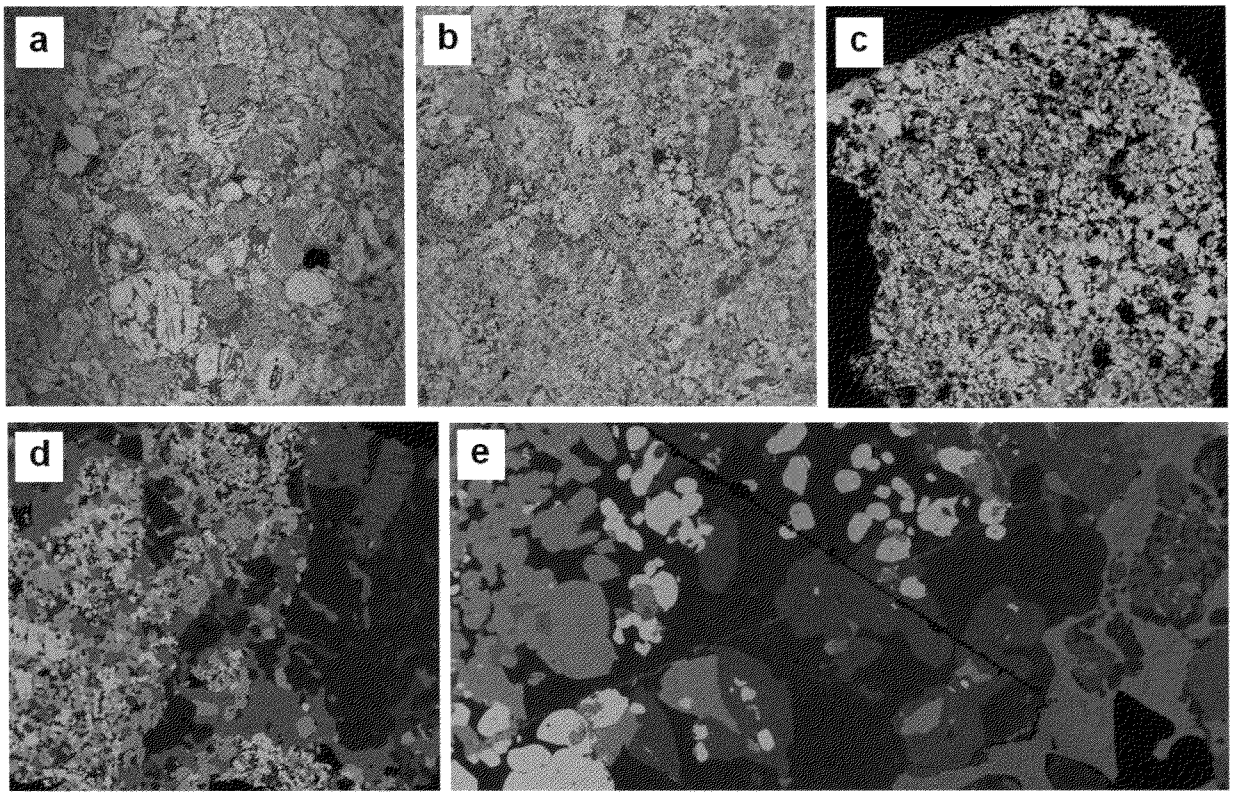

Fig. 1. Color composite elemental maps (Red: Fe, Green: Mg, Blue: Na) of (a)Y-792772 LL4 chondrite (FOV: 7 mm), (b) Y-793506 LL6 chondrite (FOV: 8 mm), (c) Y-82067 LL7 chondrite (FOV: 4 mm) (d) LEW 86220 acapulcoite-lodranite (FOV: 9 mm) and (e) silicate inclusion of Caddo County IAB iron (FOV: 15 mm). Red indicates FeNi metal and troilite, bright green shows olivine and orthopyroxene, dark green shows diopside, and blue indicates Na-rich plagioclase.

Heterogeneous distribution of ^{26}Al in the solar protoplanetary disk – insights from chondritic components and angrite meteorites.

M. Bizzarro[1], M. Olsen[1], M. Schiller[1], J.N. Connelly[1], S. Itoh[2], N. Kawasaki[2], H. Yurimoto[2] & T. Mikouchi[3]. [1]Centre for Star and Planet Formation, University of Copenhagen, Copenhagen, Denmark. [2]Natural History Sciences, Hokkaido University, Sapporo 060-0810, [3]Japan, Department of Earth & Planet. Science, University of Tokyo, Tokyo, Japan.

With a half-life of 0.73 Myr, the ^{26}Al-to-^{26}Mg decay system is the most widely used short-lived chronometer for understanding the formation and earliest evolution of the solar protoplanetary disk. However, the validity of ^{26}Al-^{26}Mg ages of meteorites and their components relies on the critical assumption that the canonical ^{26}Al/^{27}Al ratio of ~5×10^{-5} recorded by the oldest dated solids, calcium-aluminium-rich inclusions (CAIs), represents the initial abundance of ^{26}Al for the solar system as a whole.

Improved techniques for the measurements of magnesium isotopes by multiple collection inductively coupled mass spectrometry (MC-ICPMS) now allow for the determination of the radiogenic ^{26}Mg resulting from the in situ decay of ^{26}Al (μ^{26}Mg*) with an external reproducibility of ~2.5 ppm [1]. This permits, for the first time, to test the assumption of ^{26}Al homogeneity in the solar protoplanetary disk and, thus, the chronological significance of the ^{26}Al-^{26}Mg clock. Using these techniques, Larsen *et al.* [2] recently demonstrated that a high-precision bulk ^{26}Al-^{26}Mg isochron for CAIs and amoeboid olivine aggregates (AOA) from the pristine Efremovka carbonaceous chondrite defines an ^{26}Al/^{27}Al of $(5.252 \pm 0.019) \times 10^{-5}$ and initial μ^{26}Mg value of -15.9 ± 1.4 ppm (Fig. 1). The μ^{26}Mg* value of the Efremovka CAI-AOA isochron at a solar ^{27}Al/^{24}Mg ratio of 0.101 is 22.2 ± 1.4 ppm, which is much higher than that defined by CI chondrites (μ^{26}Mg = 4.5 ± 1.0) as well as other bulk solar system materials with solar or near solar ^{27}Al/^{24}Mg ratios. Collectively, these data have been interpreted as reflecting widespread ^{26}Al heterogeneity in the protoplanetary disk at the time of CAIs formation. However, the observed μ^{26}Mg* heterogeneity could also predominantly reflect magnesium-isotope heterogeneity, although it is unclear how a late addition of ^{26}Al to the nascent solar system would result in a homogenous distribution of ^{26}Al, but a heterogeneous distribution of magnesium-isotopes.

Distinguishing between these two interpretations can be achieved by comparing U-Pb and ^{26}Al-^{26}Mg ages of pristine samples, given that the U-Pb chronometer provides absolute ages that are free from assumptions of parent nuclide homogeneity. We have thus initiated a study aimed at comparing U-Pb and ^{26}Al-^{26}Mg for samples with simple thermal histories such as CAIs, chondrules and angrites.

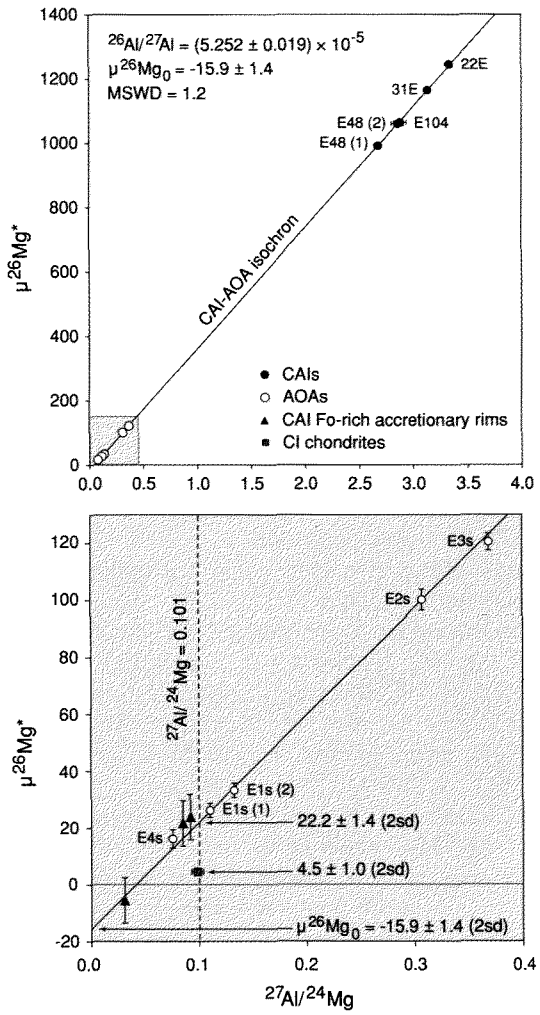

Figure 1: ^{26}Al-^{26}Mg evolution diagrams [2].

Angrite meteorites are the most alkali-depleted rocks in our solar system and they can be divided into plutonic and volcanic angrites [3]. Volcanic angrites record ancient crystallization Pb-Pb ages that are within ~4 Myr of CAI formation [4-5] and, thus, formed during the lifespan of ^{26}Al. Of particular interest is the NWA 1670 quenched angrite, as it contains significant amounts of olivine xenocrysts of up to 5 mm in size thereby allowing us to precisely define the initial ^{26}Mg* composition at the time of crystallization. Our new U-corrected Pb-Pb date for NWA 1670 indicates crystallization at 4564.37±0.19 Myr, making it the oldest known angrite. Individual olivine xenocrysts and multiple analyses of groundmass material of NWA 1670 define an

^{26}Al-^{26}Mg isochron yielding a slope corresponding to an ^{26}Al/^{27}Al of (6.14±0.88) × 10^{-7} and initial ^{26}Mg of −10.8±1.2 ppm. This corresponds to an age difference of 4.69±0.16 Myr between formation of CAIs and crystallization of NWA 1670, which is not consistent with the age difference of 2.93±0.25 Myr inferred from U-corrected Pb-Pb dating. This age discrepancy is similar to that observed between the ^{26}Al-^{26}Mg and Pb-Pb dates of the younger SAH 99555 and D'Orbigny quenched angrites, which record ^{26}Al-^{26}Mg ages that are systematically ~1.5 Myr younger than the Pb-Pb dates [6]. Reconciling the ^{26}Al-^{26}Mg ages of these angrites with their Pb-Pb dates require an initial ^{26}Al/^{27}Al of ~1.25 × 10^{-5} in the accretion region of the angrite parent body. This result supports the claim of ^{26}Al heterogeneity in the early solar system [2] and a reduced abundance of ^{26}Al in the accretion regions of asteroids and terrestrial planets compared to the ^{26}Al/^{27}Al value of ~5 × 10^{-5} defined by canonical CAIs.

To evaluate the extent of ^{26}Al heterogeneity in the inner solar system, we have extended our study to chondrules, as these represent the major constituent of chondrite meteorites and, by extension, the precursor material of asteroidal bodies and terrestrial planets. We obtained ^{26}Al-^{26}Mg ages through the internal isochron approach for three U-corrected Pb-Pb dated chondrules from the carbonaceous chondrite Allende and the unequilibrated ordinary chondrite NWA 5697 [7]. Internal isochron relationships were defined by combining *in situ* ^{26}Al-^{26}Mg systematics of Al-poor and Al-rich phases obtained by secondary ionization mass spectrometry (SIMS) at the of Hokkaido University with high-precision bulk analyses of the same chondrules by MC-ICPMS obtained at the University of Copenhagen. In detail, we investigated the internal ^{26}Al-^{26}Mg systematics of two ferro-magnesian porphytitic olivine-pyroxene chondrules from Allende (C30) and NWA 5697 (C1) as well as one barred olivine-pyroxene chondrule from NWA 5697 (C3). The C30, C1 and C3 chondrules have U-corrected Pb-Pb dates of 4567.32 ± 0.42 Myr, 4566.67 ± 0.43 Myr and 4566.02 ± 0.26 Myr, respectively [7]. Note that these chondrules record primitive initial Pb isotope compositions, which precludes a complex thermal history of their precursors.

Chondrule C30 defines an ^{26}Al-^{26}Mg isochron based on multiple analyses of spinel and olivine crystals as well as one bulk measurement that record an initial ^{26}Al/^{27}Al of (1.46 ± 0.29) × 10^{-5}. Chondrules C1 and C3 define ^{26}Al-^{26}Mg isochrons based on multiple analyses of olivines, glassy mesostasis and bulk measurements that record initial ^{26}Al/^{27}Al values of (8.15 ± 1.00) × 10^{-6} and (8.14 ± 2.8) × 10^{-6}, respectively. Thus, similar to angrite meteorites, the ^{26}Al-^{26}Mg systematics of the three chondrules analyzed here record ^{26}Al-^{26}Mg ages that are younger than their Pb-Pb dates by ~1.3-1.9 Myr.

The observed discrepancy between the ^{26}Al-^{26}Mg and Pb-Pb dates for the Allende and NWA 5697 chondrules could, in principle, reflect selective disturbance of the ^{26}Al-^{26}Mg system. However, the bulk of the U in chondrules is believed to be hosted by pyroxene which, similarly to the glassy mesostasis, is susceptible to thermal metamorphism. As such, disturbance of the ^{26}Al-^{26}Mg systematics is predicted to also be accompanied by U-Pb disturbance, which would be reflected by the loss of linearity in Pb-Pb isochron diagrams. The excellent linearity of the Pb-Pb isochron diagrams for the C30, C1 and C3 chondrules, coupled with the primitive Pb isotope compositions recorded by these three chondrules [7] is not consistent with disturbance of their U-Pb systematics. Therefore, we conclude that the ^{26}Al/^{27}Al ratios recorded by the chondrules reflect the initial abundance of ^{26}Al in their precursors at the time of crystallization inferred from the Pb-Pb dates.

The reduced ^{26}Al abundance in chondrule forming regions deduced from our measurements provides unequivocal evidence for heterogeneous distribution of ^{26}Al the time of CAI formation. We note that the initial abundance of ^{26}Al inferred for the various bulk solar system reservoirs correlates with their ^{54}Cr [2] as well as their ^{84}Sr [8], ^{43}Ca, ^{46}Ca and ^{48}Ca compositions [9], thus providing evidence for a relationship between the distribution of short-lived nuclides and that of stable isotope anomalies in the early solar system. Thus, similarly to the ^{54}Cr heterogeneity, we suggests that ^{26}Al heterogeneity in solar system objects reflects variable degrees of thermal processing of their precursor material, probably associated with volatile-element depletions in the inner solar system. In this view, CAIs and AOAs represent samples of the complementary gaseous reservoir enriched in ^{26}Al by thermal processing, which resulted in the widespread ^{26}Al depletions observed among inner solar system bodies.

A reduced abundance of ^{26}Al in the accretion regions of asteroidal bodies requires shorter timescales for the timing of accretion of differentiated planetesimals if melting resulted from ^{26}Al decay. Indeed, thermal modeling indicate that accretion within 100,000 years of CAI formation is necessary to fully melt a body that formed with an initial ^{26}Al/^{27}Al value of ~1 × 10^{-5}.

References:

1-Bizzarro, M. *et al.* (2011) *JAAS* **26**, 565. 2-Larsen K. *et al.* (2011) *ApJL* **735**, L37. 3-Keil, K. (2012) *Chem. Erde-Geochem* **72**, 191. 4-Connelly, J.N. *et al.* (2008) *Geochim. Cosmochim. Acta* 72, 4813. 5-Amelin, Y. (2008), *Geochim. Cosmochim. Acta* **72**, 4874. 6-Schiller, M. *et al.* (2010) *Geochim. Cosmochim. Acta* **74**, 4844. 7-Connelly, J.N. *et al.* (2012) *Science* **338**, 651. 8-Paton, C. *et al.* (2013) *ApJL* **763**, L40. 9-Schiller, M. *et al.* (2013) *Sci. Rep.*, submitted.

A new curation facility for Antarctic meteorites at the Royal Belgian Institute of Natural Sciences. M. De Ceukelaire, W. De Vos & M. Dusar, RBINS, Royal Institute of Naturals Sciences.

Founded in 1846, RBINS houses a diverse and exceptionally rich zoological collection, palaeoanthropological and mineralogical collections and prehistoric items involving about 37,000,000 specimens with around 100,000 primary types. This places RBINS among the world top ten collections in terms of volume of specimen stored and available for research.

A curation facility for Antarctic meteorites has become operational at the Royal Belgian Institute of Natural Sciences (RBINS). The meteorites collected through the Antarctic campaigns in the Sør Rondane Mountains during three joint Japanese-Belgian expeditions between 2009 and 2013, will be shared evenly between the two countries. This sharing will be accomplished by cutting in half the larger samples (> 50g). The smaller samples (<50g) will not be cut to avoid wasting precious small samples. They will be shared evenly between Japan and Belgium based on either total weight or total number. Priority access for research to the samples curated by the other partner is guaranteed. Specific sharing agreements will be tailored according to the circumstances, for the largest samples (> 4kg) because of their importance in terms of outreach and exhibits. Cutting them should be avoided, except for classification purposes.

The facility manages the meteorite collection for optimal preservation and provides national and international meteorite scientists access to the samples hosted at RBINS. It also handles loans for exhibits and supports public outreach and educational initiatives concerning meteorites and solar system evolution. The existing regulations of NIPR Japan will stand as a model for finalizing RBINS meteorite-allocation regulations. The Belgian Parties have set up a Scientific Loan Committee (SLC), which includes VUB, ULB and RBINS representatives. The SLC will handle the loan requests in coordination with the Committee at AMRC-NIPR. Before any decision, AMRC-NIPR and the SLC will systematically inform each other of all loan requests and will regularly keep each other informed of the loan follow-up.

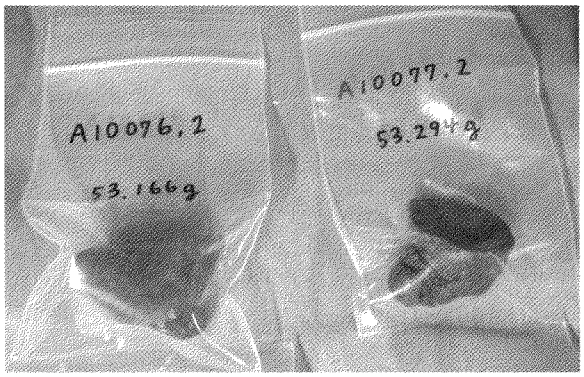

The entire database will be made available online (DaRWIN.naturalsciences.be), with photographs, sample descriptions, downloadable loan requests, research sample request forms etc.. DaRWIN stands for Data Research Warehouse Information Network. It's a home-made (RBINS) open source web base tool published on AGPL to manage Natural Sciences collections.

A special laboratory, exclusively for meteorite preparation work, was set up in an air-conditioned room of about 16 m^2 on the ground floor of the Geological Survey. It gradually became operational in September-October, especially after installation of the Escil wire saw. Several scientists were trained in the use of the saws and in the procedure of making Aluminum-ring polished sections of meteorites. The RBINS collection of Saharan meteorites was used for this exercise. In this way, a core group of researchers became familiar with the use of the meteorite lab and of the delicate wire saw in particular.

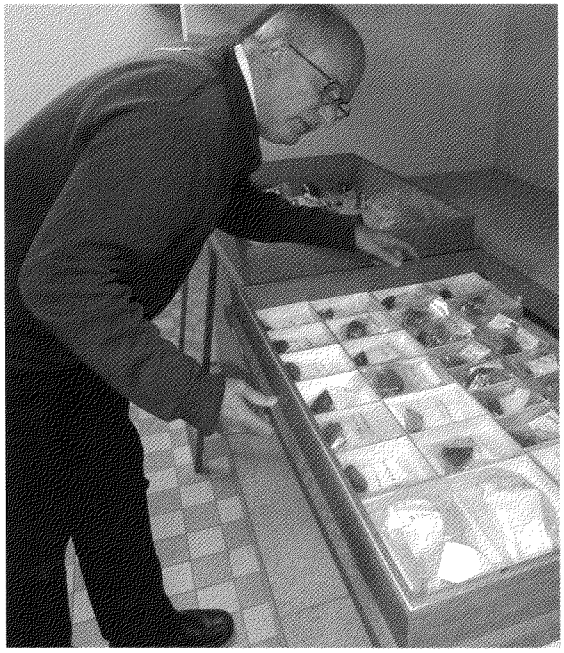

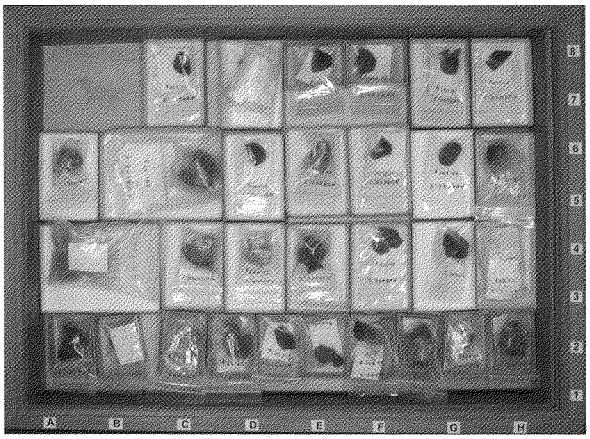

The 2012-2013 Joint Field Campaign for Collecting Meteorites in Antarctica: an Efficient Collaboration between Japan and Belgium. V. Debaille[1], N. Imae[2], A. Yamaguchi[2], S. Goderis[3], T. Mikouchi[4], W. Debouge[1], G. Hublet[1], N. Van Roosbroek[1], H. Zekollari[3], H. Kojima[2], Ph. Claeys[3], [1]Laboratoire G-Time, Université Libre de Bruxelles, Brussels, Belgium. [2]National Institute of Polar Research, Tachikawa, Japan. [3]Earth Science Systems, Vrije Universiteit Brussel, Brussels, Belgium. [4]Department of Earth and Planetary Science, University of Tokyo, Tokyo, Japan. (e-mail address: vinciane.debaille@ulb.ac.be)

Introduction:

For the last 5 years, Belgium and Japan have joined forces, logistics and knowledge to organize three successful meteorite expeditions in Antarctica. The first joint JARE 51 mission sampled the Balchen Ice Field, in the eastern Sør Rondane Mountains region, in 2009-2010 and recovered more than 600 meteorites. The second joint BELARE SAMBA 2010-2011 on the North-West part of the Nansen Ice Field (area A, Fig. 1), located to the South of Sør Rondane Mountains, recovered 220 meteorites (Fig. 2). Finally, this year, a third JARE 54 - BELARE SAMBA 2012-2013 joint expedition has been organized in the Nansen Ice Field during the austral summer 2012-2013. This was the largest recovery party organized, with a total of 10 members searching for meteorites. On the Belgian side, this program is funded by the Belgian Science Policy (BELSPO) and benefits from the logistic support of the International Polar Foundation (IPF).

The meteorite search team consisted of 5 Belgian scientists from Université Libre de Bruxelles (ULB) and Vrije Universiteit Brussels (VUB), a field guide provided by the IPF, and 3 Japanese scientists from the National Institute of Polar Research (NIPR) and University of Tokyo, and a field guide from NIPR.

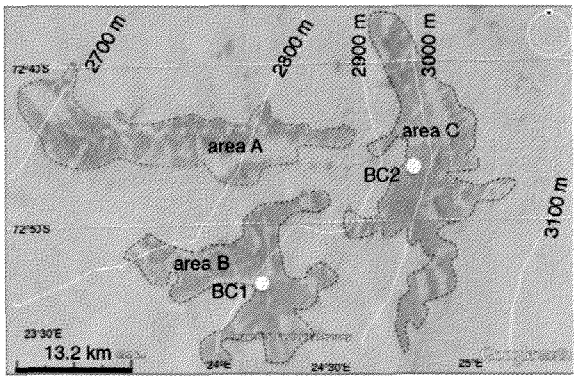

Figure 1: Nansen Ice Field subdivided in 3 parts: Area A (season 2010-2011), Area B (season 2012-2013), and Area C (partially done during the season 2012-2013). BC2 has been moved from this previous location. Map from N. Imae

Base camps and meteorite search:

Considering the shape of the Nansen Ice Field (Fig. 1), it has been decided to divide the 2012-2013 campaign in two, implying two different base camps (BC1 and BC2 on Fig. 1) located in the not yet sampled areas (B and C). All the logistics (including living containers, fuel, personal belongings, ...) were dropped off on the Nansen Ice Field Plateau on December 24 2012 by the IPF team, led by Alain Hubert. Then, the full team followed by snowmobile on December 26th 2012, when the base camp was installed, and weather acceptable. Systematic searches by skidoo were carried out from the 27th of December 2012 to the 13th of January 2013, whenever the weather was permitting (see weather conditions subsection below), and covered the entire zone B of the Nansen Ice Field. The base camp B was moved to the second area on the 15th of January 2013. There, weather degraded and searches were possible only from the 28th to the 30th of January. The team finally left the camp on the 2nd of February 2013, back to the Princess Elisabeth Station. Typically, after a first briefing in the morning to evaluate weather conditions, search started around 12 PM. Normal search-day consisted of only 4 to 6 hours in the field due to the severe weather conditions.

Weather conditions:

The weather conditions were harsh, even for the South Pole and determined the daily schedule as such. Notable difference exists between base camp BC1 and BC2 (data from T. Mikouchi and A. Yamaguchi). At camp BC1, absolute temperature ranged from -14.4 to -22.4°C (average of -18.2°C), with an average wind speed of 10.1 m/s, resulting in average wind chill corrected temperature of -31.0°C. At base camp BC2, absolute temperature ranged from -18.2 to -27.1°C (average of -21.9°C), with an average wind speed of 10.6 m/s, resulting in average wind chill corrected temperature of -36.0°C, notably lower than Area B. It is difficult to know whether tougher conditions were met in Area C because it was later in the season, or because of a slightly higher altitude (~100 m between the two base camps), or less sheltering.

In average, half of the time on the plateau was lost due to weather conditions. This is similar to the 2010-2011 campaign. However, the main difference is the repartition of bad weather days. While during the 2010-2011 season, bad weather days were distributed over a short period (every 3-4 days), during the 2012-2013 season, longer periods were observed, with 15 days in a row of good weather, and 12 days in row of bad weather.

Preliminary results:

During the 2012-2013 season, 427 meteorites were recovered (Fig. 2), for a total weight of 65.2 kg. Notably, the largest sample weighs 18.1 kg, and 9 meteorites are over 1 kg. A few achondrites have been observed when fusion crusts were partially absent (possibly eucritic), as well as a few carbonaceous chondrites.

First, the meteorites were sent to NIPR for careful defreezing. The large samples will be cut in two, and shared evenly between Japan and Belgium. After detailed classification made by both NIPR and ULB-VUB teams, including the Royal Belgian Institute for Natural Sciences (RBINS), one half will come back to Belgium where they will be available for research by the international scientific community. In addition, the most beautiful pieces will be exposed to the public at the RBINS. Scientific research will be performed on those samples, in close collaborations between NIPR and ULB-VUB teams.

Curation of meteorites:

Belgium has recently developed a meteorite curation center at the RBINS where the Belgian share of the Antarctic meteorites will be stored and curated based on sample requests made by researchers.

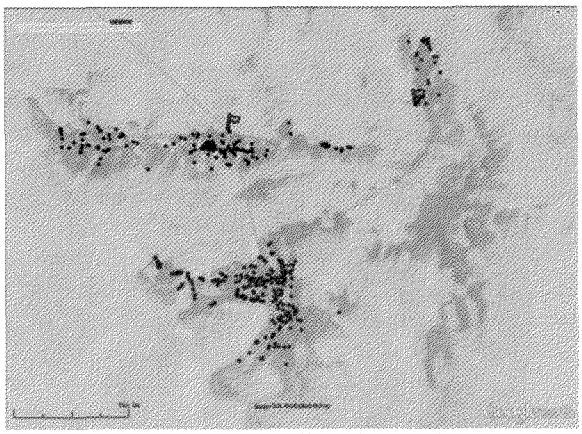

Figure 2: Summary of collected meteorites on Nansen Ice Field, during the two campaigns (blue: 2010-2011; red: 2012-13). Tracks followed by the team are in green. Orange flags indicate base camps.

Towards an Efficient Coupled Cu and Zn Purification Technique Adapted to Precious Terrestrial and Meteorite Materials. W. Debouge[1], N. Mattielli[1] and V. Debaille[1], [1]Laboratoire G-Time, Université Libre de Bruxelles, ULB, Brussels, Belgium (wdebouge@ulb.ac.be).

Introduction and study interests:

Copper is an important tracer for reconstruction of geochemical cycling in terrestrial or extraterrestrial environments. It is a transition element with three oxidation states (0, I, and II) and two isotopes (^{63}Cu and ^{65}Cu). With a condensation temperature of ~1050° to 1100° K, Cu is considered as a relatively volatile element [1-3]. In meteorites, this element is both chalcophile and siderophile as it enters in FeNi metals (60%) and sulfides (20–25%) and forms tiny metallic Cu nuggets (4–5%) [4]. To a limited extent, it also enters in silicate minerals (olivine, pyroxene). Specifically, in magmatic and non-magmatic iron meteorites (IM), Cu can provide information on primordial processes that affected the meteorite parent bodies: core formation [5] [6] and fractional crystallization [7]. These processes induce metal-silicate-sulphide segregation that might produce mass dependent fractionation recorded by the Cu isotopes. Accordingly, the study of Luck et al. [8] on carbonaceous and ordinary chondrites shows that Cu is isotopically heterogeneous in the solar nebula. In addition, Cu isotopic variations observed in chondrites suggest the existence of two isotopically distinct reservoirs [8]. As Cu is moderately volatile, some other processes like accretion and shock metamorphism can also produce Cu isotope fractionation and hence can be traced by the variations in Cu isotope ratios [5, 9]. Consequently, Cu isotopes can be a sensitive and powerful tracer for understanding primordial nebular and planetary processes.

The continuous development of the HR-MC-ICP-MS (high resolution multi-collector inductively coupled plasma- mass spectrometry) renews interest in heavy stable isotope systems, whose subtle natural isotopic variations require high precision, accuracy and reproducibility. However, significant inaccuracy in MC-ICP-MS measurements of Cu or Zn isotopic composition may be caused by inorganic and organic resin-derived components added to samples during column chemistry or/and to incomplete separation of the analyte from the sample matrix [10, 11]. In addition, previous studies [12] have shown that mass bias corrections, using sample-standard bracketing and external normalization (Zn as dopant for Cu isotope measurements, and Cu as dopant for Zn isotope measurements), may fail to accurately correct for these matrix effects.

Therefore, special attention is paid to the total recovery of Cu or Zn analyte during the chemical purification, and optimal elimination of potentially interfering matrix elements.

Analyses of Cu, as well as Zn, are important for understanding early planetary differentiation processes, and efficient purification procedure is required to ensure high-precision measurements. In this study, we present a new anion exchange chromatography procedure developed at Laboratoire G-Time (ULB) for Zn and Cu separation.

Analytical procedure and Results:

Compared to Zn or Fe, Cu is much more difficult to purify and to recover totally. In order to purify and collect Cu and Zn from a single aliquot of a sample, previous studies have been mainly using AG-MP1. This macroporous resin has a high level of crosslinkage but is very difficult to wash and has relatively poor blank levels (J.C.J. Petit, PhD thesis). Therefore a two passages column separation method on Bio Rad AG®1-X8 has been considered. The first column separates Zn from Cu, while the second column refines the purification of the Cu cut.

First for digestion of the samples, about 100 mg of finely ground powdered sample is dissolved with concentrated HF and HNO_3 (3:2) in PFA beaker. All reagents (hydrobromic acid, hydrochloric acid, nitric acid and hydrofluoric acid) that were used for this study were subboiled in PFA bottleneck systems. The necessary dilutions were performed with Milli-Q water (18.2 MΩcm) (Millipore system). After 48 hours on a hot plate at 120°C, samples are dried and dissolved again with 6M HCl on a hot plate at 100°C for 8h. Evaporation temperature is never higher than 100 C in order to avoid burnt crust.

The distribution coefficients on anion-exchange resin (Bio Rad AG®1-X8) (determined by [13]) for many elements at various concentrations of nitric acid, hydrochloric acid and hydrobromic acid have been used to determine the optimal combination. Copper is first separated from Zn using 2 ml Bio Rad AG®1-X8 100–200 mesh in HCl. Digested samples are redissolved in 1 ml 8 M HCl, centrifuged and loaded on the resin. Copper is recovered with 8 M HCl. Iron is subsequently discarded by rinsing with 1 M HCl. Zn is then eluted with a mixture of 1 M HNO_3/0.1 M HBr. If needed, Cd can also be recovered by using HNO_3. The procedure is detailed in Fig. 1a.

Elemental concentrations were determined by ICP-MS Agilent 7700 at Laboratoire G-Time for each sample before purification and Cu cut to monitor both Cu recovery and the presence of potential matrix interferences. Calibration curves (Fig. 1a) indicate a recovery close of 100 % for both Zn and Cu (Fig. 1b).

The second column to refine the purification of the Cu fraction of this first column is in development. Several tests have been performed using hydrobromic acid in order to purify the Cu cut from the presence of Ti that generates an important isobaric interference with Cu. However, despite promising experimental data [14], the results were deceptive. Copper should be purified on a micro column of 0.2 ml Bio Rad AG®1-X8 using a similar procedure.

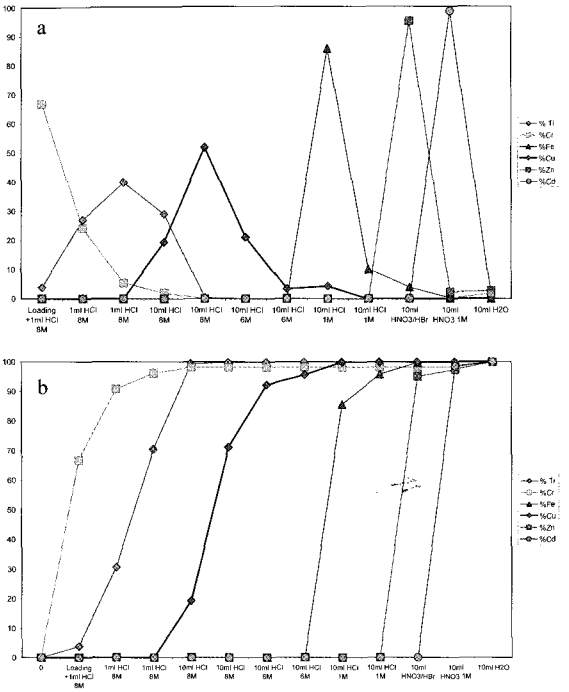

Fig. 1: a) Elution curve in percent, b) cumulative elution curve in percent, for Ti, Cr, Fe, Cu, Zn and Cd.

References:

[1] Wasson J. T. (1985), *Meteorites (Berlin: Springer),* 267 p. [2] Palme H. et al. (1988), *Meteorites and the early solar system,* 436-461. [3] Cassen P. (1996), *Meteorit. Planet. Sci.,* 31, 793-806. [4] Rubin A. E. (1994), *Min. Mag.,* 58, 215-221. [5] Luck J. M. et al. (2005), *Geochim. Cosmochim. Acta,* 69, 5351-5363. [6] Moynier F. et al. (2007), *Geochim. Cosmochim. Acta,* 71 4365-4379. [7] Williams H. M. and Archer C. (2011), *Geochim. Cosmochim. Acta,* 75, 3166-3178. [8] Luck J. M. et al. (2003), *Geochim. Cosmochim. Acta,* 67, 143-151. [9] Moynier F. et al. (2006), *Geochim. Cosmochim. Acta,* 70, 6103-6117. [10] Petit J. C. J. et al. (2008), *Geostand. Geoanalyt. Res.,* 32, 149-166. [11] Shiel A. E. et al. (2009), *Anal. Chim. Acta,* 633, 29-37. [12] Petit J. C. J. et al. (2013), *Geostand. Geoanalyt. Res.,* 37, 319-335. [13] Strelow F. W. E. (1980), *Talanta,* 27, 727-732. [14] Strelow F. W. E. (1978), *Anal. Chem.,* 50, 1359-1361.

Speciation of Iron as a Monitor of Oxidation, Reduction and Sulfidation in Ordinary and Enstatite Chondrites. T. J. Fagan, H. Wakai, C. Niki and D. Kato, Department of Earth Sciences, Waseda University, Tokyo, Japan. (fagan@waseda.jp)

Introduction:

Chondrites formed in the solar nebula and hence contain clues about the conditions and processes of the nebula. Variations in the occurrence of Fe as FeO in silicates and oxides vs. metallic Fe in Fe,Ni-rich metals show that oxygen fugacities varied in the regions of the nebula where chondrites formed [1]. Iron is progressively oxidized along a sequence from EH & EL to H to L to LL to R chondrites, reflecting increasingly oxidized settings of formation in the solar nebula [2] (see Fig. 1).

This wide range in the distribution of Fe between silicates and metals is well established [3]; however, Fe also occurs in sulfide minerals in chondrites, raising the possibility that S fugacities also may have varied among the chondrite groups. In this project, we use speciation of Fe to address sulfidation as well as reduction and oxidation in enstatite (EH, EL), ordinary (H, L, LL) and Rumuruti-like (R) chondrites.

Methods:

FeO vs. Metallic Fe vs. FeS in Chondrite Samples. Three separate data sets were used to determine speciation of Fe in different samples of chondrites. Data (1) is based on modes and quantitative electron microprobe analyses of Fe-bearing minerals in the following set of chondrites: Bensour (LL6, fall); Mt. Tazerzite (L5, fall); Tamdakht (H5, fall); St. Marks (EH5, fall); Lewis Cliff 88180 (EH5, find); Northwest Africa 974 (E6, find); Northwest Africa 753 (R3, find). Meteorite falls were emphasized in order to limit the effects of terrestrial weathering; high petrologic types were preferred because coarse-grained samples with homogeneous mineral compositions are well suited for calculation of rock composition by modal recombination. The R- and E-chondrites are relatively rare, so some finds were used and the R-chondrite used here (NWA 753) is a type 3. Modes were determined from elemental X-ray maps of polished thin sections. Modes were counted manually from grids overlain on the elemental maps. Mineral compositions were determined by wavelength dispersive spectroscopy using a JEOL JXA electron microprobe at Waseda University.

In data sets (2) and (3), the speciation of iron among FeO, metallic Fe (Fe^0) and FeS was determined from wet chemical analyses of whole rocks. Data (2) is from analyses conducted by E. Jarosewich [4,5] on LL (n = 17), L (N = 57) and H (n = 31) finds, and 1 fall and 3 finds of E-chondrites. Data (3) is from analyses conducted by H. Haramura of NIPR (and compiled by Yanai and Kojima [6]) on Antarctic finds (59 LL, 158 L, 162 H, 6 E).

Mass Balance Model for Reactions in Chondrites. Understanding Fe-speciation requires a model for the reactions that transfer Fe between the silicate, sulfide and metal subsystems within the whole-rock reacting systems for O, E and R chondrites. We use a linear algebraic approach to model whole-rock mass balance using independent reactions as vectors, and then combining the vectors as multi-dimensional reaction progress or "reaction space" [6,7].

Results:

Mass Balance Model. Potential variations in abundances of the major minerals in O, E, and R chondrites can be described as linear combinations of four independent reactions: (R1) $NaAlSi_3O_8$ = $NaAlSi_2O_6$ + SiO_2; (R2) Mg_2SiO_4 + SiO_2 = 2 $MgSiO_3$; (R3) $FeSiO_3$ = Fe-metal + SiO_2 + 0.5 O_2; (R4) $FeSiO_3$ + 0.5 S_2 = FeS + SiO_2 + 0.5 O_2. R1 does not appear to be important in most chondrites. R2 is very important as it describes variations in olivine vs. pyroxene, but it occurs entirely within the silicate subsystem. Reduction of FeO to Fe-metal occurs on R3, and sulfidation of FeO to FeS occurs on R4. The reactions as written above do not indicate that all Fe transferred from silicate to metal originates in pyroxene; nor do the model reactions indicate the true volatile species present during true reaction (e.g., in R3, oxygen lost from silicate might have been transferred to H_2O vapor instead of O_2). Rather the model reactions should be considered book-keeping tools to keep track of changes in abundances and compositions of minerals. R3 and R4 can be used as monitors of Fe transferred between the silicate, metal and sulfide subsystems (Figs. 2, 3).

Speciation of Fe in Data Sets (1), (2) and (3). The three data sets show internally consistent distributions of Fe among silicates, sulfides and metals among ordinary and enstatite chondrites. For most ordinary chondrites, 10 to 25% of Fe occurs in sulfides, and the progression from LL to L to H chondrites shows a wide range in the extent of reduction of FeO to Fe-metal on R3 (Figs. 2, 3). E-chondrites from Data (1) show that all Fe in these samples occur as FeS or Fe-metal. The presence of some FeO in E-chondrites in Data (2) and Data (3) is probably due to terrestrial weathering of meteorite finds. The only R-chondrite analyzed in this study (NWA 753) is in Data (1); modal recombination was determined for two areas, both showing all Fe in FeO or FeS (Fig. 2), consistent with previous interpretations of the R-chondrites as indicators of high oxygen and sulfur fugacities in the solar nebula [3].

The NIPR Antarctic finds (Data 3) show a

greater extent of scatter than the other data sets (compare Fig. 3 with Fig. 2). Most of the scatter appears to be from oxidation of FeS (negative progress on R4) or of Fe-metal (negative progress on R3) and is likely due to terrestrial weathering.

References:

[1] van Schmus W.R. and Wood J.A. (1967) *GCA, 31,* 747-765. [2] McSween H.Y., Jr. (1999) Meteorites and their Parent Planets, 310 p. [3] Weisberg M.K. et al (2006) in Lauretta D.S. and McSween H.Y. Jr. (editors) *Meteorites and the Early Solar System II,* p. 19-52. [4] Jarosewich E. (1990) *Meteorit. Planet. Sci., 31,* 323-337. [5] Jarosewich E. (2006) *Meteorit. Planet. Sci., 41,* 1381-1382. [6] Yanai K. and Kojima H. (1995) *Catalog of the Antarctic Meteorites, NIPR,* 230 p. [7] Thompson et al (1982) *Jour. Petrol., 23,* 1-27. [8] Fagan T.J. and Day H.W. (1997) *Geology, 25,* 395-398.

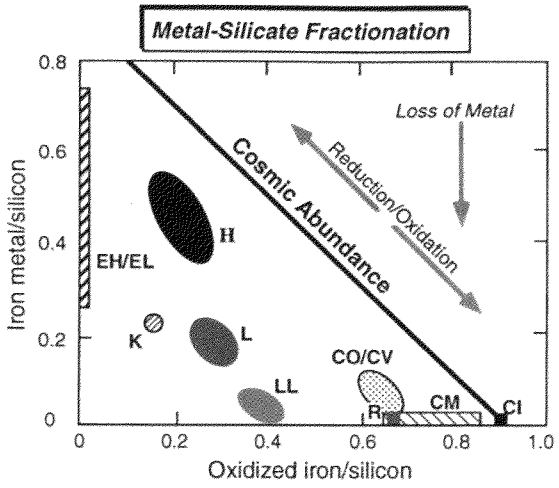

Fig. 1. Speciation of Fe into Fe,Ni-metal vs. silicates and oxides in several chondrite groups (from McSween, 1999 [2]). Iron abundances are presented as ratios of metallic Fe/Si and FeO/Si. All chondrites other than CI's have Fe/Si lower than the cosmic abundance. Increasing proportions of oxidized iron from EH/EL to H to L to LL to R reflect increasing f(O2) in nebular regions where these chondrite groups formed.

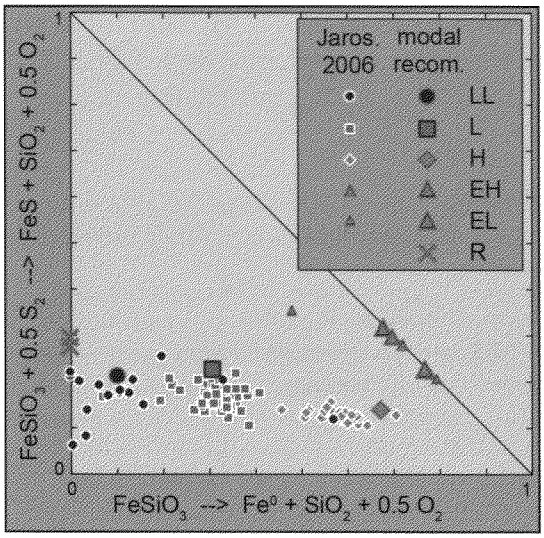

Fig. 2. Speciation of Fe into silicates, metals and sulfides for chondrites analyzed by modal recombination (this study) and by wet chemical techniques of Jarosewich [4,5]. Reaction progress on the horizontal axis shows speciation of all Fe in silicates (at origin) to all Fe in metal (x = 1). Progress on the vertical axis shows speciation of all Fe in silicates (at origin) to all Fe in sulfides (y = 1).

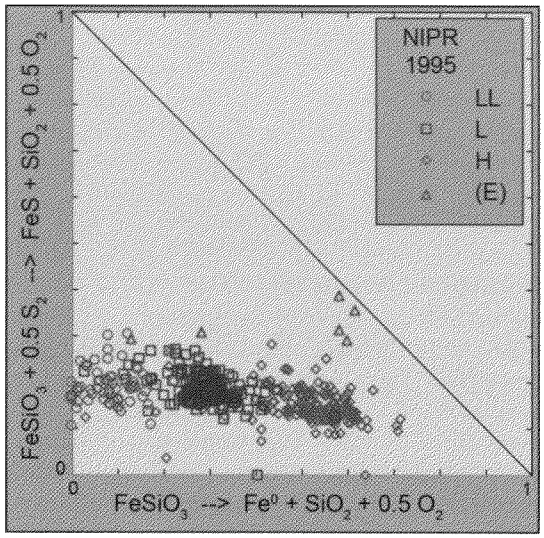

Fig. 3. Speciation of Fe into silicates, metals and sulfides for chondrites analyzed by wet chemical techniques by H. Haramura of NIPR [6]. See Fig. 2 for explanation of reaction progress along horizontal and vertical axes.

Discovery of New hibonite-bearing FUN inclusions from the Murchison(CM2)meteorite.

K. Fukuda[1], H. Hiyagon[1], S. Sasaki[1], W. Fujiya[2], T. Mikouchi[1], N. Takahata[3], Y. Sano[3] and Y. Morishita[4], [1]Department of Earth and Planetary Science, Graduate School of Science, The University of Tokyo, Tokyo 113-0033, Japan (k.fukuda@eps.s.u-tokyo.ac.jp), [2]Max Planck Institute for Chemistry, Particle Chemistry Department, 55128 Mainz, Germany, [3]Atmosphere and Ocean Institute, The University of Tokyo, Chiba 277-8564, Japan, [4]Department of GeoSciences, Graduate School of Science, Shizuoka University, Shizuoka 422-8529, Japan.

Introduction:

Refractory inclusions [Calcium-aluminum-rich inclusions, (CAIs)] are the oldest known solar system solids and would retain information about the early solar system evolution [1]. There is a minor group of CAIs, so called FUN (*F*ractionation and *U*nidentified *N*uclear effects [2]) CAIs, which exhibit distinct isotopic characteristics: (i) large mass-dependent fractionation in O, Mg and Si preferring heavy isotopes (F-signature), (ii) presence of unknown nuclear effects, esp., positive or negative anomalies in ^{48}Ca and ^{50}Ti (UN-signature), and (iii) little or no excess ^{26}Mg (and excess ^{41}K) from the decay of ^{26}Al (and ^{41}Ca). Absence of excess ^{26}Mg suggests either their late formation *after* the complete decay of ^{26}Al, or their early formation *before* injection of ^{26}Al into the solar system from (a) stellar source(s). The presence of Ca and Ti isotopic anomalies may suggest their earlier formation. The origin of FUN CAIs is still not well understood, but they may have important information about evolution and isotopic homogenization process(es) in the early solar system.

We found three FUN-like hibonite-bearing inclusions (MC037, MC040, MC003) from the Murchison (CM2) meteorite, which exibit extremely large mass-dependent fractionation in Mg isotopes (up to ~55‰/amu) but almost no excess in ^{26}Mg. Assuming a Rayleigh distillation process, more than 95% of Mg must have been lost (evaporated) from the molten precursors of these inclusions [3]. In order to better understand their origin and evolution, we conducted electron backscattered diffraction (EBSD) analyses and ion microprobe analyses of Mg, Ca and Ti isotopes on these inclusions.

Samples:

Two inclusions, MC037 (~150μm x ~200μm) and MC040 (~200μm x ~200μm), consist of abundant hibonite grains (5-30μm) with some spinel grains (5-10μm for MC037 and 10-30μm for MC040) embedded in Fe-rich silicates. Numerous μm-sized perovskite grains are almost uniformly distributed in Fe-rich silicate portion of MC040. They are probably the exsolution product from rapidly cooling melt. MC037 also contains perovskite in the Fe-rich silicate portion. Seven μm-sized ultra-refractory metal grains (enriched in Pt, Ru, Ir, etc.) are found in both inclusions. They also may be produced by severe evaporation of more volatile Fe-Ni-rich metal grains [4].

MC003 (~100μm x ~100μm) are composed mostly of spinel with rounded hibonite grains (3-20μm). This inclusion is similar to Blue Spinel by Ireland et al. [5].

Analytical conditions:

EBSD analyses: Silicates and perovskites of MC037 and MC040 were analyzed by a SEM-EBSD (Hitachi S-4500) at The University of Tokyo. The EBSD was used to identify mineral phases by Kikuchi lines. The obtained Kikuchi patterns were analyzed using a software developed by Kogure [6].

Mg isotopes: Magnesium isotopes were measured using a NanoSIMS at AORI, The University of Tokyo. Analytical details were previously described in [7]. In order to precisely estimate excess ^{26}Mg, a correction for mass-dependent fractionation, presumably caused by an evaporation process, is essential and we adopted the formula recommended by Davis et al. [8], where $\varphi(^{25,26}\mathrm{Mg})$ is defined by $1000 \times \ln\{(^{25,26}\mathrm{Mg}/^{24}\mathrm{Mg})_{sample}/(^{25,26}\mathrm{Mg}/^{24}\mathrm{Mg})_{std}$ and $\Delta^{26}\mathrm{Mg} = \varphi(^{26}\mathrm{Mg}) - \varphi(^{26}\mathrm{Mg})/0.514$. The fractionation factor (0.514) was experimentally determined using a CAI-like melt composition [8], which may also be applied to the FUN-like inclusions in this study.

Ca and Ti isotopes: Calcium and titanium isotopes were measured using a CAMECA ims-1270 ion microprobe at AIST, Tsukuba, Japan. Analytical details were previously described in [7,9,14]. An exponential law was applied for Ca and Ti isotopes, with ^{40}Ca and ^{44}Ca for reference isotopes of Ca, and ^{46}Ti and ^{48}Ti for reference isotopes of Ti [9]. Measured ratios for Madagascar hibonite standard were consistent with the literature values within uncertainties [10,11].

Results and discussion:

EBSD analyses obtained no Kikuchi pattern from Fe-rich silicates of MC037 and MC040, indicating that it is indeed amorphous. The result is considered that two inclusions were quenched from molten precursors.

Magnesium isotope data are plotted in the $\varphi(^{25}\mathrm{Mg})$ *vs* $\varphi(^{26}\mathrm{Mg})$ diagram (Fig. 1). All the data for MC037, MC040 and MC003 lie on the mass

fractionation line within uncertainties. Data for MC040 and MC003 show rather homogeneous composition with $\varphi(^{26}Mg)$ from ~97‰ to ~107‰ and ~29‰ to ~35‰, respectively. However, MC037 data show highly heterogeneous composition with $\varphi(^{26}Mg)$ from ~27‰ up to ~95‰. Hibonite and spinel in MC037 probably crystallized at various stages of the evaporation event, while those in MC040 and MC003 only at the last stage of the evaporation event, suggesting slightly different heating conditions for these inclusions. Figure 2 shows a $\Delta^{26}Mg$ *vs* $^{27}Al/^{24}Mg$ diagram. All the data for these inclusions show no excess ^{26}Mg ($\Delta^{26}Mg$ ~0) within uncertainties. Again MC037 data show large variations in the $^{27}Al/^{24}Mg$ ratio.

The obtained Ca and Ti isotopic compositions are shown in Figs. 3 and 4, respectively. These inclusions have small (< ± 10‰) but resolvable anomalies in ^{48}Ca and ^{50}Ti.

Highly fractionated Mg isotopes, lack of resolvable excess in ^{26}Mg and existence of ^{48}Ca and ^{50}Ti anomalies suggest that they are newly found FUN CAIs. The present results and previous works show that there are variations in F, UN, and ^{26}Mg excess signatures among different types of FUN (F) CAIs [11,12,13].

Outlook:

We are planning to measure oxygen isotopic compositions of these inclusions using SIMS, and the results may be presented at this meeting if possible.

References:

[1] Connelly J. N. et al. (2012) *Science, 338,* 651-655 [2] Wasserburg G. J. et al. (1977) *GRL, 4,* 299-302. [3] Sasaki S. et al. (2011) *NIPR Antarctic Meteorite XXXIV.* [4] Fukuda K. et al. (2012) *NIPR Antarctic Meteorite XXXV.* [5] Ireland T. R. et al. (1986) *GCA, 50,* 1413-1421. [6] Kogure T. (2003) *J. Crystal. Soc. Japan, 45,* 391-395 [7] Fukuda K. et al. (2013) *LPS XXXXIV,* Abstract #1870. [8] Davis A. M. et al. (2005) *LPS XXXVI,* Abstract #2334. [9] Fahey A. J. et al. (1986) *GCA, 51,* 329-350. [10] Niederer F. R. and Papanastassiou D. A. (1984) *GCA, 48,* 1279-1293. [11] Niederer F. R. et al. (1981) *GCA, 45,* 1017-1031. [12] Ireland T. R. et al. (1992) *GCA, 56,* 2503-2520. [13] Ushikubo T. et al. (2007) *EPSL, 254,* 115-126. [14] Jacobsen B. et al. (2008) *EPSL, 272,* 353-364.

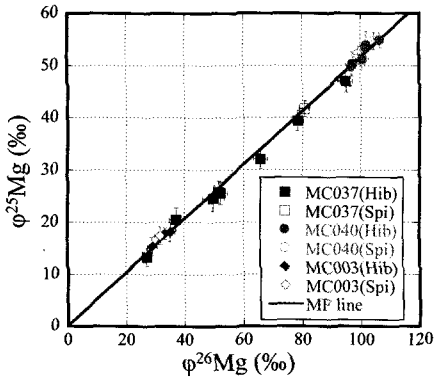

Fig. 1. The $\varphi^{26}Mg$-$\varphi^{25}Mg$ plot for MC037, MC040 and MC003. Hibonite and Spinel in these inclusions show extremely large mass fractionation of up to ~55‰/amu.

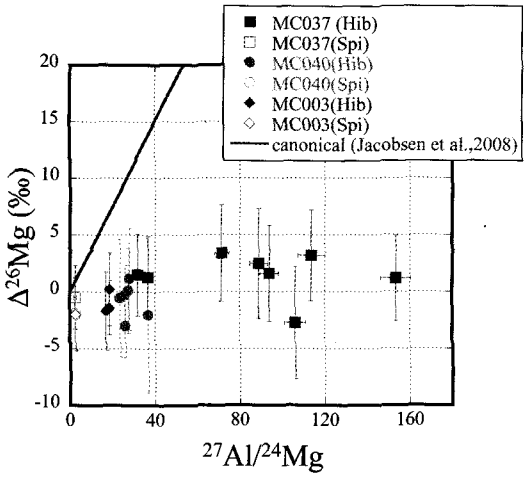

Fig. 2. Excess ^{26}Mg ($\Delta^{26}Mg$) *vs* $^{27}Al/^{24}Mg$ diagram for MC037, MC040 and MC003. The Blue line represents the canonical $^{26}Al/^{27}Al = (5.23 \pm 0.13) \times 10^{-5}$ by Jacobsen et al. [14]. All the data for these inclusions show almost no excess ^{26}Mg.

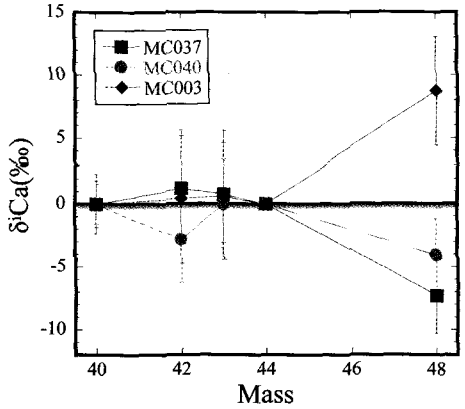

Fig. 3. Normalized Ca-isotopic compositions of the MC037, MC040 and MC003. MC037 and MC040 have negative anomaly in ^{50}Ti, but MC003 has positive one relative to the terrestrial value [10].

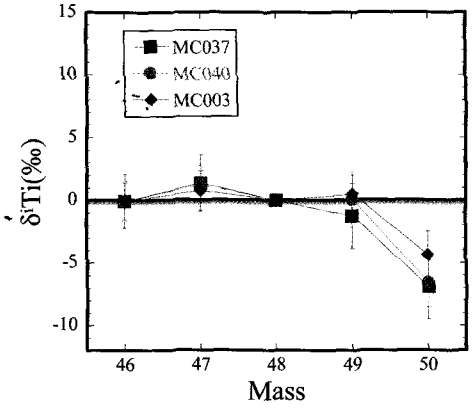

Fig. 4. Normalized Ti-isotopic compositions of the MC037, MC040 and MC003. All the data for these inclusions show negative anomaly in ^{50}Ti relative to the terrestrial value [11].

ARTIFICIAL COSMIC SPHERULES PRODUCED BY MELTING EXPERIMENTS OF THE POWDERED CARBONACEOUS CHONDRITES.

T. Gondo[1] and H. Isobe[1], [1]*Dept. Earth Envi. Sci., Grad. Sch. Sci. Tech., Kumamoto Univ., Kurokami, Kumamoto, 860-8555, Japan, e-mail: isobe@sci.kumamoto-u.ac.jp*

Introduction: Micrometeorites (MMs) are extraterrestrial fine particles derived from asteroids and comets and continuously falling to the Earth. Depending on their velocity, mass and entry angle, micrometeorites have undergone various degrees of heating during the atmospheric entry within a few seconds. This heating lead to significant textural, mineralogical and chemical modifications to MMs.

Micrometeorites are steady accumulation flow of planetary materials to the Earth. The annual mass is estimated at approximately 30,000 tons. The MM samples can be collected from Antarctia, ocean floor sediments and suspended particles in the stratosphere. Some MMs show remarkable similarity on mineralogy and chemical compositions to carbonaceous chondrite [1, 2].

MMs can be classified into two groups based on their size and textures: (1) fine-grained MMs (FgMMs), which are dominated by a fine-grained porous groundmass of micron-sized minerals, and (2) coarse-grained MMs (CgMMs), which are dominated by anhydrous silicates with larger than several micron meters, generary with glassy mesostasis [3].

The MMs larger them 70 μm in diameter show variously melted textures. In particular, completely melted micrometeorites are known as cosmic spherules. Cosmic spherules have experienced large degrees of melting of precursor materials during atmospheric entry, and form molten droplets. Cosmic spherules show considerable diversity in textures, compositions and mineralogy depending on characteristics of precursor materials and atmospheric heating [3,4].

In this study, we carried out rapid heating and quenching experiments on fine particles of the Allende meteorite and Murchison meteorite to reproduce cosmic spherules by atmospheric entry.

Experimental: We used powdered Allende meteorite (typical CV3 chondrite) and Murchison meteorite (CM2 chondrite) with approximately 100 μm in diameter as the starting material. The rapid heating and quenching within a few seconds are implemented by free fall of starting material particles through a high temperature vertical furnace with regulated gas flow of H_2, CO_2 and Ar to control oxygen fugacity and total gas flow [5]. Upward gas flow in the furnace tube can reduce falling velocity of the particles to reproduce thermal history of the cosmic spherules. The maximum temperature of the particles in this study is approximately 1520 °C. In the furnace, fO_2 is controlled to oxygen partial pressure of the upper atmosphere at approximately altitude of 86 km where MMs heated. Run products are retrieved from the bottom of the furnace tube and observed with a field-emission scanning electron microscope (FE-SEM, JEOL JSM-7001F) and analyzed with an energy dispersive X-ray spectroscopy (EDS, Oxford INCA system).

Results and Discussion: The run products show quite analogous textures to micrometeorites including scoriaceous, porphyritic olivine and barred olivine. Almost molten particles show spherical shape due to surface tension of the silicate melt. The outside shape of the particles is various depending on melt fraction of the particle.

1. Result of Allende meteorite as starting material

Fe-rich rim in olivine crystals found in the porphyritic olivine spherules, can be considered to be formed during quenching (Fig. 1). Olivine phenocrysts in porphyritic spherules are characterized by hexagonal shape with sharp

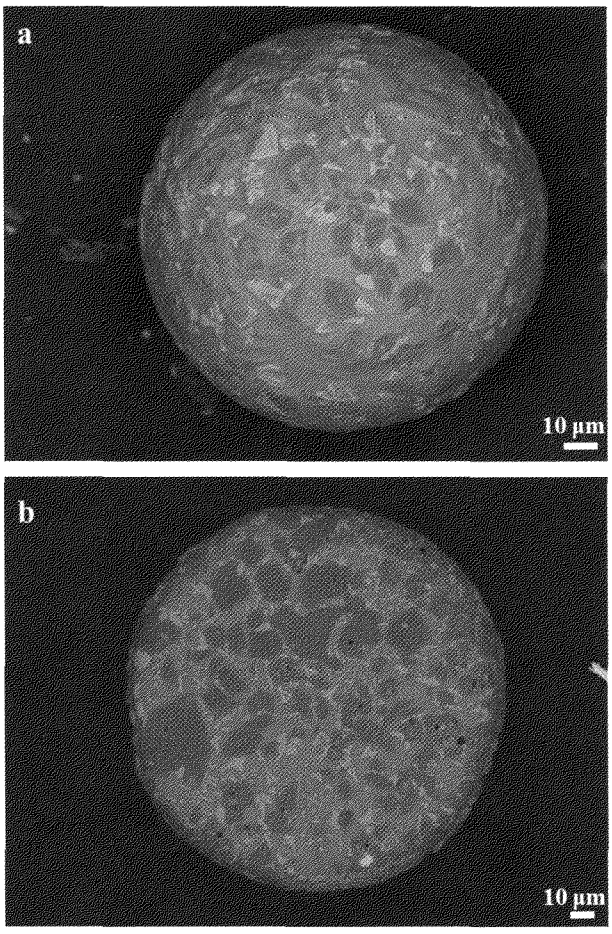

Fig. 1 Backscattered electron images of a porphyritic olivine spherule in the run product as the starting material of powdered Allende meteorite. (a) surface of the spherule, (b) polished section of the spherule shown in (a).

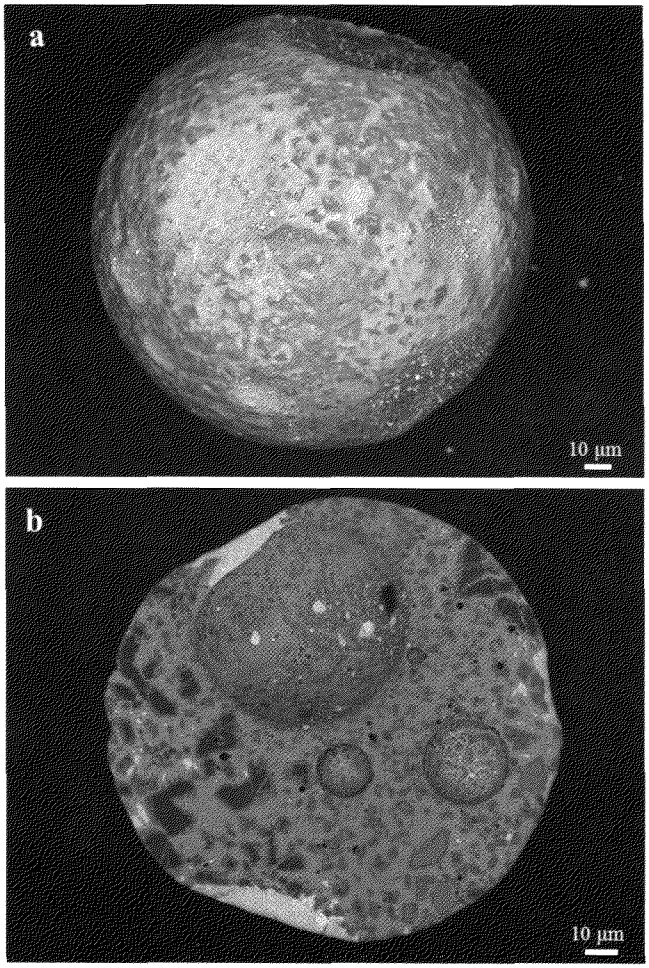

Fig. 2 Backscattered electron images of a porphyritic spherule showing a porous texture with olivine relict grains in the run product from powdered Murchison meteorite as the starting material. (a) surface of the spherule, (b) polished section of the spherule show in (a).

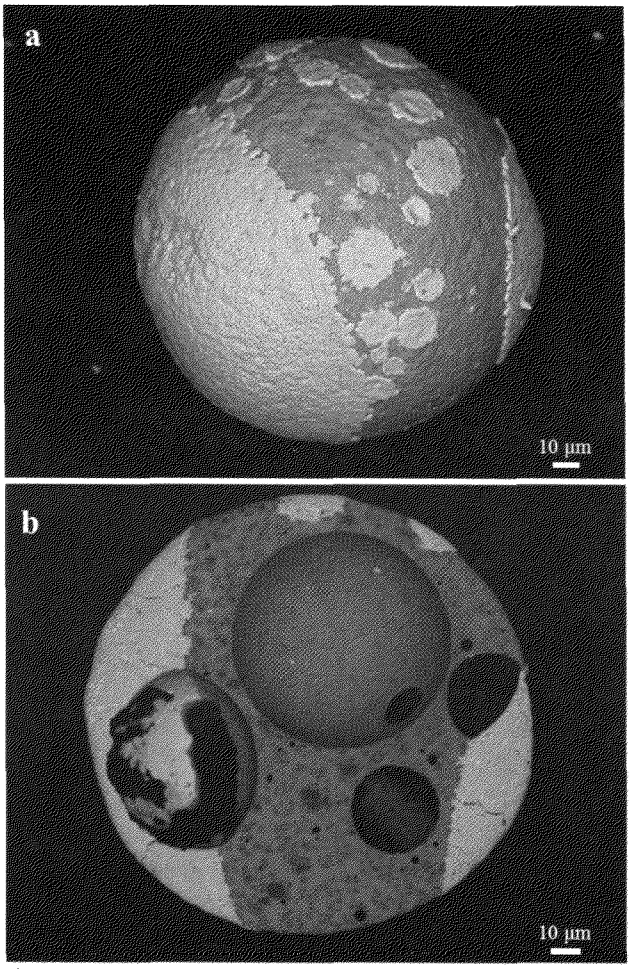

Fig. 3 Backscattered electron images of a porphyritic spherule showing a porous texture with olivine relict grains. (a) surface of the spherule, (b) polished section of the spherule show in (a).

edge. The sharp-edged olivine phenocrysts are quite rare in chondrules. It occurs, however, in molten micrometeorites, known as cosmic spherules. Internal texture of the artificial cosmic spherule produced in this work shown in Fig. 1(b) is remarkably similar to that of the natural porphyritic spherules shown in Figs. 1(A) and (B) of Cordier et al. (2011) [6].

2. Result of Murchison meteorite as starting material

Many run products show relict-bearing PO spherules containing relict anhydrous silicates (olivine and pyroxene) derived from mineral fragments in Murchison meteorite (Fig. 2). Olivine phenocrysts in porphyritic spherules are also characterized by hexagonal shape with sharp edge. Olivine phenocrysts are smaller than those in the run product of the Allende meteorite, and many voids numerous bubbles with various diameter can be seen in the spherules of run products. Internal texture of the artificial cosmic spherule produced in this work shown in Fig. 2(b) and Fig. 3(b) are remarkably similar to those of the natural porphyritic spherules shown in Figs. 1(C) and (D) of Cordier et al. (2011) and Fig. 1 (u) and (v) of Genge et al (2008) [3, 6].

On the surface of molten spherules, Fe sulfide also occur (Fig. 3). Immiscibility between sulfide melt and silicate melt may induce sulfide melt discharge from silicate melt. Iron-nickel metal is contained in the sulfide melt of spherules both run products (Figs. 2, 3).

In this study, we successfully reproduced artificial cosmic spherules with remarkably analogous textures to natural ones. We can compare each of the natural ones and these run products, and analogy of the run products to micrometeorites can be discussed on textural, mineralogical and chemical modifications during atmospheric entry of inter planetary materials.

References: [1] Love, S.G. & Brownlee, D.E. (1993) *Science, 262*, 550-553. [2] Reietmeijer, F.J.M. (2000) *Meteoritics & Planetary Science, 35*, 1025-1041. [3] Genge, M.J. (2008) *Earth Moon Planet, 102*, 525–535. [4] Love, S.G. & Brownlee, D.E. (1991) *Icarus, 89*, 26-43. [5] Isobe, H. & Gondo, T. (2013) *Jour. Mineral. Petoral. Sci.*, 108, 227-237. [6] Cordier, C. et al. (2011) *Meteoritics & Planetary Science, 46*, 1110–1132.

Cathodoluminescence Microscopy and Spectroscopy of a Plagioclase Particle from Asteroid Itokawa: Results of a Preliminary Investigation.

A.Gucsik[1,2](argu1986@hotmail.com), T. Nakamura[3], H. Nishido[4], K. Ninagawa[5], Y. Kimura[3], M. Kayama[6], A. Tsuchiyama[7], Sz. Bérczi[8] and Á. Kereszturi[1] [1]Konkoly Thege Miklos Astronomical Institute, Research Centre for Astronomy and Earth Sciences, H-1121 Budapest, Konkoly Thege Miklós út 15-17., Hungary, [2]Department of Geology, University of Johannesburg, Johannesburg, 2600 Auckland Park, South Africa, [3]Department of Earth and Planetary Materials Science, Graduate School of Science, Tohoku University, Sendai 980-8578, Japan, [4]Department of Biosphere-Geosphere System Science, Okayama University of Science, 1-1 Ridai-cho, Okayama, 700-0005, Japan, [5]Department of Applied Physics, Okayama University of Science, 1-1 Ridai-cho, Okayama, 700-0005, Japan, [6]Department of Earth and Planetary Systems Science, Graduate School of Science, Hiroshima University, Kagami-yama 1-3-1, Higashi-Hiroshima, Hiroshima 739-8526, Japan, [7]Kyoto University, Faculty of Science, Graduate School of Science, Division of Earth and Planetary Sciences, Kitashirakawaoiwake-cho, Sakyu-ku, Kyoto-shi, 606-8502, Japan, [8]Institute of Physics, Department of Material Physics, Eötvös University, Pázmány P. s. 1/a, Budapest, H-1117, Hungary

Introduction:

Cathodoluminescence (CL) is the emission of photons in the visible range from a material stimulated by an incident electron beam, being applicable for high-spatial resolution (~1 μm) spectroscopy. CL studies for minerals, especially feldspar, have been conducted in the planetary sciences to characterize shock metamorphic effects, to identify high-pressure minerals and shock-induced microdeformations such as planar deformation features (PDFs), to observe their distribution in meteorites and impactites, and to clarify the degree of the irradiation damage. An Itokawa sample was used to demonstrate the further capabilities to use of ScanningElectron Microscope-Cathodoluminescence (SEM-CL) methods in studies of the fine-grained astromaterials.

Sample and Experimental Procedure:

A plagioclase-dominated particle containing a relatively high albitic content was allocated by JAXA (RB-QD04-0022, length: 25 μm, width: 13 μm), which was obtained by the Hayabusa sample return mission in 2010. CL spectral data were recorded by a photon counting method using a photomultiplier tube (Hamamatsu: R2228) and converted to digital data. Corrected CL spectra in energy units were deconvoluted into the Gaussian components corresponding to each emission center. A peak-fitting software (Peak Analyzer) in OriginPro 8J SR2 was used for the correction and deconvolution of each emission center. Further details of the CL equipment and analytical procedure can be found in Kayama et al. [1] and references therein.

Results and Discussion:

The result shows that two components in blue region were assigned to defect center related to Al-O--Al/Ti centered at 2.83 eV (maxima at 438 nm) and impurity center of Ti at 3.06 eV with maxima at 405 nm (Fig. 1). However, any emissions of Fe^{3+} and Mn^{2+} usually found in terrestrial plagioclase could not be detected in this particle. Its CL image exhibits bright emissions in blue region with relatively homogeneous intensity. It implies that the plagioclase formed from nonferrous silicate melt at slightly higher temperature and after that has not been affected by thermal or hydrothermal alteration, which easily eliminates defect centers [1].

Conclusions:

This preliminary CL study of an Itokawa particle shows that the SEM-CL technique as a multiple technological approach is applied to investigate tiny samples as a powerful method, and could provide the first evidence of impact related micro-deformation on such a small body. However, further studies must be performed to understand how the irradiation could change the spectral properties of the sample, for instance.

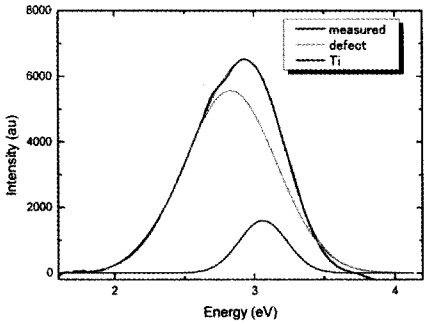

Figure 1. *Energy vs Intensity plot of the Hayabusa plagioclase particle showing the defect and Ti-related peaks.*

References:

[1] Kayama et al. (2012) *JGR: Planets, 117*, E09007.

Petrology and mineralogy of ALH-77005 shergottite

I. Gyollai[1,2], Sz. Nagy[3], Sz. Bérczi[2], H. Nishido[4]

[1]*Department of Lithospheric Research, Impact Research Group, Althanstrasse 14., 1051-Vienna, Austria.,* [2]*Institute of Physics, Department of Material Physics, Cosmic Material Space Research Group, H-1117 Budapest, Pázmány Péter sétány 1/a., Hungary,* [3]*University of Szeged, Department of Mineralogy, Petrology and Geochemistry, H-6722 Szeged, Hungary,* [4]*Okayama University of Science, Department of Biosphere-Geosphere Science,1-1 Ridai-Cho, Okayama 700-0005, Japan.*

Introduction:

The ALH-77005 Martian meteorite (lherzolitic type) was found at Allan Hills area in South Victoria Land on Antarctica in 1977-1978 [1]. Nyquist et al. [2] described the lherzolitic texture in ALH-77005 meteorite. Moreover, Ikeda [3] suggested the shergottite formation in the plutonic subsurface environment on Mars. We give an overview here about our new microscopical observations that could explain some details of its formation by shock-metamorphism overlapped with magmatic processes.

Methodology:

Petrographical studies were carried out using a Nikon Eclipse LV100POL optical microscope. The phase transitions and lattice defects in constituent minerals were examined by a Renishaw RM-2000 Raman spectrometer attached to a Leica DM/LM microscope. A 785 nm diode laser with 8 mW power as an excitation source was focused onto the surface with a spot size of 1 μm.

Petrography:

The ALH-77005 consists of dominant pyroxene and olivine associated with minor feldspar and chromite. It has coarse-granular texture with locally-arranged microgranular and poikilitic textures (Fig. 1.) as well as melt pockets including recrystallized needle-like crystallites in glassy matrix. The length of the needles is between 10-75 μm and their width between 1-5 μm. In the vicinity of the melt pockets resorption rim can be observed in olivine and the intrusion of dark melt. The textural characteristics above mentioned imply its formation during crystal differentiation in plutonic processes.

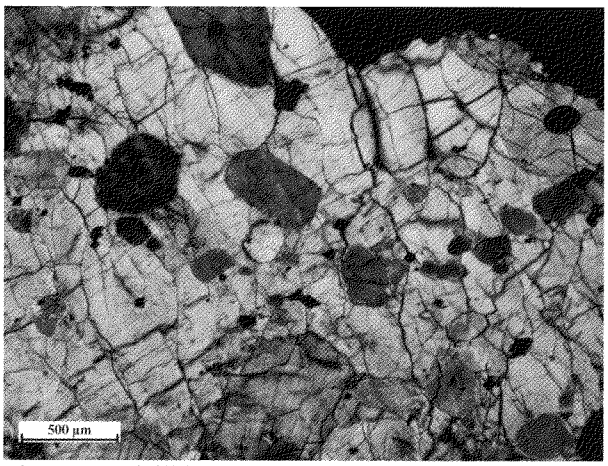

Figure 1: Poicilitic texture in our ALH-77005 sample

Shock metamorphic effects:

The isotropic lath-shaped plagioclase and maskelynite occur close to the melt pockets. Multiple parallel kink-band system is discernible in olivine. Poelchau and Kenkmann [4] described a new shock-metamorphic feature (feather features, FF) in quartz, which might be produced in low shock-pressure regime (7-10 GPa). Their appearances are in a good agreement with our observations in olivine from ALH-77005. Commonly, the FF lamellae tilt to the fractures in a low angle. The ALH-77005 shergottite contains patchy olivine grains with reduced interference color resulted from the thermal annealing followed by postshock melting, which formed melt pockts. Such patchy olivine also occurs in the ringwoodite-bearing shocked chondrite (e.g. NWA 5011) [5].

Raman spectroscopy:

The Raman spectra obtained from the boundary areas and the inside of the melt pocket suggest a recrystallization history related to the annealing in the postshock stage (Fig. 2). The Raman spectra were obtained from four areas characterized by the microtexture related to post-shock annealing as follows: sp1) normal olivine, sp2) olivine with deformation microtextures, sp3) boundary zone between olivine and melt pocket, sp4) recrystallized melt pocket (Fig. 2.). The olivine grain in the vicinity area to the melt pocket shows characteristic Raman peaks at 823, 853 (doublet main vibration) 535, 600, 918 and 957 cm^{-1} (minor peaks).

The main doublet peak seems mostly unchanged among the areas, but second peak of doublet became broader with reduction of its intensity, of which behaivor might be affected by the formation of lattice defects due to post-shock annealing. These facts imply that the duration of postshock pulsation was too short to induce a phase transition to high pressure-temperature minerals, such as wadsleyte and ringwoodite, which have been observed in NWA-5011.

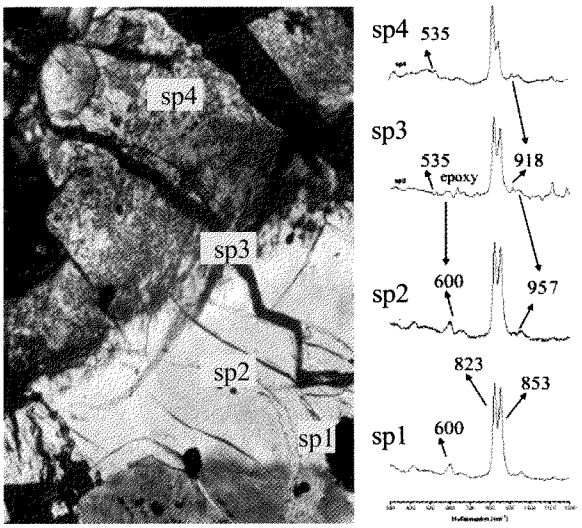

Fig. 2: Raman spectra of differently shocked olivine.

Conclusion:

The ALH-77005 formed by plutonic processes had experienced impact-metamorphic event estimated at 45-55 GPa peak shock pressure (S5 stage). The lack of high-pressure olivine polymorphs suggests that shock pressure pulsation was not enough to reach the activation energy for phase transformation. Therefore, patchy olivine might be corresponding to an intermediate phase on the way to higher-pressure stage during phase transformation.

Acknowledgement

We are grateful to H. Kojima for the loan of Antarctic Meteorite Educational Thin Section Set, and to M. Veres (Research Institute for Solid State Physics and Optics of the Hungarian Academy of Sciences) for assistance in Raman measurements.

References:

[1] Yanai K. (1979) *Mem. NIPR Res. Spec. Is., 12,* 1–8. [2] Nyquist L. E. (2001) *Space Sci. Rev., 96,* 105–204. [3] Ikeda Y. (1994) *Proc. of NIPR Symp. of Ant. Met. Res., 7,* 929, [4] Poelchau und Kenkmann T. (2011): *JGR, 116,* 13. [5] Nagy Sz. et al. (2010) *Lunar and Planet. Sci. Conf.*, abs#1228.

Characteristic features shock-induced on Mócs chondrite (L6)

I. Gyollai[1,2], K. Fintor[3], Sz. Nagy[3], Sz. Bérczi[2], H. Nishido[4], A. Gucsik[5,6]

[1]*Department of Lithospheric Research, Impact Research Group, Althanstrasse 14., 1051-Vienna, Austria.*, [2]*Institute of Physics, Department of Material Physics, Cosmic Material Space Research Group, H-1117 Budapest, Pázmány Péter sétány 1/a., Hungary,* [3]*University of Szeged, Department of Mineralogy, Petrology and Geochemistry, H-6722 Szeged, Hungary,* [4]*Okayama University of Science, Department of Biosphere-Geosphere Science,1-1 Ridai-Cho, Okayama 700-0005, Japan.* [5]*Konkoly Thege Miklos Astronomical Institute, Research Centre for Astronomy and Earth Sciences, H-1121 Budapest, Konkoly Thege Miklós út 15-17., Hungary,* [6]*Department of Geology, University of Johannesburg, Johannesburg, 2600 Auckland Park, South Africa*

Introduction:

The Mócs L6-type chondrite was found in Kolozs-county (Transylvania) in 1882. Raman spectroscopy of the sample revealed the shock-induced deformation microtextures in the vein-forming olivine, exhibiting strong mosaicism [1]. No shift of the major Raman vibration has been observed in the spectra of the olivine. This fact implies almost no p-T transition in the adjacent mineral assemblage. Chen et al. [2] reported characteristic K-Na fractionation in shock-induced veins. In this study, therefore, the fracture/vein system of Mócs meteorite has been investigated ,to clarify a signature of shock-induced melting.

Methods:

Petrographical studies were worked out using LV100POL microscope under plane polarized light and crossed polarized light modes with a polarizing microscope at Eötvös University, Budapest (Hungary). The polished thin section of 35 μm thickness was coated with carbon for the SEM-EDX, BSE, and element mapping studies, which were done at University of Szeged, Hungary by using a Hitachi S4700 electron microscope (10 kV acceleration voltage) combined with a Röntec QX2 energy dispersive X-ray fluorescence spectrometer.

Petrography:

The Mócs meteorite corresponds to L6-type, where shock metamorphosed and recrystallized matrices and several well-distinguished chondrule remnants have been observed. The chondrules in the meteorite are characterized by the follows: 3 pieces of pyroxene radial chondrules (1-3mm diameter), 4 pieces of olivine porphyritic chondrules (2 mm diamater), 2 pieces of recrytallized glassy chondrules (1mm diameter), 1 granular olivine chondrule, 1 composite chondrule and several porphyritic chondrule fragments. In the matrix we recognized a zoned part (~2mm) composed of feldspar, which was crossed by melt inclusion linked to fractures toward the rim.

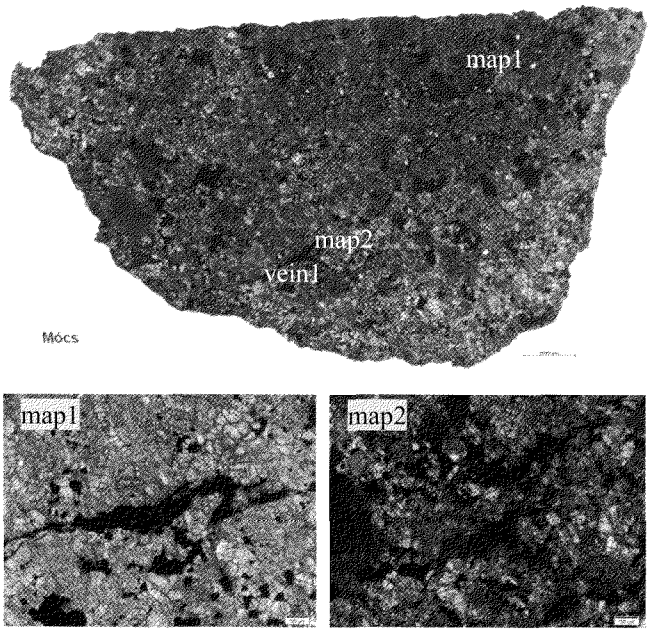

Figure 1: Stereomicroscopic image of thin section of Mócs meteorite marked with the measuring areas. Optical microscopic photos of area map1 (plain polarized light) and map2 (crossed polars)

Shock metamorphic effects:

The Mócs meteorite exhibits highly dense fractures or fissures, mostly which are filled by opaque minerals (iron-oxide and troilite), mineral fragments and melt. In the case of L6-type chondrites such as Tenham and NWA-5011[2], mineral assemblages indicating shock-induced phase transformations have been observed. Hence, two wide parts in a vein with 500 μm width were selected for the BSE measurements and element mappings. Several chondrules were also selected for the BSE imaging for checking inhomogenities, which show the signature of partial melting or the presence of the relict with lower metamorphic petrologic type. Among the chondrules, large the higher acoustic-impedance opaque mineral assemblages (troilite and chromite) could enhance shock wave velocity and peak shock p-T in adjacent olivine grains resulting strong mosaicism and deformation microstructure. One of the wide part in the shock vein (vein1 in Fig. 1) and 2 chondrules (map1 and map2 in Fig. 1) were selected for the element mapping.

Elemental mapping:

The map1 area contains chromite grains (Fig. 2A), which is altered to iron oxide via secondary processes. According to the composite map (Fig. 2B), the melt pocket area indicates near composition of feldspar minerals, whereas chondrules are composed of both pyroxene and olivine. The melt packet is enriched in Na compared to its vicinities (Fig. 2C). The P and Ca enrichments correspond to the area rich in K (Fig. 2D).

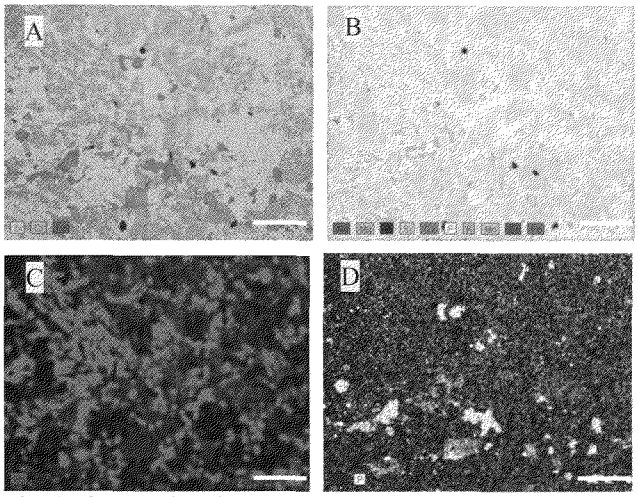

Fig. 2. Composite element maps of upper part in shock vein (map1 in Fig. 1.) including chondrule fragments (A: Si-Cr-Fe, B: composite element map of major elements and Cr, C: Na-K, D: Ca-P, scale: 200 μm)

The map 2 shows chromite grains (with high Cr concentration), troilite (with higher Fe and S concentrations), suggesting the oxidation with iron oxide phases with only higher Fe concentrations (Fig. 3A). The dark area in SE map is enriched in Na, which is significant for melt pockets. Moreover, the high Al content in Fig. 3/B confirms the presence of feldspar. On the Mg-Si-Ca-Fe elemental map (Fig. 3D), there are well distinguishable by the presence of olivine (Mg-Si), pyroxene (Ca-Si), and the opaque (Fe) phases. The chondrule fragments are mostly made up of olivine, whereas pyroxenes are concentrated in the groundmass and the melt regions.

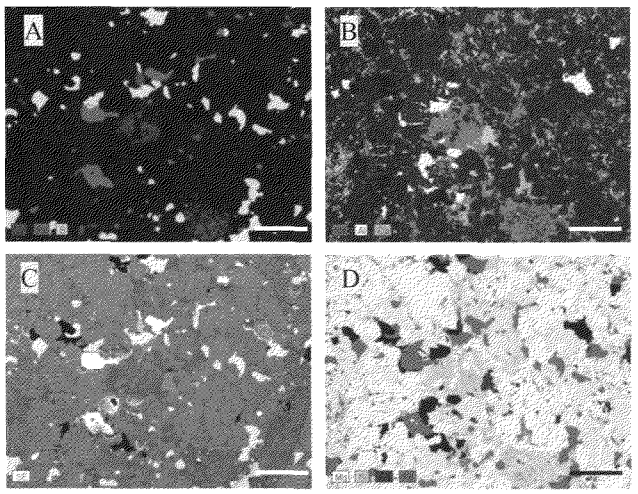

Fig. 3. Composite element maps of lower part of shock vein (map 2 area) including mineral and chondrule fragments (A: Cr-Fe-S, B: Na-Al-Ca-K, C: secondary electron image, D: Mg-Si-Ca-Fe, scale: 200 μm)

The map 2 within the vein is characterized by Cr, P, S, Al, Ca enrichments comparing to the neighboring large mineral grains (Fig. 4A). However, the vein is not so rich in Na comparing to its environment, which is not concordant with the presence of mineral melt. The upper left part in the map is occupied by an olivine grain (higher Fe and Mg concentrations), whereas the lower right part with higher Ca-Si is a pyroxene (Fig. 4B). The vein is composed of troilite and iron-oxide. The patchy-like Cr enrichment corresponds a chromite inclusion. The Ca has moderately enrichment near to the pyroxene- vein boundary, whereas Fe is dominant in the inner part of the vein. The tiny lath-shaped particles in the vein have higher Na and K at their boundaries, which might be identified to the feldspar.

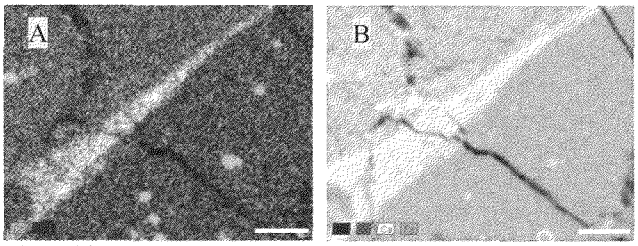

Fig. Thin vein cutting across olivine and pyroxene grains (near the map 2 in Fig. 1.). (A: Cr-Fe-S, B: Mg-Si-Ca-Fe, scale: 200 μm)

Conclusion:

The petrologic texture observed in Mócs meteorite results from both of thermal and impact metamorphic processes. The lack of the high-pressure olivine polymorphs suggests that shock pressure pulsation was not enough to reach the activation energy for its phase transformation. Therefore, the patchy olivine corresponds to an intermediate phase formed by postshock temperature involved in shock metamorphism.

Acknowledgement

We are grateful to Félix Schubert (University of Szeged) for the support to obtain element maps.

References:

[1] Gyollai, I. et al. (2009) *AIP Conference Proceedings, 1163*, 75-85,[2] Chen, M. et al. (2004) *European Journal of Mineralogy, 16/2*, 203-211, [3] Nagy Sz. et al. (2010) *Lunar and Planet. Sci. Conf.*, abs#1228.

Systematic Isotopic Studies of Sr, Ba, Ce, Nd and Sm in Eucrites. H. Hidaka[1], K. Sera[1] and S. Yoneda[2], [1]Department of Earth and Planetary Systems Science, Hiroshima University, Higashi-Hiroshima 739-8526, Japan, [2]Department of Science and Engineering, National Museum of Nature and Science, Tsukuba 305-0005, Japan.

Introduction:

Most eucrites have basaltic composition and represent lava flows or shallow intrusions from a differentiated parent body, possibly asteroid 4 Vesta. Chronological information of eucrites provide important constraints of the evolutional history of the eucrite parent body (EPB). Although many isotopic studies have been conducted by several kinds of geochronometers using decay systems with long-lived and short-lived radioisotopes to understand the processes of accretion, core formation, mantle differentiation, and the formation of primary basalts on the EPB [1-4], the exact time-scales for eucrites petrogenesis are still unclear. Complex post-crystallization events such as impact heating and remelting may have reset the isotopic systems in eucrites to some degree, showing in inconsistent results from several kinds of geochronometers.

In this study, systematic isotopic analyses of Sr, Ba, Ce, Nd and Sm were performed on each eucrites sample for better understanding of differentiation on the EPB.

Samples and experiments:

Eight eucrites, Juvinas, Millbillillie, Stannern, DaG 380, Dag 391, DaG 411, DaG 443, and DaG 480, were used in this study. About 1 g of each powdered sample was decomposed by treatment with HF-$HClO_4$ with heating. Then, the samples were taken to dryness and redissolved in 10 mL of 2M HCl. The solution was divided into two portions: the main portion for isotopic measurements by TIMS and the rest for the determination of elemental abundances of Sr, Ba, and REE by ICP-MS.

A variety of geological reference materials (JA-1, JB-1a, JG-1, JGb-1) and chemical reagents (standard solutions produced from SPEX CertiPrep for Ba, Ce, Sm, and Gd; JNdi-1 for Nd; NIST SRM-987 for Sr) were also analyzed as terrestrial standard samples.

Each solution for the isotopic study was loaded onto a cation exchange resin packed column (Bio-Rad AG50WX8, 200-400 mesh, H^+ form, 50 mm length × 4.0 mm diameter). The column was washed with 2 M HCl for Sr elution. Next, the column was washed with 2 M HNO_3 for Ba elution. Finally, the column was washed with 6M HCl for REE elution. The solution was then evaporated to dryness and redissolved in a drop of 0.1 M HCl. The first Sr fraction was purified using a quartz column packed with Sr-specific resin (Eichrom, Sr resin, particle size of 100-150 μm, 100 mm length × 2.5 mm diameter). The REE fraction was loaded onto a second column packed with lanthanide-specific resin (Eichrom, LN resin, particle size of 100-150 μm, 100 mm length × 2.5 mm diameter) to separate Ce, Nd, Sm and Gd using 0.15, 0.25, 0.35 and 0.5 M HCl, respectively.

A Triton thermal ionization mass spectrometer equipped with nine Faraday cup collectors was used for the isotopic measurements of Sr, Ba, Ce, Nd, Sm, and Gd. The purpose of Gd isotopic measurement is to cross-check the neutron capture effect of the samples in combination with Sm isotopic data.

Sr was measured on single Re filament with Ta_2O_5 activator. Instrumental isotopic mass fractionation was corrected by the exponential law using $^{88}Sr/^{86}Sr = 8.375209$ as a normalizing factor.

Ba, Ce, Nd, Sm and Gd were measured on double Re filaments. For their isotopic measurements, $^{134}Ba/^{136}Ba=0.307776$, $^{140}Ce/^{142}Ce=7.941$, $^{146}Nd/^{144}Nd=0.7219$, $^{147}Sm/^{152}Sm=0.56081$, $^{156}Gd/^{160}Gd=0.9361$ were used to correct for instrumental mass fractionation using the exponential law. When the isotopic depletions of ^{155}Gd were found in the analyses, the Gd isotopic data sets were normalized by $(^{155}Gd+^{156}Gd)/^{160}Gd=1.61290$. Cerium was measured as oxide ions (CeO^+), while Ba, Nd, Sm and Gd were measured as mono-atomic ions (M^+).

Another minor aliquot of each sample solution was once evaporated to dryness, and redissolved using 5 mL of 0.5 M HNO_3. A 0.05 g quantity of a 10 ppb indium solution was added to the individual sample solutions as an internal standard element to optimize the analytical conditions for REE measurements. An ICP-MS (Agilent 7500cx) was used for determination of the elemental abundances of Sr, Ba, and REE.

Results and Discussion:

^{87}Sr includes radiogenic component from the decay of ^{87}Rb, and its isotopic variation correlates with Rb/Sr elemental ratios. In order to estimate the initial $^{87}Sr/^{86}Sr$ of the EPB, namely basaltic achondrite best initial (BABI) [5], from our Rb-Sr data, precise determination of Rb/Sr elemental ratios by isotope dilution method are in progress.

Ba has seven stable isotopes consisting of p-, s-, and r-process nucleosynthetic origin. Most previous Ba isotopic studies of meteorites focused on the variation of r- and s-process nucleosynthetic components due to additional inputs in the early solar system. ^{135}Ba and ^{137}Ba isotopes are sensitive to s- and r-process variations, and often have deficits

and/or excesses in chemical separates in carbonaceous chondrites due to the existence of presolar grains [6]. However, in case of eucrites, there are no significant isotopic variations of all Ba isotopes.

Since ^{138}Ce isotopic excesses of eucrites correlate with their La/Ce elemental ratios, these excesses are identified to be decay product from ^{138}La. Our data are consistent with the results from previous study on the EPB evolution of Ce isotope [7], showing the La-Ce isochron of 4.56 Ga with the initial Ce isotopic ratio of ^{138}Ce/^{142}Ce=0.0225321 .

The isotopic deviations of ^{142}Nd of eucrites show slightly negative to zero values relative to terrestrial standard materials (ε^{142}Nd=-0.2 to 0), and no positive values which are observed in typical cumulate eucrites having high Sm/Nd elemental ratios. These results are consistent with previous study [8].

Sm isotopic compositions of the eucrites show the depletions of ^{149}Sm and excesses of ^{150}Sm caused by neutron capture reactions due to cosmic rays irradiation. These Sm isotopic shifts correspond to the neutron fluences ranging from 3.2 to 6.1x10^{15} n cm^{-2}. The estimated neutron fluences are almost consistent with their cosmic-ray exposure ages, suggesting no strong evidence of initial cosmic-ray irradiation on the surface of EPB. The isotopic shifts of Sm are caused by the cosmic-ray irradiation after release from the EPB. The variation of ^{157}Gd-^{158}Gd isotopic shifts also show the consistency with that of ^{149}Sm-^{150}Sm.

Systematic isotopic data obtained in this study provide a hint to understand the evolution processes of differentiated meteorites. We are now applying this technique for the analyses of cumulate eucrites and diogenites.

References:

[1] Lugmair G.W. and Shukolyukov A. (1998) Geochim. Cosmochim. Acta 62, 2863-2886. [2] Misawa K., Yamaguchi A. and Kaiden H. (2005) Geochim. Cosmochim. Acta 69, 5847-5861. [3] Srinivasan G., Whitehouse M.J., Weber I. and Yamaguchi A. (2007) Science 317, 345-347. [4] Quitté G. et al. (2011) Geochim. Cosmochim. Acta 75, 7698-7706. [5] Papanastassiou D.A. and Wasserburg G.J. (1969) Earth Planet. Sci. Lett. 5, 361-376. [6] Hidaka H. and Yoneda S. (2011) Geochim. Cosmochim. Acta 75, 3687-3697. [7] Makishima A. and Masuda A. (1993) Chem. Geol. 106, 197-205. [8] Boyet M. and Carlson R.W. (2005) Science 309, 576-581.

Chemical composition of primitive achondrites: Clues for understanding the early differentiation processes of their parent bodies. Y. Hidaka[1, 2], N. Shirai[2], A. Yamaguchi[3, 4], M. Ebihara[2], and V. Debaille[1] [1]Laboratoire G-time, Université Libre de Bruxelles, 50 Av. F. D. Roosevelt, Brussels, Belgium, [2]Department of chemistry, Tokyo Metropolitan University, 1-1 Minami-Osawa, Hachioji, Tokyo, Japan, [3]National Institute of Polar Research, Tachikawa, Tokyo, Japan, [4]Department of Polar Science, School of Multidisciplinary Science, Graduate University for Advanced Sciences, Tachikawa, Tokyo, Japan.

Introduction:

Primitive achondrites, acapulcoite-lodranites and winonaites, are the most suitable materials for understanding the early differentiation processes in the solar system bodies, because they preserve partially melted features in their textures and show primitive chemical compositions. Partial melting processes are believed to represent the early stages of differentiation of bodies and there are two types of processes proposed for chondritic materials: silicate partial melting and metallic partial melting [1]. Primitive achondrites have been well studied for their petrology [1, 2, 3, 4], but not enough for their bulk chemical composition, especially those for their metals. Therefore, in this study, we determined the chemical composition of a number of primitive achondrites to understand the partial melting processes that had occurred on their parent bodies.

Samples and analyses:

We have determined lithophile and siderophile element abundances of 13 primitive achondrites, including 9 acapulcoites (Dho 125, Dho 290, GRA 95209, MET 01195/01198/01244 Y-74063, Y 981505 and Y 981725), 2 lodranites (NWA 2235 and Y-791491) and 2 winonaites (NWA 725 and Y-8005). Among the analyzed meteorites, an acapulcoite Y-74063 and a winonaite NWA 725 have been reported as the relict chondrule-bearing primitive achondrites [5, 6]. Each meteorite was ground into powder in an agate mortar and was magnetically separated into the non-magnetic fraction and the magnetic fraction. The sample amount is ~200-300 mg for each meteorite. The non-magnetic fraction was analyzed by INAA and ICP-MS at Tokyo Metropolitan University (TMU). The magnetic fraction was analyzed by ICP-MS and ICP-AES at TMU. For Dho 125, Dho 290 and NWA 2235, we could not prepare the magnetic fraction, so they are unavailable for discussion of metallic partial melting.

Results:

The chemical composition of the non-magnetic fraction of each primitive achondrite is characterized in the abundances of light-rare earth elements (LREE), Eu and plagiophile elements (Na, Al and K). Acapulcoite Y-74063, winonaites NWA 725 and Y-8005 have nearly chondritic composition of REE and plagiophile elements. Acapulcoites Dho 125, Dho 290, GRA 95209 and MET 01195/01198/01244 have slightly depleted composition of LREE and plagiophile elements compared with chondrites. Acapulcoites Y 981505 and Y 981725 are more depleted in LREE but less depleted in plagiophile elements compared with Dho 125, Dho 290, GRA 95209 and MET 01195/01198/01244. Lodranites NWA 2235 and Y-791491 are severely depleted in plagiophile elements and Eu, but chondritic in LREE.

The chemical composition of the magnetic fraction of each primitive achondrite is characterized in the abundances of platinum group elements (PGE) and volatile elements (Cu, Ga, Sb, Ge and Sn). Among acapulcoite-lodranites, acapulcoite Y-74063 has chondritic composition of PGEs, while others are enriched in PGE except for an acapulcoite Y 981505. Lodranite Y-791491 has the highest PGE abundances among them. Y 981505 is clearly depleted in Re and Ir. Between winonaites, NWA 725 and Y-8005 have similar PGE abundances, but clearly different in volatile element abundances. The abundances of Ga, Sb, Ge, and Sn in Y-8005 are nearly chondritic. On the other hand, NWA 725 is depleted in Ga, Ge and Sn and slightly depleted in Sb relative to Y-8005.

Discussion:

In the non-magnetic fraction, primitive achondrites have wide variety of REE abundances that is difficult to explain by simple silicate partial melting process. The relationship between incompatible trace element (Th) and plagiophile elements is also difficult to explain by a single event (Fig. 1). Based on these observations, we assume the existence of different process(es) in addition to the silicate, basaltic partial melting on the parent body of acapulcoite-lodranites. From Fig. 1, we assume that phosphate must relate to the compositional transition of acapulcoite-lodranites. The phosphate mobilization process was proposed by [2] from their petrologic observations. They found the veins of phosphates and of metals with phosphates in meteorites they studied. We suggest that this phosphate mobilization process must have important role for the early differentiation processes and chemical compositional evolution on the acapulcoite-lodranite parent body.

The abundances of REE in winonaites NWA 725 and Y-8005 are nearly chondritic. This indicates that these winonaites are scarcely melted meteorites.

In the magnetic fraction, to explain the compositional variation of acapulcoite-lodranites, we

model the metallic partial melting in Fe-S and Fe-S-C systems. Partition coefficients are from [7, 8, 9]. The Fe-S system melting has been considered as the common process for primitive achondrite metals [1, 10]. On the other hand, it was suggested that if there were C in the system, Fe-S-C system melting had to occur [9, 11]. Acapulcoite GRA 95209 has been reported as having large amount of carbon in its metal [12]. Here, acapulcoite Y-74063 is used as the starting material of this calculation.

Modeling of Fe-S and Fe-S-C system melting can reproduce metals that have broadly similar chemical composition to those of measured primitive achondrites. In Ir/Ni vs. W/Re, model calculation results of the Fe-S system and Fe-S-C system melting are both mostly consistent with acapulcoites, but slightly inconsistent with lodranite and clearly different from winonaites (Fig. 2). However, we could not explain the reasons for low W/Re ratio in Y-791491 and difference in the abundances of some elements (Mo, Fe and Cu for Fe-S system, and Co, As and Cu for Fe-S-C system) between model and Y-791491. Therefore, it is difficult to conclude which type of partial melting process had occurred in the acapulcoite-lodranite parent body.

Compositional difference between two winonaites was difficult to explain by parent body processes. Considering that a winonaite parent body may have experienced several large impact events that caused secondary heating or the breakup-reassembly [4, 13], such a difference can be explained by the contribution of materials from different reservoirs.

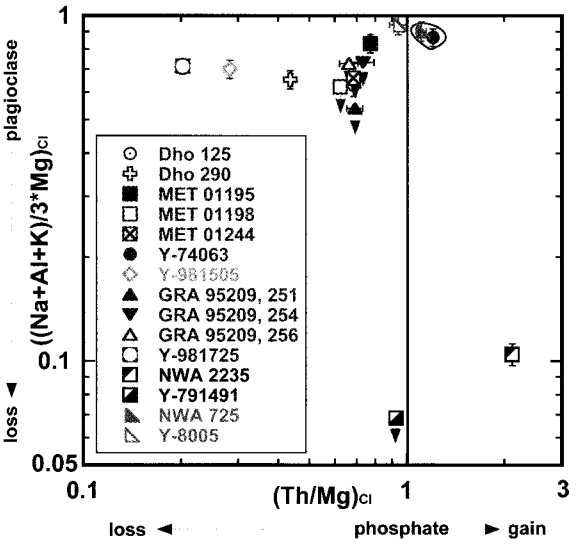

Fig. 1. CI-normalized plagiophile element abundances vs. Th abundances for the non-magnetic fraction of primitive achondrites. CI values are from [14].

References:

[1] McCoy T. J. et al. (1997) *GCA, 61*, 639-650. [2] McCoy T. J. et al. (1996) *GCA, 60*, 2681-2708. [3] McCoy T. J. et al. (1997) *GCA, 61*, 623-637. [4] Benedix G. K. et al. (1998) *GCA, 62*, 2535-2553. [5] Yanai and Kojima, (1991) [6] Patzer A. et al. (2004) *Meteorit. Planet. Sci., 39*, 61-85. [7] Chabot N. L. and Jones H. (2003) *Meteorit. Planet. Sci., 38*, 1425-1436. [8] Chabot N. L. et al. (2009) *Meteorit. Planet. Sci., 44*, 505-519. [9] Hayden L. A. et al. (2011) *GCA, 75*, 6570-6583. [10] Mittlefehldt D. W. et al. (1996) *GCA, 60*, 867-882. [11] Goodrich C. A. et al. (2013) *GCA, 112*, 340-373. [12] McCoy T. J. et al. (2006) *GCA, 70*, 516-531. [13] Schulz T. et al. (2009) *EPSL, 280*, 185-193. [14] Anders E. and Grevesse N. (1989) *GCA, 53*, 197-214.

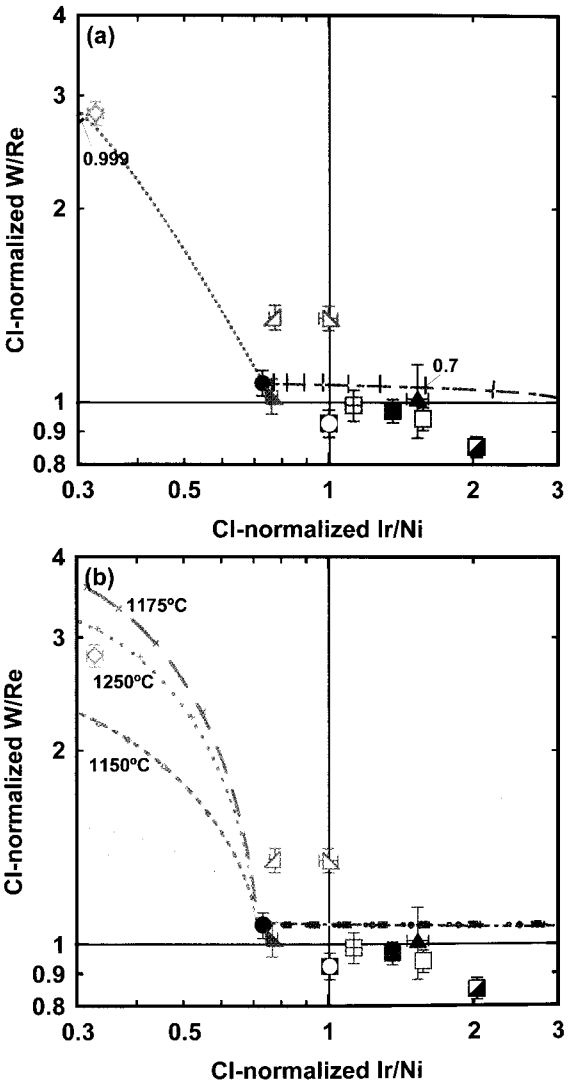

Fig. 2. CI-normalized W/Re vs. Ir/Ni ratios for the magnetic fraction of primitive achondrites. (a) Dotted lines show model calculation results of Fe-S eutectic melting. (b) Dotted lines show model calculation results of Fe-S-C melting. Legends are the same as shown in Fig. 1.

Visible and Near-Infrared Spectral Survey of Select Carbonaceous Chondrite Samples of the National Institute of Polar Research: Results of CI/CM Chondrites. T. Hiroi[1,2], H. Kaiden[2], N. Imae[2], A. Yamaguchi[2], H. Kojima[2], S. Sasaki[3], T. Misu[4], M. Matsuoka[4], T. Nakamura[4]. [1]Department of Geological Sciences, Brown University, Providence, RI 02912, USA, [2]Antarctic Meteorite Laboratory, National Institute of Polar Research, 10-3, Midori-cho, Tachikawa, Tokyo 190-8518, Japan, [3]Department of Earth and Space Sciences, Osaka University, 1-1 Machikaneyama-cho, Toyonaka, Osaka 560-0043, Japan, [4]Department of Earth and Planetary Materials Sciences, Tohoku University, 6-3, Aoba, Aramaki, Aoba-ku, Sendai, Miyagi 980-8578, Japan.

Introduction:

In June 2010 we started a visible and near-infrared (VNIR) spectral survey of meteorite samples stored at the National Institute of Polar Research (NIPR) and finished lunar, Martian, and HED meteorite samples. Then, we started surveying carbonaceous chondrite (CC) samples since November 2012. In this presentation we are reporting the initial results of CI and CM chondrite chip samples.

Experimental:

Out of 95 catalogued CCs of the NIPR, 3 CI/C1 and 17 CM samples were selected and studied so far by considering weight, freshness, and texture (having a natural, broken surface). Bidirectional VNIR diffuse reflectance spectra of one or two spots on each chip sample were obtained at every 5 nm over the wavelength range of 0.25-2.5 μm at RISE Project of the National Astronomical Observatory of Japan (NAOJ). A detailed description of the procedure is described in a separate paper on Martian meteorite samples [1]. For this study, incident beam size was about 3 × 2 mm. In addition, biconical Fourier Transform infrared (FTIR) reflectance spectra of those spots were measured at 4 cm^{-1} resolution over the wavelength range up to either 15 μm at Tohoku University or 25 μm at RELAB [2]. The FTIR spectra were scaled to connect with the VNIR spectra at 2.5 μm in wavelength.

Preliminary Results:

An example of CC chips and measured spots is shown in Fig. 1. Two spots were chosen for each of the CI/C1 chip samples: Spot A from fresh-looking, dark areas, and Spot B from light, weathered (evaporite?) areas.

Shown in Fig. 2 are VNIR-FTIR combined reflectance spectra of three CI/C1 chondrite chip spots. As expected, Spot B spectra have high visible albedos and totally different (negative) spectral slopes from those of typical CC spectra. In addition, while Spot A spectra show very shallow 3-μm hydration bands, Spot B spectra shows deeper and more complex 3-μm absorption bands. The shallow 3-μm bands combined with the absence of UV absorption of Spot A spectra may indicate that these CI/C1 chondrites were dehydrated by thermal metamorphism based on our previous study [3].

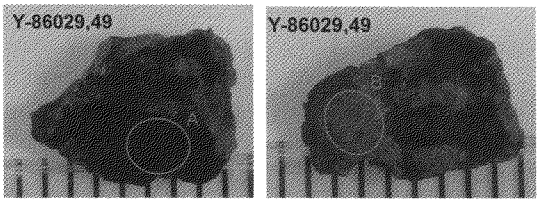

Fig. 1. Example images of measured spots on a Y-86029 chip sample viewed from two different sides, showing fresh dark Spot A and terrestrially-weathered light Spot B. The spot size is about 2 × 3 mm, and the scale is 1 mm.

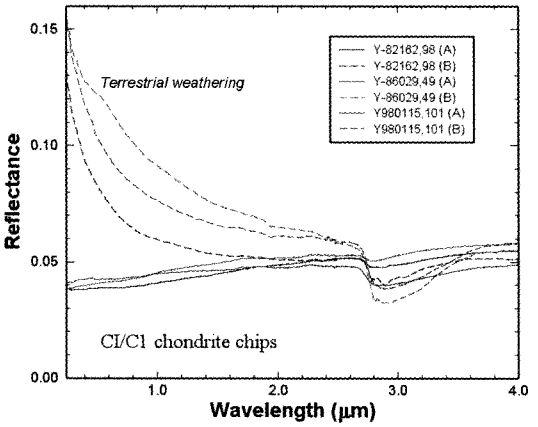

Fig. 2. VNIR-FTIR combined reflectance spectra of CI/C1 chondrite chip samples.

Shown in Fig. 3 are examples of CM chondrite chips and measured spots. Most of the CM chips studied here show fine dark-light textures as on the A-881458 chip, while some of them showing relatively large, 1-mm size clasts as seen on the B-7904 chip.

Fig. 3. Example images of two of CM chondrite chip spots measured here. The scale is 1 mm.

VNIR reflectance spectra of these CM chip spots are grouped into the following three plots. Although their FT-IR spectra were also measured, their data have not been processed yet and will be presented at the meeting.

Shown in Fig. 4 are VNIR reflectance spectra of select CM chondrite spots showing prominent UV abosortion and extended visible absorption bands near 0.7, 0.9, and 1.1 μm allegedly due to Fe^{2+}-Fe^{3+} charge transfer in certain types of serpentine. These serpentine absorption features can be detected by the ONC multicolor images onboard Hayabusa 2 spacecraft if present on its target asteroid (1999 JU_3).

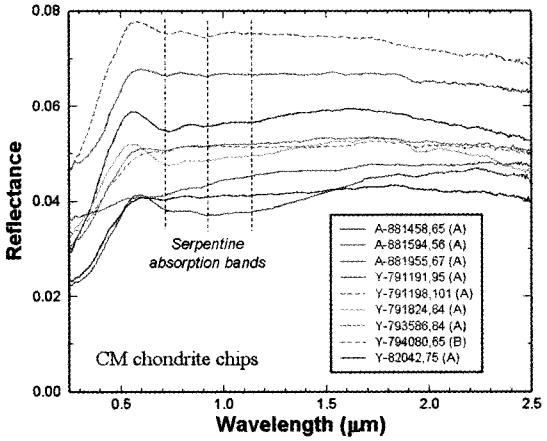

Fig. 4. VNIR reflectance spectra of CM chondrite chip spots showing Fe^{2+}-Fe^{3+} charge-transfer absorption bands of certain types of serpentine.

Next, shown in Fig. 5 are VNIR spectra of CM chip spots showing no or little serpentine absorption bands other than some UV absorption. Especially, B-7904 is known well as a thermally-metamorphosed CM chondrite and thus exhibits a totally feature-free VNIR spectrum with moderately weak UV absorption, consistent with our previous study [4].

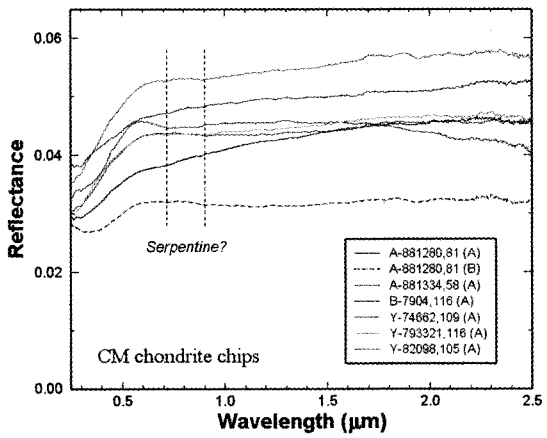

Fig. 5. VNIR reflectance spectra of CM chondrite chip spots showing no particular absorption features or possible serpentine bands as in Fig. 4.

Lastly, shown in Fig. 6 are VNIR spectra of CM chip spots showing olivine absorption bands near 0.85, 1.05, and 1.3 μm in wavelength. Based on these results, the large 1-mm size clasts on B-7904 chip in Fig. 3 are now identified as olivine-rich ones formed probably by thermal metamorphism. The A-881655 spectrum shows much weaker olivine bands than the B-7904 Spot B spectrum. The Y-793601 spectrum also shows a weak 0.7-μm band and an upward-pointing 0.55-μm feature, suggesting serpentine coexisting with olivine.

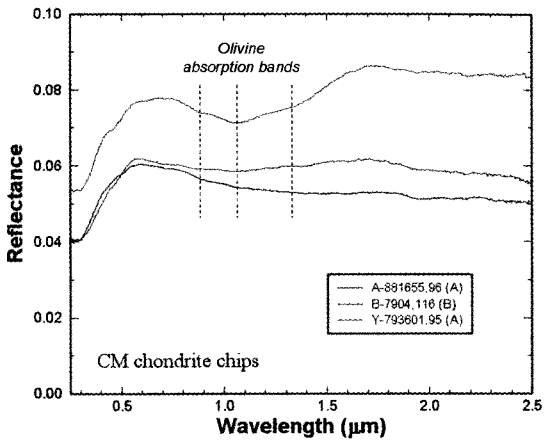

Fig. 6. VNIR reflectance spectra of CM chondrite chip spots showing olivine absorption bands.

Conclusions:

This study has proven that VNIR spectral measurements of CC chips is highly useful for identifying and characterizing meteorite types, major component minerals, and parent-body or terrestrial alterations. Therefore, this technique will be valuable in future spacecraft missions to small primitive asteroids such as Hayabusa 2 and OSIRIS-REx, especially during their close-up observation and touch-down phases and lander/rover operations. Because of its nondestructive nature, this survey can potentially be done for all the samples of our meteorite collections if proper arrangement is made in terms of security and contamination control. In addition, future analyses may include spectral deconvolutions employing the modified Gaussian model [5].

References: [1] Hiroi T. et al. (2011) *Polar Sci. 5*, 337-344. [2] Pieters C. M. and Hiroi T. (2004) *LPS XXXV*, Abstract #1720. [3] Hiroi T. et al. (1996) *Meteorit. Planet. Sci. 31*, 321-327. [4] Hiroi T. et al. (1993) *Science 261*, 1016-1018. [5] Sunshine J. M. et al. (1990) *JGR 95*, 6955-6966.

Acknowledgment: A part of this research was supported by JSPS Grant-in-Aid for Scientific Research (C).

^{26}Al-^{26}Mg Systematic and ^{26}Mg* Anomaly in Ureilites. G. Hublet[1] and V. Debaille[1], [1]Département des Sciences de la Terre et de l'Environnement, Université Libre de Bruxelles, CP 160/02, 50, Av. F.D. Roosevelt, 1050 Brussels, Belgium (ghublet@ulb.ac.be)

Introduction:

Short-lived radioactive isotopic systems such as ^{26}Al-^{26}Mg are powerful to study the chronology of the early solar system due to their high timeframe resolution during the lifetime of their parent elements. As such, they can be considered as the most efficient chronometers for the first few million years (Ma) of the solar system history. The now extinct radionuclide ^{26}Al, decayed to ^{26}Mg with a half-life of ~0.73 × 10^6 years [1]. This chronometer can thus date only the objects that formed during a period of ~5 Ma after the solar system formation.

Ureilites are the second largest group of differentiated meteorites (260 specimens) after the HED (Howardite-Eucrite-Diogenite) meteorite group. They are ultramafic achondrites mainly composed of olivine and low-Ca pyroxene (pigeonite). They are highly fractionated igneous rock but have also some minor primitive characteristic [2] suggesting a complex history for their formation. Ureilites have been defined as partial melting residues [3] or ultramafic igneous cumulates of a chondritic precursor [2]. Today, there is a consensus about the partial melting residues origin of ureilite. Chemical composition and texture argue that ureilites are mantle residues of ~15-30% partial melting of the Ureilite Parent Body (UPB) mantle after the extraction of basaltic magma [4, 5]

However, the UPB is still unknown. First, O isotope and high C-content (up to 5%) [6] suggest that this UPB could be carbonaceous chondrite but a recent study shows that some chemical and textural characteristics are particular and not found in the known C-rich chondrite types [7]. New investigations confirm that UPB is a single parent body for all ureilites that underwent heating and differentiation very early in the Solar System but disrupted by a major impact rapidly after its formation [8]. Fragments of this first asteroid re-accreted to form a daughter asteroid from which are issued ureilites. However, ureilites recorded the differentiation process of the primary UPB. Dating these rocks can thus give the formation age of ureilites before the disruption of the initial UPB. Some previous studies have dated ureilites with short-lived isotopic systems like ^{53}Mn-^{53}Cr and ^{182}Hf-^{182}W and suggested a differentiation of the UPB and formation of ureilites within 1 to 2 Ma after CAI formation [9, 10]. This implies these meteorites are old enough to be dated by the ^{26}Al-^{26}Mg isotopic system.

In this study, Al-Mg systematic has been investigated in five different monomict ureilites to date these type of achondrite: Yamato (Y-)790981, Y-791538, Y-981750, Y-981810, Asuka (A-)881931.

Analytical techniques:

All the preparation and chemical procedures were realized in clean laboratory at ULB. Around 200 mg of each sample were gently crushed in an agate mortar and sieved for obtaining a fraction between 64 to 150 µm. A fraction of ~50 mg was kept for bulk analyze. We proceeded to mineral separation on all samples. The metallic phase was separated with a hand magnet. The lighter metallic phase was obtained by density separation with heavy liquid (methylene iodide). Mg will be measured in this light fraction only. Magnetic separation using a Frantz magnetic separator was used on the silicate phase to obtain three different fractions: pure olivine (ol.) fraction; pure pyroxene (px.) fraction and a second pyroxene (px.2) fraction. All sample and mineral fractions were dissolved with an HNO_3/HF mixture (2:1) followed by a step in concentrated HNO_3 (+H_2O_2) to destroy the organic matter and a step in concentrated HCl. All samples and fractions were dissolved again in HNO_3 before the Mg separation procedure. An aliquot of each sample was taken without any purification for the ^{27}Al/^{24}Mg ratio measurements. For the whole rock data presented here, Mg was separated using cation-exchange resin (Bio Rad AG®50W-X12, 200–400 mesh). Elution and sample collect were performed with 1N HNO_3. The purification was repeated three times in order to insure a perfect separation of Mg and limited interferences with matrix.

Mg isotopes were measured on ULB MC-ICP-MS Nu-plasma. Samples were introduced in 0.05N HNO_3 using an Aridus desolvating nebulizer. Measurements were performed in medium resolution in order to avoid the possible isobaric interferences ($^{12}C^{14}N$) [1]. The instrumental mass bias was corrected by standard-bracketing with DSM-3 standard. Each measure cycle for standards and samples consisted of a cycle of three blocks of 20 integrations with a concentration of ~200 ppb, corresponding to ~7 volts on ^{24}Mg. Terrestrial standard BCR-2 was measured between each sample with a δ^{26}Mg* value of 0.006±0.011 to control the accuracy of the measurements.

Result and discussion:

The preliminary results obtained for δ^{26}Mg* on whole rock ureilites are showed in Fig. 1. Ureilites Y-791538 and Y-981750 and Y-981810 show a negative anomaly in δ^{26}Mg* that encompasses the terrestrial value and are respectively -0.031 (±0.030), -0.011 (±0.023) and -0.002 (±0.017). Y-790981 ureilite is fully comprised in the terrestrial domain with a value of 0.001 (±0.005) for δ^{26}Mg*. Finally, only A-881931 ureilite present an excess in δ^{26}Mg* (δ^{26}Mg* = 0.023 ±0.032) partially not resolvable

from the terrestrial average. Error bars are relatively large and need to be reduced with further measurements. However, these preliminary results suggest that some ureilites have a deficit in ^{26}Mg*.

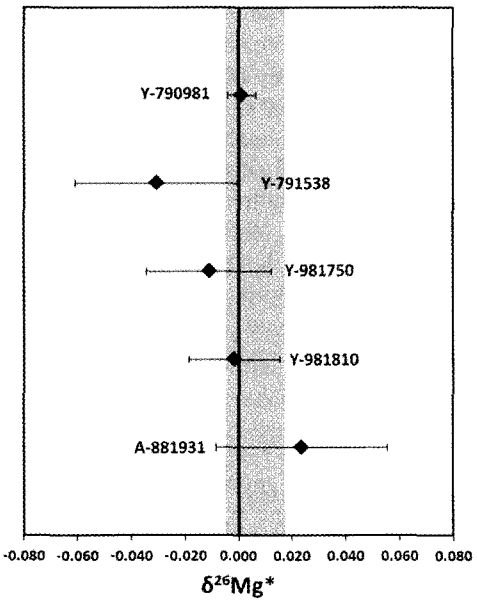

Figure 1: δ^{26}Mg* measurement in the different ureilites analyze. Grey zone corresponds to the terrestrial standard (BCR-2 range value). All sample comprised in this range do not have any δ^{26}Mg* anomaly. Errors shown in this diagram correspond to standard error ($s_e = s_d/\sqrt{n}$). The δ^{26}Mg* is reported relative to the DSM-3 standard.

All these five ureilites have also a sub-chondritic value for the ^{26}Al/^{24}Mg ratios (0.003 to 0.009). Baker et al. [11] observed a correlation between a deficit in δ^{26}Mg* in achondrite (pallasites, ureilites) with a low value of Al/Mg ratios. This observation can be explained by a silicate differentiation of the UPB very early in the solar system history with a lack of ^{26}Al in the ultramafic component of the parent body. This is also an evidence that this type of achondrite formed during the life of the ^{26}Al.

Conclusion:

Preliminary results on ureilites presented here indicate that four of the five ureilites analyzed have an anomaly in δ^{26}Mg*. Internal isochrons on these samples will be performed to date precisely these ureilites with ^{26}Al-^{26}Mg isotopic system. However, the resolvable ^{26}Mg* anomaly is associated with large errors. Further analyzes are required in order to validate our results.

References:

[1.] Jacobsen B., et al. (2008) *Earth Planet. Sc. Lett., 272,* 353-364. [2.] Goodrich C.A. (1992) *Meteorit. Planet. Sci., 27,* 327-352. [3.] Mittlefehldt D.W. (2004) *in Treatise of Geochemistry, vol. 1,* 291-324. [4.] Kita N.T., et al. (2004) *Geochim. Cosmochim. Acta, 68,* 4213-4235. [5.] Goodrich C.A., et al. (2007) *Geochim. Cosmochim. Acta, 71,* 2876-2895. [6.] Krot A.N., et al. (2004) *in Treatise of Geochemistry, vol. 1,* 83-128. [7.] Warren P.H. (2010) *Geochim. Cosmochim. Acta, 75,* 6912-6926. [8.] Herrin J.S., et al. (2010) *Meteorit. Planet. Sci., 45,* 1789-1803. [9.] Lee D.-C., et al. (2009) *Earth Planet. Sci. Lett., 288,* 611-618. [10] Yamakawa A., et al. (2010) *Astrophys. J., 720,* 150-154. [11.] Baker J.A., et al. (2012) *Geochim. Cosmochim. Acta, 77,* 415-431.

Mars: A Perspective from NWA 7533. M. Humayun[1], A. Nemchin[2], M. Grange[2], A. Kennedy[2], B. Zanda[3], R. H. Hewins[3,4], J.-P. Lorand[5], C. Göpel[6], E. Lewin[7]. S. Pont[3] & D. Deldicque[8]. [1]Florida State Univ., Tallahassee, USA; humayun@magnet.fsu.edu. [2]Curtin Univ., Perth, AUS. [3]MNHN & CNRS, Paris, FR. [4]Rutgers Univ., Piscataway, USA. [5]LPGN, Univ. Nantes, FR. [6]IPGP, Paris, FR. [7]ISTerre, Univ. J. Fourier, Grenoble, FR. [8]ENS, Paris, FR.

Introduction:

Meteorites from Mars provide us with the only detailed chronological and chemical constraints on the geological evolution of Mars. Most of the known Martian meteorites are igneous rocks, comprising shergottites ranging in age from 160-600 Ma, or nakhlites/chassignites of about 1.4 Ga. The known exceptions are ALH 84001, a monomict orthopyroxenite breccia of 3.8 Ga age [1], and the newly reported NWA 7034 polymict breccia [2]. This amazing meteorite is represented by a set of five paired stones that are named NWA 7034, NWA 7475 and NWA 7533. An enduring enigma in the Mars-meteorite connection is the lack of samples from the ancient cratered terrain when there are over 60 Martian meteorites that appear to come from younger volcanic terrains. Even ALH 84001, the oldest known Martian meteorite, has among the lowest siderophile element contents of Martian meteorites, i.e., ALH 84001 is a "pristine" rock. Pristine rocks from the Moon are comparatively hard to find in both Apollo collections and among lunar meteorites compared with lunar highlands breccias that contain abundant meteoritic debris [3-4].

NWA 7533 has now been recognized to be a polymict breccia containing mafic and feldspathic clasts in a matrix of alkali basaltic bulk composition [5]. Prior Rb-Sr dating yielded an age of 2.1 Ga [2], and preliminary K-Ar dating yielded an age of ~1.56 Ga [6], inconsistent with an origin from the ancient cratered highlands. In this report, we summarize recent findings on the study of NWA 7533, particularly new compositional and U-Pb zircon dating, and discuss their implications for early Mars.

Analytical Methods:

An uncoated section, NWA 7533 section-3, was analyzed by laser ablation ICP-MS using an ElectroScientific Instruments™ New Wave UP193FX ArF excimer (193 nm) laser ablation system coupled to a Thermo Electron™ Element XR [7-8]. Altogether, 76 peaks for major and trace elements and their interferences were monitored. Spot sizes of 50-150 μm were used, and the laser repetition rate was 50 Hz, with a fluence of >2 GW/cm^2. Raster rates were 10 μm/s. Laser dwell times on a spot were 20 s, resulting in a pit depth of ~100 μm determined by focussing of the optical microscope on the top and bottom of the pit. Relative sensitivity factors obtained from separate standards for many well-characterized lithophile elements agreed to 2-5%, but the accuracy is worse for elements for which only one standard was available, e.g., for NIST SRM 610 (~10-20%).

U-Pb isotope analyses on polished and Au-coated NWA 7533 section-4 were performed on a Shrimp II high-resolution ion microprobe at Curtin University (Perth, Western Australia) under analytical conditions described previously [9]. The beam spot was reduced to 7 μm to effectively analyze the small zircons observed with a primary O^{2-} beam current of 0.5 nA.

Results:

Analyses of 5 zircon grains large enough to obtain one or more spots with no beam overlap yielded a discordia line with an upper intercept of 4,428±25 Ma and a lower intercept of 1,712±85 Ma. Three zircons plotted concordantly on the upper intercept, supporting a very ancient origin of the zircon-bearing, leucocratic lithologies.

Chemical compositions of matrix and clasts from NWA 7533 is presented in figures 1-3, and discussed further below.

Discussion:

The excess Ni in Martian rocks and soils has been interpreted in terms of a meteoritic component [10], or as an indigenous protolith formed by partial melting of an oxidized early Martian mantle [11]. In this study, ubiquitous meteoritic contaminant is observed in the interclast crystalline matrix (ICM), in clast-laden impact melt rocks (CLIMR) analyses, and in many of the coarse lithic clasts from NWA 7533 (Fig. 1), indicating that many of the coarse clasts originated from impact melts. The refractory siderophile elements, Os, Ir, Ru, Rh and Pt, require a chondritic source for the excess siderophiles. The excess Ni is equivalent to ~4-5% CI chondrite in the NWA 7533 breccia. However, the meteoritic material is not represented by a single metallic component, but the Ni and Ge have been oxidized and merged with the silicate components. Our interpretation of excess Ni in NWA 7533 also extends to the Martian rocks and soils observed at Gusev crater (Fig. 1). The presence of ancient zircons indicates that the siderophiles in NWA 7533 originate from the southern highlands. Dust storms are likely to distribute meteoritic material from the southern highlands to all Martian basins. We found no evidence to support an early oxidized mantle on Mars.

The NWA 7533 ICM and CLIMR are

compositionally similar to soils from Gusev Crater in all major element ratios (Fig. 2) and Ni abundances, although more Mg-rich. In Fig. 2, the cpx-rich nakhlites plot above the SNC trend while the soils plot below the SNC trend in a complementary fashion. This implies a relative depletion of Ca in Martian soils, a feature shared by NWA 7533. The ICM/CLIMR in NWA 7533 is also depleted in Sc, while nakhlites are enriched in Sc, indicating that the soils reflect a cpx depletion of magmatic origin in their protolith (Martian crust) rather than loss of Ca during aqueous alteration of the source region [12]. However, there are key differences between modern Martian soils, all of which are enriched in S, Cl and Zn relative to the rocks, and NWA 7533 components which strikingly lack these enrichments (Fig. 3). We infer that the ancient Martian hydrosphere removed these volatiles from the ancient soils lithified in NWA 7533, supporting recent geological evidence for former oceans on Mars [13].

The NWA 7533 matrix REE pattern is consistent with a low degree partial melt of a fertile garnet peridotite source. It agrees well with an end-member of ~20% crustal contamination of shergottite magma [14], with the exception that the NWA 7533 REE pattern is steeper in the HREE. The Martian mantle is inferred to have refractory incompatible elements (Ba, Th, U, Nb) at ~2 x CI [12, 14]. These elements are enriched 45-48 x CI implying ~4-5% partial melting of a fertile source for Martian crustal origin. If the whole mantle of Mars is melted to an average melt fraction of 4-5% it implies an average crustal thickness of 45-60 km, consistent with geophysical estimates of Martian crustal thickness [15].

In summary, NWA 7533 is a polymict breccia containing 4.4 Ga zircons, abundant chondritic impactor debris, and lithified Martian soil modified by interactions with an early hydrosphere.

References: [1] Lapen T. J. et al. (2010) *Science 328*, 347-351. [2] Agee C.B. et al. (2013) *Science Express*, doi 10.1126/science. 1228858. [3] Warren, P. H. et al. (2005) *Meteoritics Planet. Sci. 40*, 989-1014. [4] Korotev R. L. et al. (2009) *Meteoritics Planet. Sci. 44*, 1287-1322. [5] Hewins R. H. et al. (2013) *Meteoritics Planet. Sci. 48* (abstract). [6] Cartwright J. A. et al. (2013) *Lunar Planet. Sci. 44*, abstract#2314. [7] Humayun M. et al. (2010) *JAAS 25*, 998-1005. [8] Gaboardi M. and Humayun M. (2009) *JAAS 24*, 1188-1197. [9] Nemchin A. et al. (2009) *Nature Geoscience 2*, 133-138. [10] Yen A. S. et al. (2006) *JGR 111*, E12S11, doi:10.1029/2006JE002797. [11] Tuff J. et al. (2013) *Nature 498*, 342-345. [12] Newsom H. E. et al. (2007) *JGR, 112*, E03S12, doi:10.1029/2006JE 002680. [13] DiAchille G. and Hynek B. M. (2010) *Nature Geoscience 3*, 459-463. [14] Norman M. D. (1999) *MAPS, 34*, 439-449. [15] Zuber M. T. et al. (2000) *Science, 287*, 1788-1793. [16] Gellert R. et al. (2006) *JGR 111*, E02S05, doi:10.1029/2005JE00255. [17] McSween H. Y., Jr., et al. (2009) *Science, 324*, 736-739.

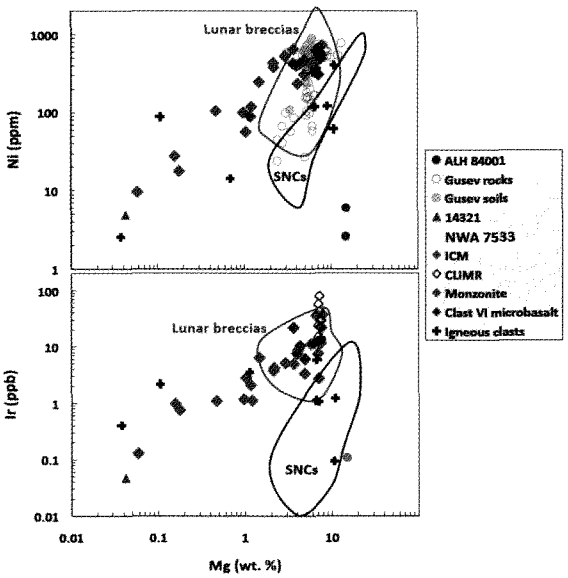

Fig. 1: Siderophile element abundances in components from NWA 7533 compared with SNC meteorites and Gusev rocks and soils [3-4, 16-17].

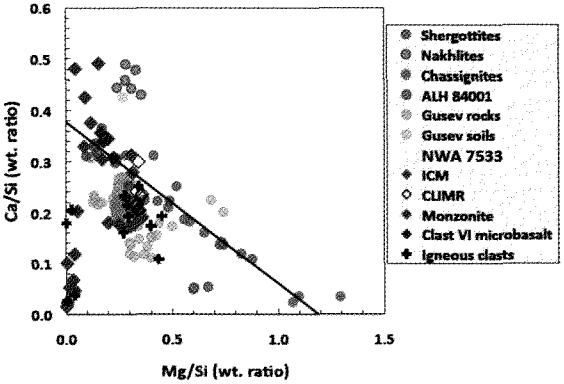

Fig. 2: Major element composition of components from NWA 7533 compared with SNC meteorites and Gusev rocks and soils (modified from [17]).

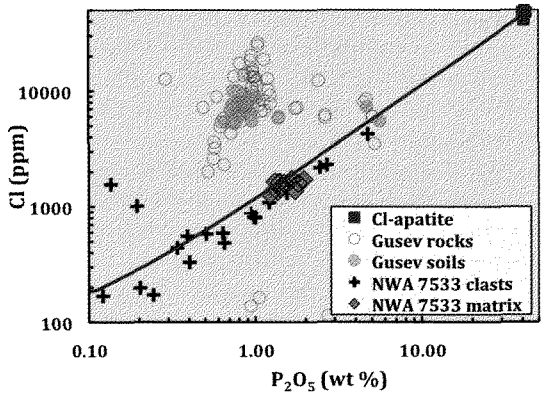

Fig. 3: ICM, CLIMR (matrix) and lithic clasts from NWA 7533 contain Cl only as chlor-apatite (green squares, EMP analyses); Gusev analyses from [16].

An experimental study of chondrule formation under the nebular pressures controlling gas conditions.

N. Imae[1] and H. Isobe[2], [1]National Institute of Polar Research, Tachikawa, Tokyo 190-8518, Japan [2]Kumamoto University, Chuo-ku, Kumamoto 860-8555, Japan. e-mail: imae@nipr.ac.jp.

Introduction: Chondrules have formed at the beginning of the solar system, most probably in the primordial solar nebula. The standard pressure of the primordial solar nebula has been assumed to be 1-100 Pa based on the theoretically estimated gas density. Experiments on chondrule formation have been carried out mainly under the atmospheric pressure (10^5 Pa), controlling oxygen fugacity. Experiments on chondrule formation in the pressure of the primordial solar nebula have been insufficiently carried out. We set up a new furnace controlling the nebula pressure range, and started to reproduce the chondrules. The focus is on the interaction of chondrule melt with the surrounding gas, and the condition is probable in the primordial solar nebula when the precursor materials are heated.

Experiments: The total pressure in the newly installed vacuum furnace was controlled to be ~100 Pa by a batterfly valve (Fuji Technology), indicated from the diaphragm-seal type pressure gauge (MKS Baratron Type 626). Under the condition, the hydrogen gas is introduced by the electric decomposition of water (~50 cc/min), and the total pressure nearly equals to hydrogen molecule pressure. The small chip of the Allende CV3 chondrite was used per one run with the weight of ~30-50 mg (~3 mm in size), being avoid of large CAIs. The size may nearly represent bulk composition, considering the size of chondrules. Two type experiments were carried out: one is that the charge is held in the capsule (cruicible 1 in Fig. 1), and another is that it is held and silica powder is on the bottom of the cruicible (cruicible 2 in Fig. 1).

The charge was holded mainly using the platinum (Pt) wire with the diameter of 0.2 mm for #Al runs and using the molybdenum (Mo) wire with the diameter of 0.2 mm for #Al-T runs. The absorption of iron content in the charge into Pt was much larger than that of Mo. When the capsule is heated in the furnace, the interior of the capsule is dominant of H_2 gas (Figs. 2 and 3). The expected partial pressures were calculated using the JANAF thermochemical tables.

The activity coefficients of the melt were assumed to be unity as the maximum estimation. Even if taking account into consideration of the maximum estimation of partial pressures from melt, the oxygen fugacity of the interior of the capsule is estimated to be in the range of IW-2 and IW-4.

When the silica powder is put (cruicible 2), the SiO pressure from silica is larger than that from the melt (Fig. 3). The oversaturated SiO_2 component in the gas may cause condensation of SiO_2 component into the melt during the heating.

The maximum temperatures and the cooling rates were controlled in the range of 1525-1225 °C (25 °C step) for #Al runs 13 times with the cooling rate is ~10^4/h, at the temperatures of 1450 °C and 1250 °C for #Al-S runs with the cooling rate of ~100 °C/h, and at the temperatures of 1450 °C, 1350 °C, 1300 °C, and 1250 °C for #Al-T runs with the cooling rate of ~100 °C/h.

Results: The common main mineral species from #Al runs were olivines (Figs. 4 and 5). Pyroxenes joined from #Al-S runs (Figs. 4 and 7). While, large euhedral enstatites ~several hundreds μm in size) crystallized from #Al-T1 and -T3 runs of #Al-T runs. They poikilitically enclose rounded olivines (Fig. 4). The enstatites of #Al-T5 were dominant only on the periphery (Fig. 4), and the Fe content of the enstatite is slightly higher than those of #Al-T1 and -T3. The interior of #Al-T5 was dominant of olivines. At the lower temperatures, slightly ferroan pyroxenes crystallized only near surface of the charge (Fig. 8).

Discussion: The bulk composition of the charge is saturated with olivine. Thus the crystallization of a large amount of low-Ca pyroxenes (mainly enstatites) from #Al-T runs suggests that the bulk composition changed to enstatite liquidus field from the olivine liquidus field to Si-rich composition. It has been difficult to make enstatite having the solar ratio (~1) phase of the Mg/Si ratio in the early solar nebula so far [1]. The rapid formation of enstatite in the present experiments is a new path to form enstatite in the early solar nebula. The study is also consistent with the earlier study by [2].

This study is supported by Grant-in-Aid for Scientific Research of JSPS (No. 23340165).

References: [1] Imae N. et al. (1993) EPSL, 118, 21-30. [2] Tissandier L. et al. (2002) *Meteorit. Planet. Sci., 37,* 1377-1389.

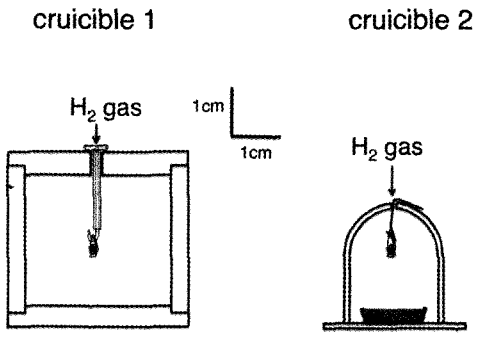

Fig. 1. Alumina cruicibles for the present experiments. The orifice diameter of the cruicible 1 and 2 is 3 mm and 1 mm, respectively.

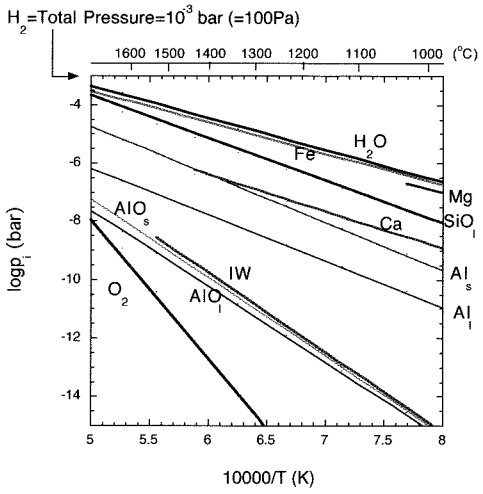

Fig. 2. Partial pressures of gas species in cruicible 1.

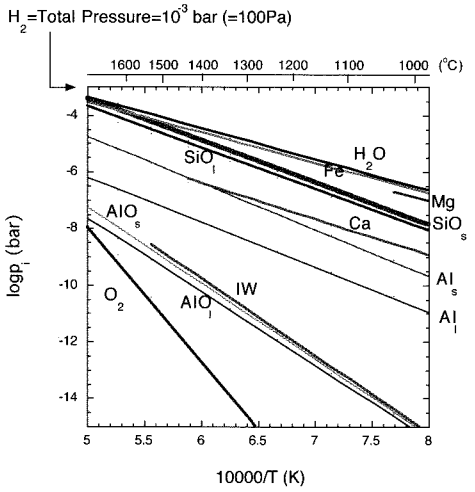

Fig. 3. Partial pressures of gas species in cruicible 2.

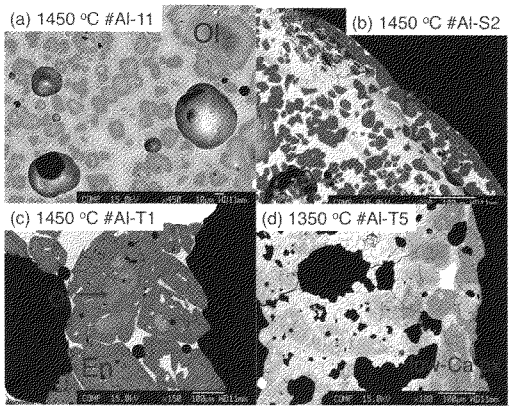

Fig. 4. Run products. Ol: olivine. Fo: forsterite. En: enstatite. low-Ca px: low Ca pyroxene.

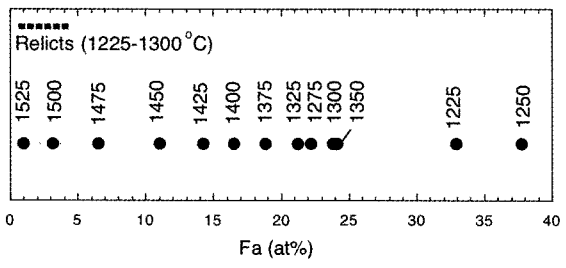

Fig. 5. Averaged olivine compositions from rapidly cooled runs (#Al-runs) using cruicible 1.

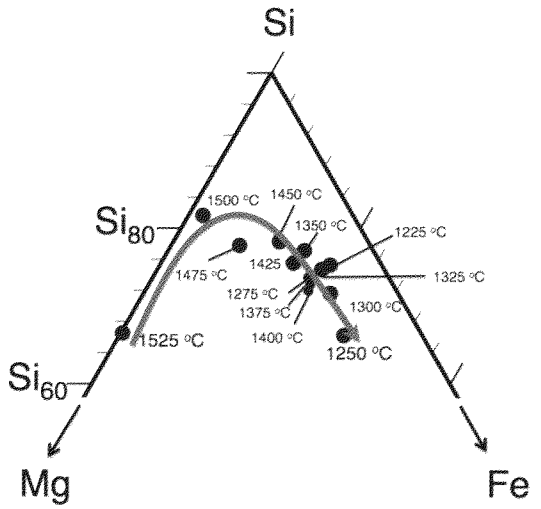

Fig. 6. Glass compositions from rapidly cooled runs (#Al-runs) using cruicible 1. Plot of atomic ratio.

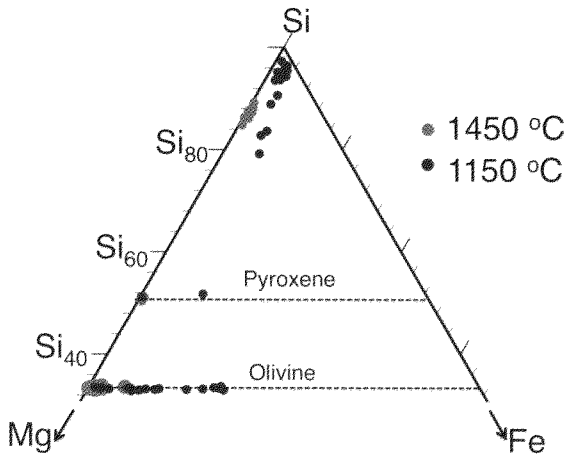

Fig. 7. Phase compositions from runs cooled at ~100 °C/h (#Al-S runs) using cruicible 1. Plot of atomic ratio.

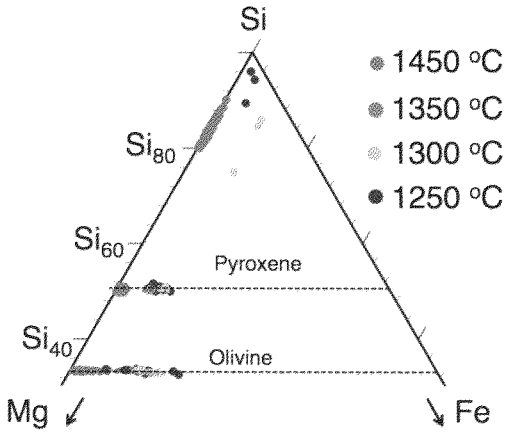

Fig. 8. Phase compositions from runs cooled at ~100 °C/h (#Al-T runs) on the gas condition of SiO_2 oversaturated using cruicible 2. Plot of atomic ratio.

Mineralogical examination of carbonaceous matter in carbonaceous chondrites by TEM and Raman spectroscopy

Chikako IWASE[1] and Junji AKAI[2], [1] Grad.School of Sci. Tech., Niigata University, [2]Faculty of Science, Niigata University

Introduction: Carbonaceous matter in chondritic meteorites has information of a complex history of the protoplanetary disk and/or meteorite parent bodies.

In this study, we have analyzed the carbonaceous matter extracted from 10 Antarctic carbonaceous chondrites (CM2, CM2 or Cl, CO3 types) and 6 Non-Anterctic carbonaceous chondrites (CM2, CV3, CO3 types) using Raman spectroscopy and transmission electron microscopy (TEM) to measure the degree of alternation.

Sample and methods: The samples used in this study are as follows.

Antarctic carbonaceous chondrites:

Yamato(Y)-86720 (CM2), Y-86789 (CM2), Y-80120 (CM2), Y-793321 (CM2), Y-74662 (CM2), Y-82054 (CM2), Asuka(A)-881655 (CM2), Y-790992 (CM2), Belgica(B)-7904 (CM2 or "CI"), Y-86751 (CV3), Y-790992 (CO3), A-882094 (CO3),

Non-Antarctic carbonaceous chondrites:

Acfer331(CM2), Murray(CM2), NWA 852, NWA 2086(CR2), Shişr 033(CR).

The meteorite samples were dissolved in HF/HCl. Then, the samples for Raman analysis are placed on a slide glass with ethanol. Samples for TEM observation were prepared on microgrids.

TEM observations were carried out using JEM-2010(JEOL) system that was operated at 200 kV with EDS attachment.

Raman spectroscopy detects the structural order of carbonaceous material, which is best parameterized by the relative intensities of the so-called D ("disordered") and G ("graphite") bands. The intensity ratio I_G/I_D increase in the case of graphite with the size of the domain. Mono-crystalline graphite shows only G band at ~1581 cm^{-1}. The second band, the D band at ~1355 cm^{-1} is caused by defect, polycrystallinity and small domain sizes, crystal boundary effects, and size reflects increasing disorder. The peak width of D band (Γ_D) generally decrease with increasing metamorphism.

Result: Raman analyses average of the signals from all constituents of the meteoritic carbonaceous material residues, which include highly interlinked macromotecular material, potentially amorphized C and small mineral grains embedded in the extracted carbonaceous matter, including presolar grains of SiC, graphite, and nano diamonds as well as oxides (e.g., chromite) of solar system origin.

The result of Raman analysis, the most primitive samples (CM, CI) show the largest values for Γ_D and D band position. CV and CO type chondrites shows smaller values than CM or CI. From this, crystallinity of carbonaceous matter differ with the meteorite types.

Using the ratio of Γ_D vs. D band position, the relative degree of crystallization of the carbonaceous matter in the meteorites becomes apparent. The peak metamorphic degrees and peak temperatures were calculated using the half bandwidth of D band [1]. Using these data, the peak metamorphic temperature of carbonaceous matter in the chondritic meteorites was estimated. The meteorite samples of B-7904, Y-793321, Y-86720 which have experienced strong thermal metamorphism [2] showed relatively low temperature for formation of carbonaceous matter: That is, 223°C (B-7904), 227°C (Y-793221), and 240°C (Y-86720). This contradicts peak temperature of thermal metamorphism calculated from phyllosilicates: Y-793321 (200-259°C), Y-86720 (700-750°C), and B-7904 (<750°C) [2]. It is suggested that carbonaceous matter in meteorites has experienced different thermal history from phyllosilicates.

In the TEM observation, we could find organic globules in the samples whose carbonaceous matter indicates low crystallinity. Organic globules show the hollow morphology. Measuring the thickness of outer envelope and radius of the organic globules observed in each sample, the ratios of the thickness of outer envelope vs. radius were similar for all organic globules even in different type carbonaceous chondrites. From this, it is not likely that there is a relationship between the type of meteorite and the size and thickness of outer envelope of organic globules.

On the other hand, in the carbonaceous matter of Allende (589°C) and A-882094 (458°C), which has well crystallized carbonaceous matter, we couldn't find organic globules. There may be a relationship between the presence of organic globules and degree of the organic material crystallization.

In addition, we conduct a carbon isotope measurement of carbonaceous material. discuss the relationship between degree of crystallinity of chondritic carbonaceous matter and abundance of organic globules.

References:

[1]Huss. G. R. et al.,2006. The University of Arizona Press. Pp. 567-586.

[2]Akai, J. 1988 *Geochemica Cosmochimica et Acta*, 52, 1593-1599.

Amino acids in cosmic dusts and carbonaceous chondrites. K. Kobayashi[1,2], H. Mita[3], T. Kogawa[1], T. Kaneko[1], Y. Obayashi[1], Y. Kawaguchi[4], K. Okudaira[5], M. Tabata[6,7], H. Yabuta[8], E. Imai[9], S. Hasegawa[7], H. Kawai[6], H. Yano[7], H. Hashimoto[7], S. Yokobori[4] and A. Yamagishi[4], [1]Yokohama National University, [2]National Institutes of Natural Sciences, [3]Fukuoka Institute of Technology, [4]Tokyo University of Pharmacy and Life Science, [5]Aizu University, [6]Chiba University, [7]JAXA/ISAS, [8]Osaka University, [9]Nagaoka University of Technology

Introduction:

Amino acids have been detected in such extraterrestrial bodies as carbonaceous chondrites and comets, and their relevance to the origin of life on the Earth is discussed. We are planning a space experiment named the Tanpopo Mission, where several experiments including capture of space dusts and exposure of organic compounds and microorganisms. As to the capture experiments, several aerogel blocks will be attached on several faces of an integrated experimental rack that will be placed on JEM/EF of ISS. High-speed dusts will make tracks in the aerogel. After recovering them to the Earth, we will separate each track with a terminal grain, and will apply to chemical analysis, including microscopic techniques (FT-IR, STXM-XANES, etc.) and amino acid enantiomers analysis after acid hydrolysis [1].

Two-stage light gas gun experiments:

Amino acid is one of the main target molecules to be found in the capture experiments. We have tested whether hypervelocity dusts can be trapped in aerogel by using a two-stage light gas gun equipped in JAXA/ISAS. Samples such as amino acids adsorbed to porous silica gel and powder of Murchison meteorite were shot out at 4- 6 km s^{-1}, and were captured in an aerogel to see whether organics could be recovered in the terminal grains or tracks. The aerogel block containing tracks of high-velocity particles was digested with HF-HNO_3 in a Teflon container [2]. The digested solution was then acid-hydrolyzed with 6 M HCl, was desalted with a cation-exchange resin (Bio-Rad AG-50WX8) or a solid-state extraction column (MonoSpin SAX), and amino acids were determined by cation-exchange HPLC after post-column derivatization for fluorometric detection.

It is of quite importance to reduce amino acids in a procedural blank. Blank amino acid level with MonoSpin SAX was much less than that with AG-50WX8. However, it should be further reduced to determine amino acids in cosmic dusts. Thus, we are planning to delete the desalting processes by applying reversed-phase HPLC.

Comparison of amino acids in cosmic dusts and carbonaceous chondrites:

It is believed that cosmic dusts (interplanetary dust particles) are originated from asteroids (meteorites) or comets. It is of great interest to compare organic compounds in cosmic dusts and those in carbonaceous chondrites. We are planning to analyze amino acids in some carbonaceous chondrites collected in Antarctica.

References:

[1] Kobayashi K. et al. (2012) *Trans. Jpn. Soc. Aero Space Sci.*, 10 (ists28), Tp_7-11. [2] Takano Y. et al. (2004) *Geochem. J., 38,* 153-161.

Revisiting the Presolar Grain Inventory of the Y-691 Enstatite Chondrite. J. Kodolanyi[1], A. de Ridder[1,2], M. Raes[1], Ph. Claeys[1], L. Polerecky[3] [1]Vrije Universiteit Brussel, [2]Katholieke Universiteit Leuven, [3]Universiteit Utrecht

Introduction:

Differences in the major element and isotope composition of carbonaceous, as well as unequilibrated ordinary and enstatite chondrites (EC) are thought to be the result of the fact that these meteorite classes sampled different regions of the solar nebula. The differences in the sampled nebular regions are also reflected in the presolar component of these meteorites, with carbonaceous chondrites showing the highest presolar grain contents among different meteorite classes (up to ~250 ppm by volume when normalised to the meteorite matrix; e.g., [1]). However, data about the presolar grain content and presolar grain composition of ordinary chondrites and ECs are limited and often rely on investigations on the bulk rock scale. ECs are believed to have sampled the least amount primitive material yet some of them have a higher presolar grain content (up to 150 ppm; [2]) and a wider range of presolar grain abundances than even unequilibrated ordinary chondrites [2-4]. How much this variability is the result of nebular heterogeneity (induced by e.g., nebular processing) or of parent body processes (e.g., metamorphism or hydrothermal alteration) is currently unknown and needs further investigation.

In the framework of a recently initiated project, we would like to revisit the presolar grain abundance and composition of the Yamato 691 (Y-691) type 3 EC. Previous work has shown that Y-691 contains presolar grains but not all presolar grain types have been searched for in the sample. Besides, the presolar grain assemblage of the meteorite was investigated using an instrument (the IMS 1270 ion probe equipped with stacked CMOS-type active pixel sensor; [4-5]) with lower sensitivity than that of the nanoSIMS, the routine tool for the detection of presolar grains. This may have caused an underestimation of the abundance of presolar grains in this meteorite (as was the case for Acfer 094, [6]). A complete and statistically more robust dataset of presolar grain types and their respective abundances in Y-691 based on nanoSIMS measurements, will be invaluable for the presolar grain record of ECs, since there are only three other ECs whose presolar grain inventory has been investigated using the nanoSIMS.

Sample description:

Y-691 is among the best studied ECs [e.g., 7,8]. We obtained a thin section of Y-691 from the NIPR to find presolar grains with the nanoSIMS 50L of the Utrecht University. Prior to nanoSIMS measurements we used secondary and back-scattered electron (SE and BE, respectively) images and X-ray maps, obtained with the JEOL JSM 7000F field emission electron microscope of the Vrije Universiteit Brussel, to locate those areas of the sample which are the most suitable for later analyses with the nanoSIMS. Y-691 consists of (1) 50-1000 μm diameter chondrules of irregular, ellipsoidal or spherical shape, (2) rounded multiphase metal-sulphide assemblages from tens to hundreds of μm in diameter, and (3) matrix of mono- or multiphase silicate, metal and sulphide minerals/mineral assemblages of irregular shape and variable diameter from <1 μm up to several tens of μm (Fig. 1). We refer to the <2 μm fraction of the latter material as "ultra-fine-grained" matrix hereafter. Such matrix regions are the primary targets of nanoSIMS investigation as most presolar grains are characterized by 0.1-1 μm grain size [9].

The ultra-fine-grained matrix of Y-691 constitutes a few ‰ of the meteorite by volume. Despite its low overall abundance, it is found throughout the sample. However, most frequently it occurs along the rims of chondrules. Its mineralogy appears to be similar to the mineralogy of the coarser grained matrix components [7,8] although we have not found niningerite or oldhamite in it. Based on X-ray mapping and semi-quantitative point analyses using energy dispersive X-ray spectroscopy (EDX) the ultra-fine-grained matrix consist largely of Mg- and Ca-Mg-silicates, a silica polymorph, Fe-Ni metal, perryite, schreibersite and troilite (Figs. 1-2). Ultra-fine matrix grains are variable in size (mostly 40-1500 nm) and shape (aspect ratio between 1:1 and 1:5) but most grains are roughly isometric (Figs. 1-2). Similar to other components of the meteorite, the ultra-fine-grained matrix of Y-691 experienced little aqueous alteration (Fig. 1).

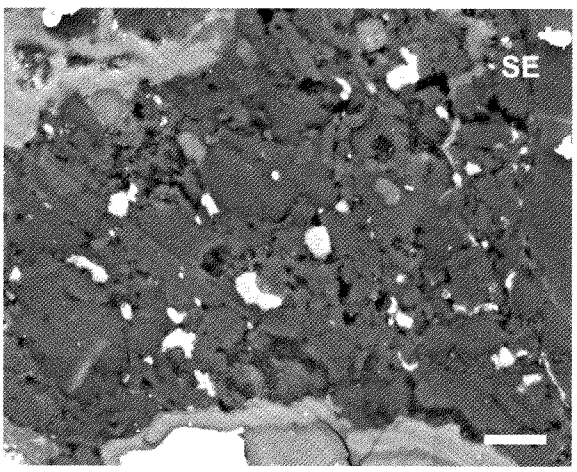

Fig. 1. Detail of the ultra-fine-grained matrix of the Y-691 (SE image). Scale bar: 1 μm. Silicates appear dark gray, phosphides and sulphides appear white. Medium gray regions are metal rich alteration products. See Fig. 2a for a more detailed mineralogy.

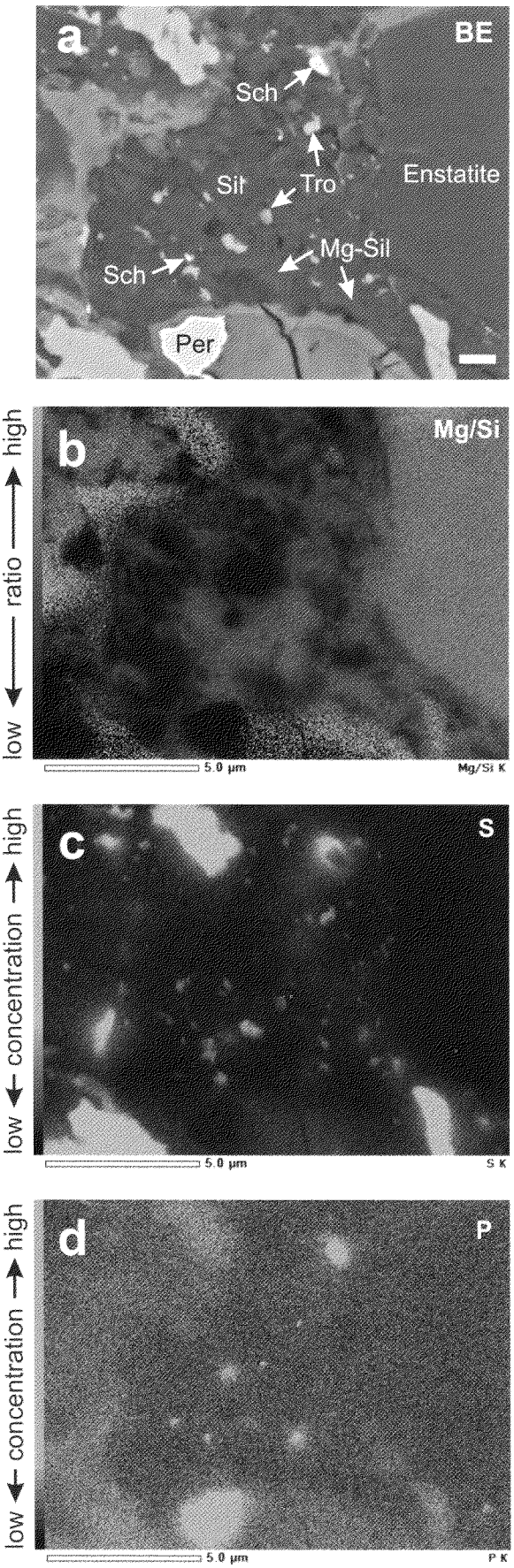

Fig. 2. BE image (a) and Mg/Si (b), S (c) and P (d) X-ray maps of part of the ultra-fine-grained matrix of Y-691. The mapped area roughly corresponds to that depicted in Fig. 1 but it is slightly larger. The scale bar in (a) corresponds to 1 µm. Tentative mineral identification (a) is based on X-ray mapping and EDX point analyses. Mineral abbreviations: Mg-Sil = Mg-silicate phase(s), Sil = silica polymorph, Sch = schreibersite, Per = perryite, Tro = troilite.

Discussion and Outlook:

Ebata et al. [3] estimated a matrix-normalised presolar carbonaceous grain abundance of 14 ppm and a presolar silicate grain abundance of 4 ppm for Y-691, based on IMS 1270 ion microprobe imaging (see above). The authors did not distinguish between carbonaceous grain types although in a later study [10] mentioned SiC and graphite among the carbonaceous grains without specifying their respective abundances. The above presolar grain abundances are in stark contrast with the nanoSIMS results of [2] who found ~100 ppm presolar silicate and ~50 ppm presolar carbonaceous grains in SAH 97159, an EH3 chondrite with almost identical mineralogy and alteration to that of Y-691. Thus, if the presolar grain abundance estimated by [3] (based on the low-sensitivity measurements) is confirmed by our nanoSIMS measurements, the lower presolar grain abundance in Y-691 relative to SAH 97159 can be interpreted as the result of the heterogeneous distribution of a presolar component in the EC source regions of the solar nebula. As mentioned above however (see Introduction), it is also possible that the observed difference in the presolar grain abundance is owing to the lower sensitivity of the analytical instrument [3] applied. Based on the isotope images of [3], these authors scanned large areas of the meteorite matrix, including large matrix areas with >1 µm grain size, to detect presolar grains. In order to improve the efficiency of presolar grain detection, we focus our efforts on the ultra-fine-grained matrix of Y-691, to detect presolar grains and use the more sensitive nanoSIMS to investigate the sample.

References:

[1] Bose M. et al. (2012) *GCA, 93,* 77–101. [2] Zhao X. et al. (2010) *Meteorit. Planet. Sci., 45,* A224. [3] Ebata S. et al. (2006) *LPS XXXVII,* 1619. [4] Ebata S. et al. (2007) *Meteorit. Planet. Sci., 42,* A38. [5] Yurimoto H. et al. (2003) *Appl. Surf. Sci., 203-204,* 793-797. [6] Nguyen et al. (2007) *ApJ, 656,* 1223-1240. [7] Kimura M. (1988) *Proc. NIPR Symp. Antarct. Meteorit., 1,* 51-64. [8] Rubin A. E. (2009) *Meteorit. Planet. Sci., 44,* 589–601. [9] Hoppe P. (2011) Proc. Sci., *NIC XI, 021.* [10] Ebata S. and Yurimoto H. (2009) *Meteorit. Planet. Sci., 44,* A65.

U-Pb dating of zircon in Mesosiderite Asuka-882023 M. Koike[1, 2], N. Sugiura[2], Y. Sano[1], N. Takahata[1], and A. Ishida[1]
[1]Atmosphere and Ocean Research Institute, University of Tokyo, [2]Department of Earth and Planetary Science, University of Tokyo.

Introduction:

Mesosiderites consist of Fe-Ni metals and HED-like silicates. Their origin is rather uncertain, while mixing between core and crust of the large parent body is suggested [1]. From molten metal and unequilibrated silicates features, their complicated reheating history is estimated [2]. After formation of silicates at 4.56 Ga, they experienced metal-silicates mixing at ≥ 4.47 Ga with rapid cooling (1-100 degree/day) near the surface of the parent body. They subsequently cooled very slowly (~0.1 degree/day around 400 C) before 3.9 Ga.

Timing of the thermal event is important for estimation of the heat source. At ancient stage of the solar system, the heat source candidates are (1) solar nebular activity and (2) short-lived radionuclides, as well as (3) accretion and impact heat. Since mesosiderites reheated at the very early age on the parent body surface, they may have recorded the early solar system evolution [3].

Meanwhile, U-Pb age information is important and can be obtained from zircon in meteorites. Previous Pb-Pb dating of Vaca Muerta zircon is reported as 4563 +/- 15 Ma, which may be the crystallization age [4]. Recently, Haba et al. [5] showed younger Pb-Pb age of 4520 +/- 27 Ma for a highly metamorphosed mesosiderite, Estherville. Here we show the U-Pb dating of zircon found in the Asuka 882023 mesosiderite.

Sample & Methods:

From A 882023 thin section, a large zircon grain (80 x 30 μm, Fig. 1) was found by SEM observation and analyzed for U-Pb age using NanoSIMS (@AORI, Univ. of Tokyo). For SIMS analysis, a ~3 nA O^- ion beam with spot size of ~10 μm is applied of 10 spots. Analyses of ^{238}U-^{206}Pb and ^{207}Pb-^{206}Pb were performed separately on the same spot. Sample $^{238}U/^{206}Pb$ ratios are calibrated using AS3 standard zircon.

Results & Discussion:

Obtained ^{238}U-^{206}Pb age and ^{207}Pb-^{206}Pb age are 4375 +/- 300 Ma (MSWD= 0.75) and 4530 +/- 81 Ma (MSWD=0.11) respectively. Since two ages are consistent within errors, the U-Pb system may be concordant. Total U-Pb age without common Pb correction shows 4527 +38/-39 Ma (MSWD= 0.46, Fig. 2). Relatively large errors are due to low U contents.

Haba et al. [5] pointed out there are two different origins of the zircons; older crystallization in silicates and secondary products of the metal-silicate mixing. Because of the large uncertainties, our age results are indistinguishable from both old Vaca Muerta [4] and younger Estherville [5]. However, the analyzed zircon is likely metamorphic origin considering the large grain size, lower U contents and somewhat younger age.

Mineral and chemical features questioned impact-origin of A 882023 [6]. If the re-heating age is 4.527 Ga, ^{26}Al does not provide enough heat. Another problem of radionuclide heat source is that they heat the parent body from inside. Surface temperature should be lower than the interior temperature. A possible way to heat surface material efficiently is external heating, due to nebular activity or impact heating. Lifetime of the solar nebular is several million years. Therefore, nebula activity is an unlikely heat source at 4.527 Ma. However, if the re-melting age is ~4.56 Ga, which is within our uncertainty, there is a possibility of the nebular activity. More precise age determination is required for further discussion.

References:

[1] Rubin A. E. (1993) Icarus, **101**, 201-212. [2] Powell B. N. (1969) GCA, **33**, 789-810. [3] Sugiura (2012) Antarctic Meteorites, XXXV, 51. [4] Ireland T. R. and Wlotzka F. (1992) EPSL, **109**, 1-10. [5] Haba et al. (2013) 地球化学会年会, pp1. [6] Tomaru et al. (2001) LPSC XXXII, 1508.

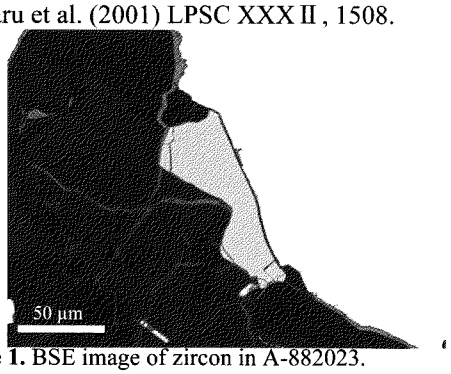

Figure 1. BSE image of zircon in A-882023.

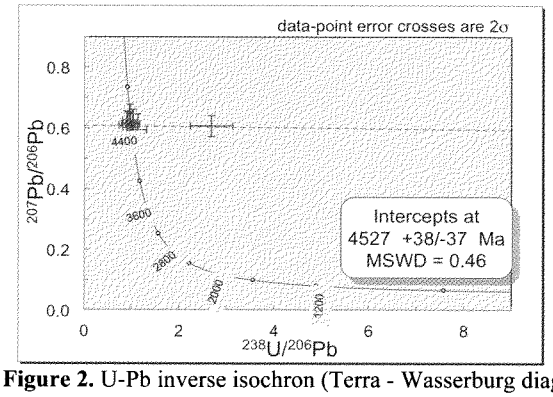

Figure 2. U-Pb inverse isochron (Terra - Wasserburg diagram)

LIME(y) Silicates in Primitive Chondrites: Records of Nebular and Parent Body Processes. M. Komatsu[1] T. J. Fagan[2] and T. Mikouchi[3], [1]Waseda Institute for Advanced Study, Waseda University (komatsu@aoni.waseda.jp), [2]Department of Earth Sciences, Waseda University, Department of Earth and Planetary Science, [3]Graduate School of Science, University of Tokyo.

Introduction:

Low-iron, Mn-enriched (LIME, Mn/FeO ≥1) silicates are important components in the primitive solar system materials. They are interpreted as indicators of nebular condensation conditions [1-4]. They have been identified in IDPs [1], chondrules and matrices of primitive chondrites [2, 3], and in Wild 2 cometary grains [4].

LIME olivine has also been observed in some amoeboid olivine aggregates (AOAs) in primitive chondrites [5, 6]. Mineralogy and chemical compositions of AOAs are similar to those predicted by equilibrium thermodynamic condensation models [e.g., 7], suggesting that AOAs formed primarily by gas-solid condensation [8]. Some AOAs have olivines that are Mn-rich, although they do not have MnO/FeO ratio as high as LIME olivines as originally defined. In this study, we refer to all of these Mn-rich olivines as `LIMEy`. We recognize that the final MnO/FeO ratios of these olivines result from enrichments and depletions in Fe and Mn in the solar nebula and in parent body settings.

In this study, we examine the distribution of LIMEy silicates in AOAs and chondrules in the primitive meteorite Y-81020, and compare to those in variably metamorphosed type 3 carbonaceous chondrites. Our goal is to assess the roles of nebular and asteroidal thermal processing on formation and alteration of LIMEy silicates.

Results:

AOAs are irregularly shaped, fine-grained objects that constitute a few volume-percent of meteorites in most carbonaceous chondrite groups.

Y-81020 (CO3.0) is one of the most primitive carbonaceous chondrites. AOAs from Y-81020 show little evidence for secondary alteration. Most AOAs in Y-81020 are composed of nodules having anorthite ±spinel cores, Al-diopside-rich mantles and closely or loosely packed forsterite rims.

LIMEy olivines are commonly observed in AOAs in Y-81020. However, the Mn-contents and distributions of LIMEy olivine grains vary from AOA to AOA. Fig. 1 shows the Mn-Kα X-ray elemental maps of three Y-81020 AOAs with variable degrees and patterns of Mn-enrichment. Strong Mn-enrichment occurs from cores to rims of individual nodules in AOA#18. In contrast, no enrichment of Mn is observed in AOA#60. AOA#61 is intermediate between AOA#18 and #60 and shows increasing Mn-enrichment toward the AOA rim. All AOAs in Y-81020 show little or no secondary Fe-enrichment.

Some Y-81020 AOAs contain low-Ca pyroxene in addition to olivine. In these cases, Mn-contents in pyroxene and olivine appear to mimic each other (i.e., if olivine is LIMEy, coexisting pyroxene also is LIMEy).

In addition to AOAs, local Mn enrichments are also observed in chondrules and CAIs. Here we describe two Mn-rich objects in Y-81020.

Mn-rich chondrule

CHD#62 is ~30 μm sized spherical Mn-rich chondrule (Fig. 1a). This chondrule looks brighter in BSE image (Fig. 2a) than other chondrules because of its higher FeO content. CHD#62 is composed of low-Ca pyroxene which contains up to 2.5 wt.% of MnO. MnO content is relatively homogeneous, but it is slightly higher in the core than the rim of the chondrule (line analysis data; Fig. 2b) and shows a negative correlation between MnO and FeO (Fig. 2c). Because Y-81020 experienced only minor parent body alteration, the higher FeO content of CHD#62 may reflect a nebular origin.

Mn-rich CAI

CAI#64 is 100×70 μm in size with concentric texture. It has a core composed of fine-grained Na-rich grains (probably nepheline); they are rimmed by high-Ca pyroxene. The high-Ca pyroxene has high up to 3.6 wt.% MnO, which is even higher than AOA olivine and low-Ca pyroxene.

Discussion:

Based on the condensation calculations [9, 10], Mn-rich silicates forms in the vapor of a solar composition. As temperature decreases, Mn in olivine increases more rapidly than Fe, which is condensing into Fe-rich metal at these low $f(O_2)$ conditions. The model increases in Mn/Fe with decreasing temperature, combined with our observed increases in Mn/Fe from core to rim suggest that some AOAs formed by core-to-rim condensation as temperature decreased [6].

Ebel et al [9] assumed that Mn partitions equally between olivine, low-Ca pyroxene and high-Ca-pyroxene in their condensation model. Our observations of similarities in Mn-enrichments of co-existing olivine and pyroxene in Y-81020 AOAs support this assumption.

Rubin [3] described some Mn-rich olivine and pyroxene in a chondrule in Allende. They are present only in the thick rim around the chondrule and contain ~4 wt.% of MnO, but also contain FeO up to ~9 wt.%. Allende experienced a higher degree of alteration than Y-81020, and FeO content in silicates is higher than less altered CV chondrites. It is possible that the Mn-rich chondrule rim of [3] has a

mixed origin, with Mn-enrichment from a nebular process and high FeO due to parent body alteration.

Our recent study [11] shows that Mn-rich olivine is commonly observed in AOAs from weakly metamorphosed Kaba and Y-86009 (CVs), as well as in CR AOAs [5] and Wild 2 grains [4]. On the other hand, AOAs in metamorphosed type 3 carbonaceous chondrites lack LIME silicates. With increasing petrologic sub-types, FeO increases and MnO decreases in AOA olivine [11].

LIMEy olivine is common in AOAs from the primitive chondrites of this study. We suggest that LIME silicates were originally formed as primary phases in AOAs, and also were rarely present as chondrule or CAIs in wide range of carbonaceous chondrites, and then were lost during a parent body alteration. If so, MnO vs. FeO concentrations in AOA olivines can be sensitive indicators of both condensation and alteration conditions.

References:

[1] Klöck W. et al. 1989. Nature 339: 126-128. [2] Ichikawa O. and Ikeda Y. 1995. Proc. of NIPR Symp. 8:63-78. [3] Rubin A. 1984. American Mineralogist 69:880-888. [4] Zolensky M. E. et al. 2006. Science 314: 1735-1753 [5] Weisberg M. K. et al. 2004. MaPS 39:1741-1753. [6] Sugiura N. et al. 2009. MaPS 44:559-572. [7] Yoneda and Grossman1995. GCA 59: 3413-3444. [8] Krot A. N. et al. 2004. Chemie der Erde 64: 185-239. [9] Ebel D. S. et al. 2012. MaPS 47:585-593. [10] Petaev et al. 2005. MaPS 40 suppl:no.5247. [11] Komatsu et al., 2013. LPSC: no.1847.

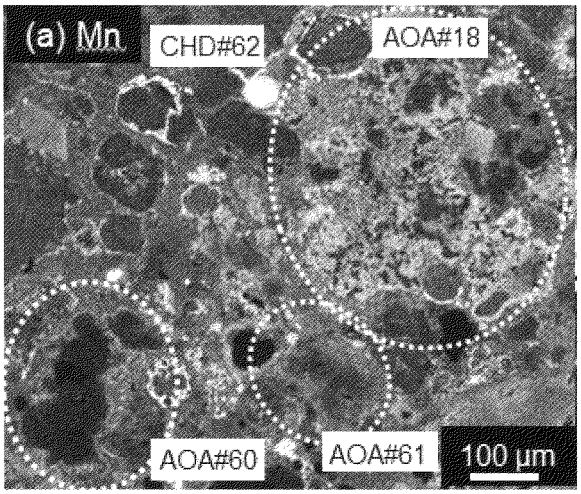

Fig.1. X-ray elemental maps of porous and compact AOAs in Y-81020. There is a clear enrichment in Mn content of olivines in porous AOA #18, whereas the two compact AOAs show minor (#61) and no (#60) Mn enrichment. Note the increase in Mn enrichment from core to rim of AOA#61.

Table 1. Representative compositions of LIMEy minerals in Y-81020.

	AOA#2				CHD#62	CAI#64
	fo	px	px	cpx	en	cpx
SiO_2	42.3	56.3	55.9	48.8	55.2	53.6
Al_2O_3	0.06	1.47	4.45	12.6	1.8	7.7
TiO2	<0.09	0.56	0.28	0.79	0.16	0.92
FeO	<0.08	0.71	0.02	0.73	3.8	1.0
MnO	0.39	0.46	0.69	0.17	2.5	3.6
MgO	56.3	35.7	33.7	17.8	32.1	11.8
CaO	0.21	3.64	4.28	18.9	1.9	16.0
Na_2O	<0.06	<0.06	<0.06	0.12	0.13	0.58
K_2O	<0.04	<0.04	<0.04	<0.04	0.08	0.23
Cr_2O_3	0.50	0.79	0.76	0.27	0.87	2.0
total	99.8	99.7	100.2	100.2	98.5	97.5
Fo	100.0	-	-	-		
Wo	-	92.2	91.6	55.9	3.9	48.3
Fs	-	1.0	0.03	1.3	6.0	2.3

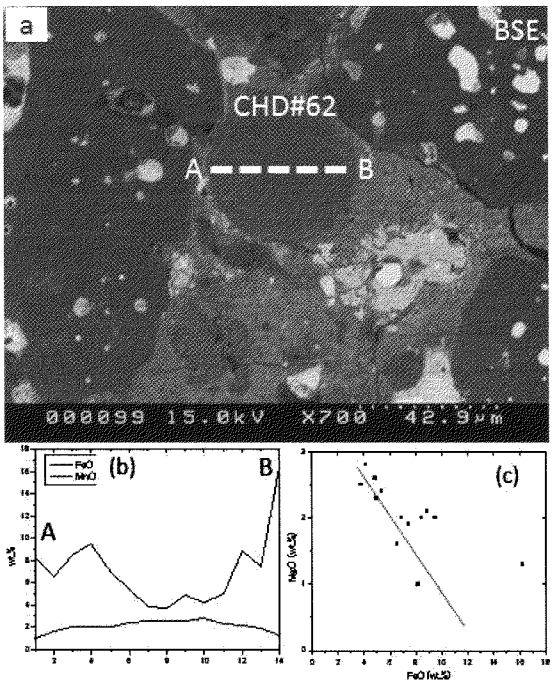

Fig.2. BSE image of chondrule #62 (a). LINE analysis shows Fe enrichment in the rim of the chondrule (b), and negative correlation between FeO and MnO contents (c).

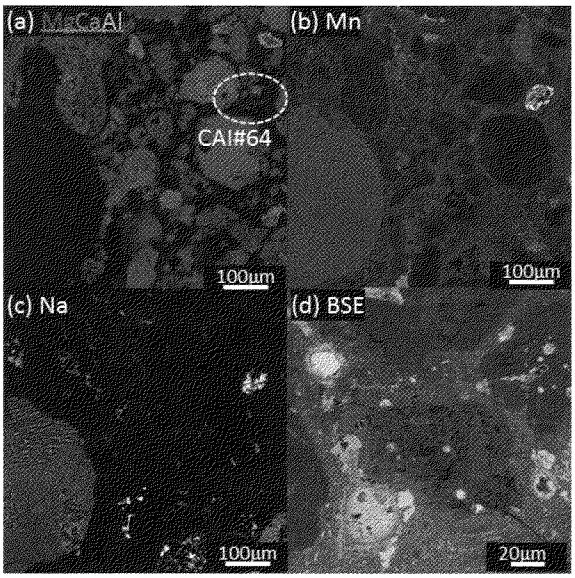

Fig.3. X-ray elemental maps of CAI #64 (a:Mg;Ca; Al, b: Mn, c:Na).and BSE image (d) of CAI #64.

Pulse-laser irradiation experiments of Murchison CM2 chondrite for reproduction of space weathering of C-type asteroids. M. Matsuoka[1], T. Nakamura[1], Y. Kimura[1], T. Hiroi[2], T. Misu[1], R. Nakamura[3], S. Okumura[1], and S. Sasaki[4], [1]Department of Earth and Planetary Materials Sciences, Graduate School of Science, Tohoku University; [2]Depertment of Geological Sciences, Brown University; [3]National Institute of Advanced Industrial Science and Technology; [4]Department of Earth and Space Sciences, Graduate School of Science, Osaka University.

Introduction:

It has been known that space weathering of S-type asteroids results in reddening of reflectance spectra due to production of nano Fe and FeS particles in the outermost layers of silicate crystals [1, 2]. H^+-ion [3] and laser [4, 5] irradiation experiments successfully reproduced space weathering by solar-wind irradiation and micrometeorite bombardment, respectively, on the surfaces of S-type asteroids, In the case of C-type asteroids, however, little has been known on the space weathering effects. According to the observation of family type asteroids, the reflectance spectra of aging C-type asteroids surfaces become bluer and exhibit a negative-slope continuum from shorter wavelength to longer [6].

Experimental procedures:

In this study, we performed reproduction experiments of space weathering on C-type asteroids by laser heating on a primitive meteorite. Pulse laser (5-15 mJ) with a diameter of 0.5 mm exposed to a pellet of powdered Murchison CM2 meteorite. The reflectance spectra in a range of wavelength from 0.25 to 14 μm were measured before and after laser irradiation in order to see heating effects on the spectra. As for the precise measurement of 2.7-μm band caused by structured water in phyllosilicates, absorption water on the surface of the samples was removed by heating the samples at ~100 degrees Celsius in a nitrogen atmosphere. A small amount of particles was recovered from the pellet surface irradiated at 15 mJ and ultra-microtomed and observed by transmission electron microscope (TEM).

Results:

Reflectance spectra:

The results of reflectance spectroscopy showed that the laser heating made Murchison spectra darker and bluer with increasing intensity of laser beam, from 5 mJ to 15 mJ (Fig. 1). The change of the spectra was significant in the range from 0.3 to 1.8 μm wavelength. These results were consistent with the tendency of the space-weathered spectra of C-type asteroids [6]. The 0.7-μm and 2.7-μm band depths decrease as the laser intensity increases. Furthermore, in the short-wavelength range (e.g., near 0.25 μm) reflectance increases in proportion to the laser intensity (Fig. 1) and thus became brighter.

TEM observation:

TEM observation indicated two apparent changes in the laser-heated areas on the pellet of Murchison. First, many nano-particles (10-15 nm in diameter) of ferroan sulfide were newly formed by melting of FeS-rich material tochilinite. The particles were identified as Fe_3S_4 and were distributed around small bubbles. Second, in the Fe_3S_4 nano-particles-rich regions, Fe-rich serpentine became amorphous, which was confirmed by high-resolution observation and selected-area electron diffraction.

Discussion:

The amorphization of Fe-rich serpentine is mainly responsible for the "bluing" of the Murchison spectra, because of the breakdown of serpentine lowers the slope of visible and near infrared spectra, especially short-wavelength range [7]. On the other hand, darkening of the Murchison spectra seems to have resulted from production of Fe_3S_4 nano-particles. Tiny sulfide particles coated the surfaces of serpentines, were able to reduce reflectivity greatly. In addition, brightening of spectra from 0.25 to 0.4 μm may indicate some structural changes of carbonaceous material, analogous to proton implantation experiment on carbonaceous material [8]

References:

[1] Noguchi T. et al. (2011) *Science, 333,* 1121–1125. [2] Keller L. P. and McKay D. S. (1993) *Science, 263,* 1305–1307. [3] Hapke B. (1965) *Ann. N.Y. Acad. Sci., 123,* 711–721. [4] Yamada M. et al. (1999) *Earth, Planets and Space, 51,* 1255–1265. [5] Sasaki S. et al. (2001) *Nature, 410,* 555–557. [6] Nesvorny D. et al. (2005) *Icarus, 173,* 132–152. [7] Hiroi T. et al. (1999) *Antract. Meteorite Res., 12,* 108–116. [8] Moroz L. et al. (2004) *Icarus, 170,* 214–228.

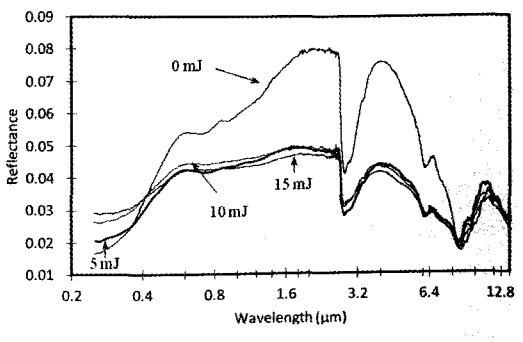

Fig. 1 Visible and infrared reflectance spectra of Murchison pellet samples.

Olivine in EH Chondrites as an indicator of metamorphism in the enstatite chondrite parent body. S. J. McKibbin[1], H. Terryn[2], L. Hecht[3], P. Claeys[1]. [1]Earth System Science, Vrije Universiteit Brussel, Belgium. [2]Research Group Electrochemical and Surface Engineering (SURF), Vrije Universiteit Brussel, Belgium. [3]Museum für Naturkunde, Berlin, Germany.

Introduction: High-Fe enstatite chondrites (EH chondrites) are samples of planetesimals accreted in a region of the solar nebula with very low oxygen fugacity [1]. A consequence of this reduction is that Fe exists as metal rather than as FeO in silicates, with pyroxene rather than olivine being the most common mineral (stabilized by low $(FeO+MgO)/SiO_2$) [1, 2]. Like ordinary chondrites, EH chondrites are divided according to textural and limited geochemical criteria, with petrologic type 3 being unequilibrated nebular rocks and types 4-6 having been increasingly metamorphosed. Suggested mineralogical and geochemical criteria for classifying this process include the presence of disequilibrium mineral assemblages e.g. olivine and silica, which react according to $Mg_2SiO_4 + SiO_2 \rightarrow Mg_2Si_2O_6$ [3], and mineral geochemistry, particularly Cr in olivine [4]. We are attempting to consolidate these classification schemes with an investigation of mineral modal abundances and geochemistry.

Methods: We are obtaining elemental maps with a JEOL 6400 SEM (20 kV, ~6 nA, EDS) using the spectral imaging function in the Thermo Scientific NSS 3 software. Olivine and pyroxene analyses are underway with a JEOL JXA-8500F Hyperprobe (15 kV, 60 nA, WDS). So far, we have investigated three EH3 chondrites (Y-691, Sahara 97079, and ALHA-77295) and one EH5 chondrite (A-881475).

Results and outlook: The major mineralogy of EH3 chondrites comprises pyroxene, olivine, silica, plagioclase/glass, Fe-Ni metal and sulfides including oldhamite (CaS), niningerite (MgS) and troilite (FeS) (Fig. 1). The higher grade EH5 lacks olivine and the rare sulfides oldhamite and niningerite (Fig. 2); silica abundance is high reflecting production by *in situ* reduction of FeO [5] which was not accounted for in the olivine and silica reaction model given by [3].

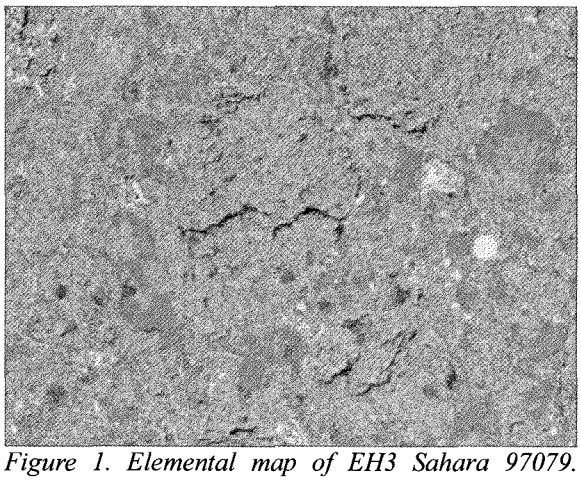

Figure 1. Elemental map of EH3 Sahara 97079. Bright blue = olivine; pale blue = pyroxene; bright yellow = silica; dark yellow = plagioclase; green = Fe-Ni; orange = FeS; red = CaS; purple = MgS.

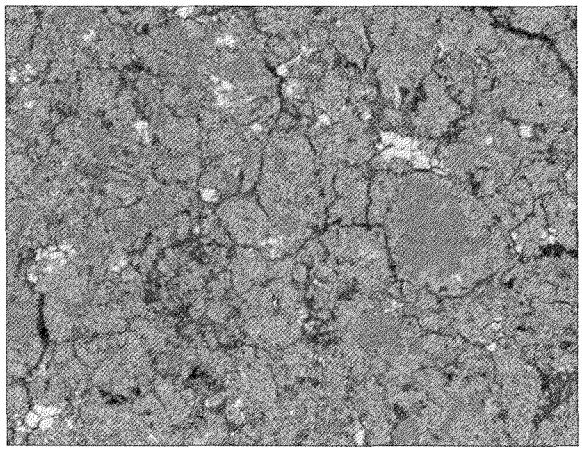

Figure 2. SEM elemental map of EH5 A-881475. Colour scheme as for Figure 1.

Our EH3 olivine compositions are in general agreement with previous work (Fig. 3) and lie on the metamorphic trend defined by [4] but are displaced to lower Cr contents and Cr standard deviations. Displacement of points along this line could arise from bias related to our criteria for finding olivine which was based on Mg counts rather than Si, since Mg-rich olivine is also Cr-poor. Alternately, accidental fluorescence of pyroxene during analysis of olivine could have biased [4] towards higher Cr and Cr standard deviation.

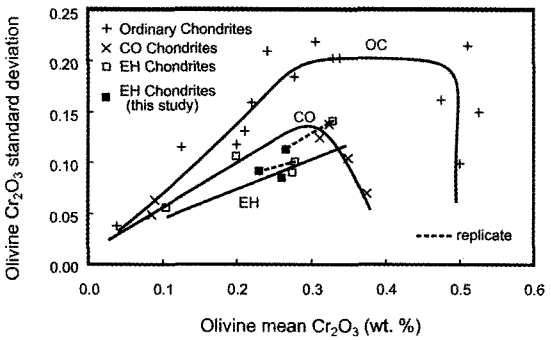

Figure 3. Cr contents and standard deviations for EH chondrite olivine compared to previous work [4].

References: [1] Weisberg M. K. and Kimura M. (2012) Chemie der Erde 72, 101-115. [2] Binns, R. A. (1967) American Mineralogist 52, 1549-1554. [3] Hicks T. L. et al. (2000) LPSC 31, 1491. [4] Bendersky C. et al. (2007) LPSC 38, 2077. [5] Weisberg et al. (1994) Meteoritics 29, 362-373.

Cathodoluminescence examination of the enstatite chondrite of Yamato 86004

M. Mishima*, K. Ninagawa, Y. Tsuchiya, N. Kusano, E. Yoshida, S. Ohgo and H. Nishido
Okayama University of Science (s10p073mm@std.ous.ac.jp)

Cathodoluminesence (CL) is the emission of light from the materials excited with an electron beam, and its appearance could be attributed to impurity, especially transition metal and rare earth elements, and to structural defects in the lattice. The applications of the CL for geological materials have been developed to clarify calcite cementation, secondary growth of quartz and radiation damage of rock-forming minerals.

According to Zhang *et al.* (1996), the enstatites in metamorphosed EL chondrites displays a distinctive magenta CL with the emission bands in blue and red regions, whereas the enstatites in metamorphosed EH chondrites shows a blue CL. We have been examining CL features of the constituting minerals in the enstatite chondrite of Yamato 86004 (EH melt rock)[2] by means of the Luminoscope (ELM-3: American Technologies) for color CL imaging and a SEM-CL for CL spectroscopy. SEM-CL analysis was conducted using a SEM (JEOL: JSM-5410) combined with a grating monochromator (Oxford: Mono CL2) to measure CL spectra ranging from 300 to 800 nm in 1nm steps at room temperature.

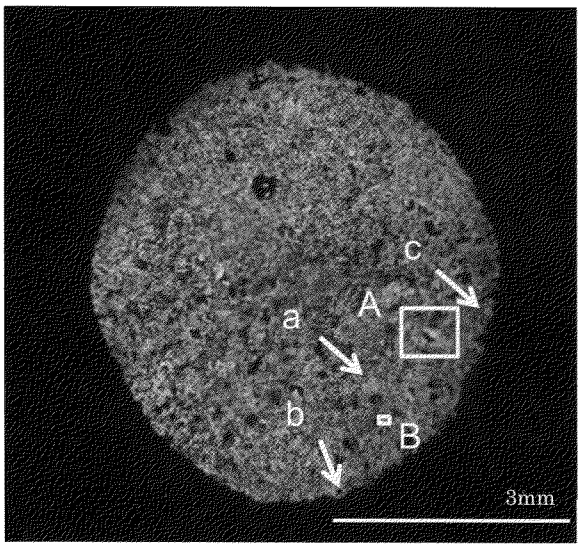

Figure 1. CL color image of Yamato 86004.

Fig. 1 shows a CL color image of Yamato 86004 collected from whole area with the Luminoscope. Three CL phases were recognized from the center to the outer rim as follows; blue, red and black, of which non-luminescent area corresponds to a fusion crust. This fact suggests that the heating during atmospheric entry might cause such CL zonation in the spherical meteorite. Fig. 2 shows CL spectra of specified grains a, b and c indicated in fig. 1, obtained with a scan mode. The grains of b and c areas give different CL spectral peaks in red emission region at 630 nm and 660 nm, respectively. The former can be assigned to an impurity center of divalent Mn ion in forsterite, and the latter to same center in enstatite[3].

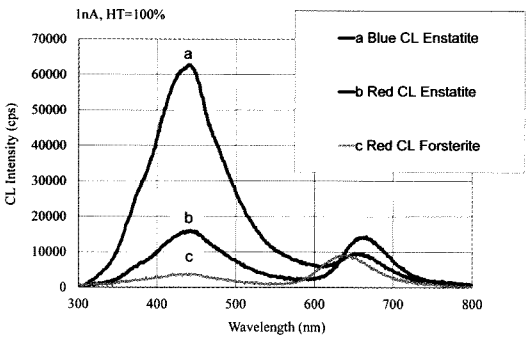

Figure 2. CL spectra of a, b and c indicated in figure 1.

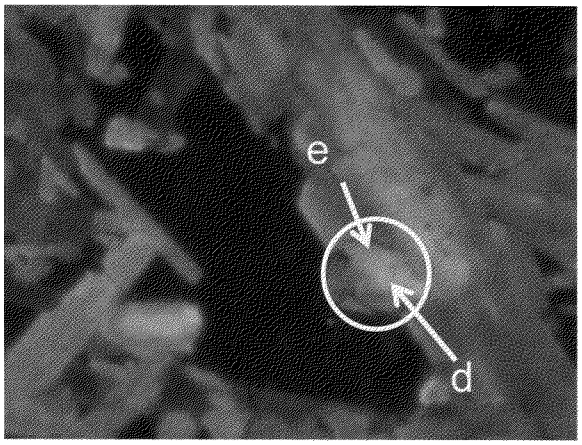

Figure 3. CL image of the square area of A in figure 1. Width is 250 μm.

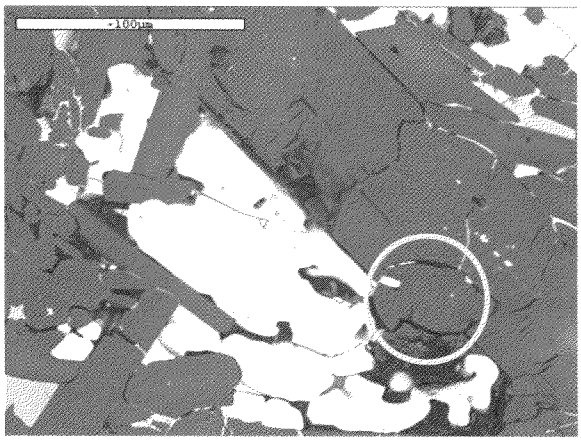

Figure 4. BSE image including the area in figure 3. The circle shows the same area of the circle in figure 3.

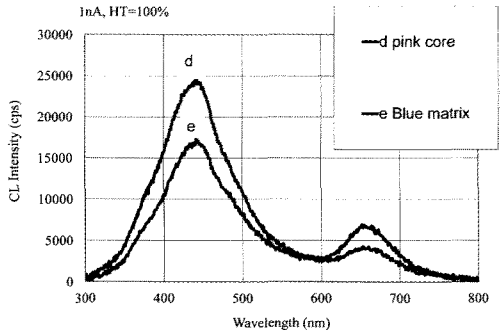

Figurer 5. CL spectra of d and e indicated in figure 3.

Fig. 3 exhibits a high-magnification CL image of the square area of A in Fig. 1. Several grains have domain texture of CL emission with a pink core in blue matrix. Fig. 4 represents a BSE image corresponding to almost same area of Fig. 3. It demonstrates no compositional heterogeneity in these grains based on the BSE information. Fig. 5 provides CL spectra of the grain of d and e areas obtained with a scan mode. They show similar CL spectral patterns, of which intensities are slightly different.

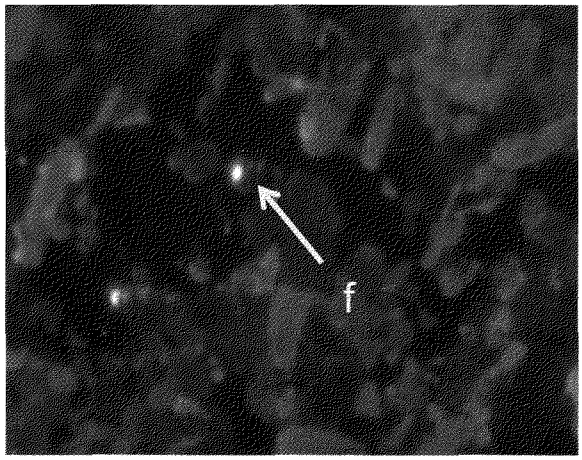

Figure 6. CL color image of the square area of B in figure 1. Width is 20 μm.

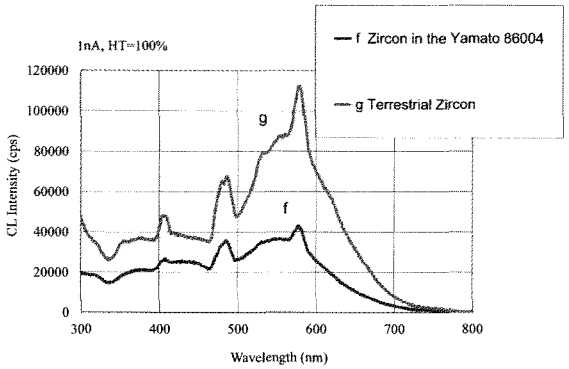

Figure 7. CL spectra of the grain of f in figure 6 and terrestrial zircon.

Furthermore, we found a tiny grain exhibiting a characteristic yellow CL emission in the blue CL area in Fig. 1. Fig. 6 shows expanded a high-magnification CL image of the square area of B in Fig. 1. The chemical analysis using EDS reveals that the grain with yellow CL has mainly Zr and Si, suggesting zircon. Fig. 7 gives CL spectra of the grain of f in Fig 6 and terrestrial zircon in granodiorite from Okayama, Japan, obtained with a scan mode. They have similar CL emission bands at 480 nm and 580nm, which are assigned to an impurity center of trivalent Dy commonly found in plutonic zircon.

References: [1] Y. Zhang *et al.* 1996. Meteoritics & Planetary Science 31, 87-96. [2] Y. Lin and M. Kimura. 1998. Meteoritics & Planetary Science 33, 501-511. [3] K. Ninagawa *et al.* 2000. 25th Symposium on Antarctic Meteorites (NIPR, Tokyo) 114-116.

VOLATILE–BEARING ASTEROIDS AND PLANETS FORMED BY IMPACT QUENCHED PROCESS.

Yasunori Miura[1, 2, 3] and G. Iancu[2]. [1]Yamaguchi University, Yamaguchi, Yamaguchi 753-0074, Japan, [2] EUA-Al.I.C University, [3]Caltech-J.P.L. yasmiura50@gmail.com

Introduction: Asteroids and some planetary bodies reveal anomalous characteristics of low or high density [1]. In order to propose possible surface model, dynamic process of volatiles (H_2O and CO_2) are discussed as the main purpose of the present study.

Low or high density of the Moon or asteroids: Figure1 shows various sizes and densities as follows:

1) Asteroids (Vesta and Massalla) show lower density (similar with the Moon) with the smallest sizes than Earth-type planets (Mercury, Venus, Earth and Mars), the Moon and a dwarf planet Pluto [1-5].
2) The above data indicate that asteroids are considered to be mixed with volatiles-bearing solids triggered by impact growth during numerous continuous collisions...

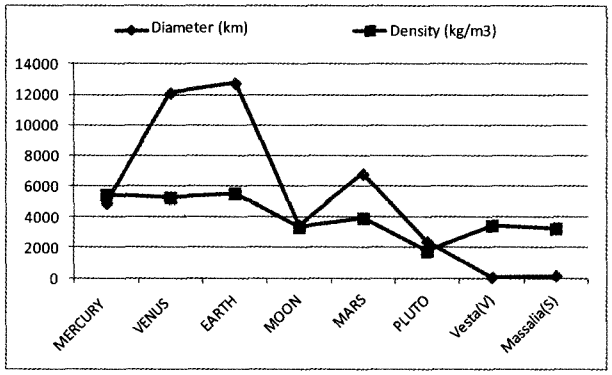

Fig.1. Diameter and density of eight bodies (Mercury, Venus, Earth, Mars, the Moon, Pluto, Vesta and Massalla) [1, 2].

Phase diagram of water and/or carbon dioxides: Water (H_2O) or carbon dioxides CO_2 diagram is expressed by phase changes of three phase-states VLS (vapor, liquid and solid) similar at the triple and critical points, which are used for dynamic changes of phase-states during impacts and quenching to lower temperatures as follows (Fig. 2) [3-5]:

1) Solidified ice (H_2O or CO_2) is normally formed by quenched after impacts to lower temperature [4, 5].
2) Fluids in primordial planets and asteroids are considered to be formed at higher temperature and pressure mainly by dynamic process of various impacts.
3) Internal fluids might be melted from solidified vapor or liquid phase (mainly by internal conditions).

Impact formation of internal fluids: Formation of internal fluids is one of the unsolved problems by previous models (without any ocean-plate movements). The most suitable model for internal fluids system is summarized as follows (shown in Fig.2) [2, 4-7]:

1) Interior fluids are considered to be formed mainly by continuous impacts through voids-rich surfaces (with icy bodies and/or some asteroids) and quenched widely to solidified surface.
2) Interior uplift of fluids H_2O and/or CO_2 molecules might be triggered by increased temperature and pressure after any impacts or the followed interior heating process [4, 5] to form gas or fluids on the shallow surface of the interior of primordial bodies.

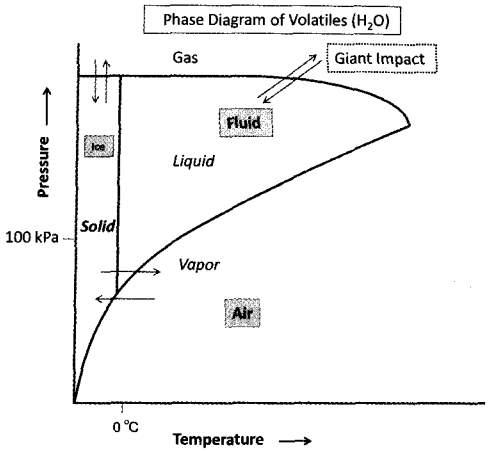

Fig.2. Phase-state diagram of H_2O phases (similar as CO_2 phases) of three VLS (vapor, liquid and solid) [4, 5].

Formation of organic molecules in space bodies: The organic molecules with hydrogen, carbon and oxy Gen (CHO) can be formed when shock-wave reaction is so generated by impacts,quakes or volcanism [4,5].

Summary: Asteroids with high density with small size might be mixtures of volatiles-bearing solids and some stony asteroidal materials through continuous im pact process on voids-rich surface.

References: [1] Williams D.R. (2012): Planetary Fact Sheet.http://nssdc.gsfc.nasa.gov/planetary/factsheet/
[2] Heiken G., D. and French B., *Lunar source book* (Cambridge Univ. Press) (1991): 27- 120.
[3] Miura Y. et al (1997): Shock Waves (World Scientific), 20. 1473-1478.
[4] Miura Y. (2011): Vexag International Workshop (Venus), #23, #24.
[5] Miura Y. (2013): Lunar and Planetary Science Conference, 44th (Woodlands), #1654, .#3098.

IMPACT-INDUCED AIR-MELTING PROCESSES ON AMORPHOUS-RICH ASTEROIDS AND PLANETS.

Yasunori Miura[1, 2, 3] and G. Iancu[2]. [1]Yamaguchi University, Yamaguchi, Yamaguchi 753-0074, Japan, [2] EUA-Al.I.C. University, [3]Caltech-J.P.L. yasmiura50@gmail.com

Introduction: Asteroids and primordial planetary bodies are used to be discussed in solid material state generally [1-3]. The active planets with geosphere are discussed high-pressure process in the solid sphere of hard rock and stable minerals, though atmosphere and ocean-water system are clearly distinguished by another material states of vapor and liquid states. Remained solid materials after impact events are used to be identified stable high-temperature and high-pressure conditions of the solid material. However, it cannot be elucidated in detail to be ignored the melting process and volatilization of various elements (including volatiles of H_2O and CO_2) at high pressures. In this paper, we propose the fluid melting process at impact-induced process based on new idea [4-7].

Problems of static high pressure in natural event: Stable high-pressure process [1-3] has been discussed in the Hugoniot curve based on volume change at high pressure of solid material. This feature has been applied to simple elements such as closed static system, such as artificial diamond of carbon element etc. However, natural state changes (such as a gas or liquid) has occurred in the compositional variation from complex composition of natural in the (Earth) process, because complex compositional changes of solids without direct observation and tracking are considered to be formed as solids with high-pressure with static reaction or shock impact event. Problem of a static high-pressure process in natural formation is to ignore the state changes formed in long geological periods resulted in final products of crystalline solidified materials. The static formation model might be serious problem when it is applied to the reaction process of dynamic location. Description of the crystalline materials used by optical, electron and X-ray beams both in Earth and extraterrestrial materials, is usually different interpretation of formed environments (statics or dynamics)

Problems of dynamic high-pressure process: Previous interpretation of dynamic high pressure process with open system has been applied incorrectly to the static environments formed quenched solids in a closed system. However, in impact experiment on the hard target materials of rocks or metals with state-changes by vapor and fluid ejecta, the residual materials after high pressure are solidified as post-shock event. From remained materials after impact process, crystalline solidified grains are mainly state-changes during dynamic high-pressure process which are considered to be representative remnants of the impacted solids without ratio of non-crystalline materials. Identification of crystalline remnants in impact event is different to generated environments [4-6].

Experiments and results: In order to collect amorphous materials after high-velocity reaction, light elements are selected from carbon and its mixed composition in soft target materials of air-molecules and liquid-molecules, which are obtained as follows [4-7]:

1) Three phases are obtained as amorphous carbon with various combinations, 2) carbonate CaCO3, and 3) carbon C.

2) At air molecules, about 90% of amorphous carbon compositions, crystalline composition of carbonates and carbon (10%) are fewer products.

3) At liquid molecules, about 45% of amorphous carbon compositions, about 5% and 50% of crystalline composition of carbonates and carbon, respectively, are obtained.

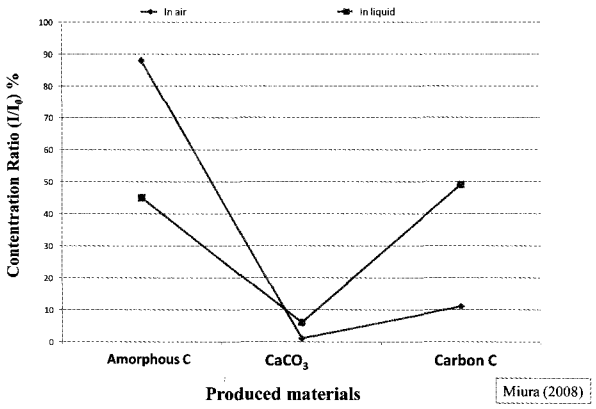

Fig.1. Diagram of products (amorphous grains and two crystalline grains of carbon-bearing materials) and content ratio (%) at high-speed reaction in air and liquid conditions [4-7].

Discussion of experimental results: From the results of the present experiments, high-speed experiments in soft air-fluids environments are obtained remarkable results as follows:

1) Amorphous solidified materials are collected in large quantities in the present experiments.

2) Impacts on soft target of voids-rich and low-density are difficult to be obtained at closed impact chamber. However, global surface of extraterrestrial surfaces has many impacted grains on regolith soils with amorphous materials-rich gain even in drilled samples as in the Apollo exploration [2, 3].

New model of impacted extraterrestrial bodies: The present new model of impacted extraterrestrial bodies and primordial Earth is summarized as follows:

1) A large amount of amorphous solidification can be obtained as state-changes among vapor, liquid and solid (VLS) states.

2) State-changes can be obtained as global system of active planet Earth, and as local system of impacted locations at all extraterrestrial surfaces of Earth-type planets, the Moon and Asteroids.

3) It was found to be important in the present experiments that the state change at the rapid reaction has a large amount of amorphous solidification. The planet Earth shows characteristic of the long-range change of composition during evolved process after impacts, however, the airless Moon crust and primordial planets reveal local state-changes because there is no continuous change at global evolution.

4) Figure 2 shows impacted and impact-related extraterrestrial bodies and active planet Earth, where main crystalline minerals formed at active Earth are completely different with present extraterrestrial bodies (without global ocean-water system to be generated the whole VLS state changes).

5) Present model called as impact-induced air-melting processes are confirmed by the feldspar minerals (composition, and lamellar textures) and volatile-bearing composition on impacted grains of the Moon and active Earth [4-7].

6) Present results can be applied for sources of Asteroids and planets for the Antarctic meteorites and other meteorites found on active Earth.

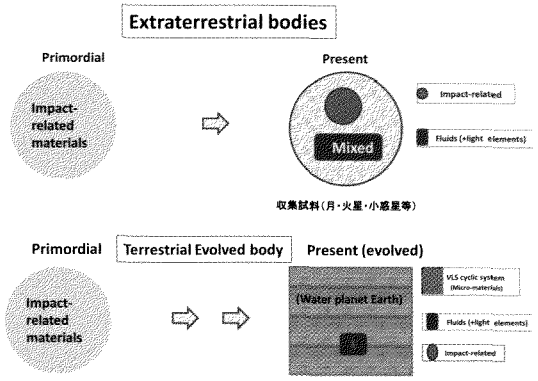

Fig.2. Comparison of amorphous and crystalline material grains on extraterrestrial bodies and terrestrial evolved planet, which are stared impact-generated bodies, and followed local impact changes, or global state-change systems of active planet Earth [4-7].

Summary: The present results are summarized as follows:

1) Significance of amorphous materials is obtained at formation of extraterrestrial bodies and primordial planet Earth.

2) A large amount of amorphous products with carbon-bearing composition are artificially obtained at impact experiments of solidified grains on air-liquid conditions in the present experiments.

3) The present results are confirmed on the sample data of extraterrestrial bodies and collected grains mainly formed by impact-induced processes.

4) Well-crystallized products (crystalline minerals) on active planet Earth are not standard for formed condition of minerals and formation model of extraterrestrial bodies (the Moon, Earth-type planets and Asteroids) because of much formation of amorphous grains as state-change during air-melting processes on extraterrestrial bodies.

5) Present results can be applied for sources of Asteroids and planets for the Antarctic meteorites and other meteorites found on active Earth.

Acknowledgements: Authors thank to Drs. T. Kato and T.Tanosaki for this discussion.

References:

[1]Ernst W.G. (1990): The Dynamic Earth (Col. Univ. Press), 280pp.

[2] Heiken G., Vaniman D. and French B. (1990): Lunar source book (Cambridge Univ. Press), 736pp.

[3] Melosh, H. J. (1989): Impact cratering: A geologic process (Oxford Univ. Press), pp.60-111.

[4] Miura, Y. and Fukuyama S. (1999): J. of Materials Proc. Tech. (Elsevier), 85, pp.192-193.

[5] Miura Y. (2012): LPSC XXXXIII (LPI). #1203, #2920.

[6] Miura Y. (2012): ELS-2012 (DLR), 76-79.

[7] Miura Y. (2013): Lunar and Planetary Science Conference, 44th (Woodlands), #1654, #3098.

High-pressure polymorphs of silica in NWA 4734. M. Miyahara[1,2], S. Kaneko[1], E. Ohtani[1], T. Sakai[1,3], T. Nagase[1], M. Kayama[2], H. Nishido[4] and N. Hirao[5] [1]Tohoku Univ., [2]Hiroshima Univ., [3]Ehime Univ., [4]Okayama Univ. of Sci., [5]JASRI.

1. Introduction

Thick brecciated rock layer (regolith) and numerous craters on the moon indicate that the moon has gone through intense meteoroid bombardment. Some meteorites originate from the moon. Considering thick regolith and many craters, it is likely that some meteorites have records of such dynamic events occurred on the moon. The existence of a high-pressure polymorph is suggestive of high-pressure and high-temperature conditions; i.e., heavily shocked meteorites include high-pressure polymorphs. However, several previous studies proposed that high-pressure polymorphs are hardly contained in lunar surface materials (lunar meteorite and Apollo samples) because most high-pressure polymorphs melted and disappeared through high-temperature condition induced by a dynamic event under rarefied atmosphere on the moon [1-2]. Nonetheless, Ohtani et al (2011) [3] investigated lunar meteorite, Asuka 881757, and identified high-pressure polymorphs of silica, coesite and stishovite. Recent studies also identify high-pressure polymorphs of olivine, wadsleyite and ringwoodite in lunar meteorites [4-5]. In this study, we investigated a lunar meteorite, NWA 4734 to clarify a dynamic event occurred on the moon, and especially focused our interests on silica.

2. Material and experimental methods

We prepared lunar meteorite, NWA 4734 thin section for this study. NWA 4734 originates from lunar basalt, and contains many shock-melt veins and melt-pockets, implying that NWA 4734 was heavily shocked. We identified minerals using a Raman spectroscopy subsequent to a filed-emission gun scanning electron microscope (FEG-SEM) observation. The compositions of minerals were determined with an electron micro-probe analyzer (EMPA). We also used focused ion beam (FIB) system, synchrotron X-ray diffraction (XRD) and transmission electron microscope (TEM) to identify high-pressure polymorphs.

3. Results and discussion

Most silica grains in NWA 4734 are cristobalite based on Raman spectroscopy analysis. Back-scattered electron (BSE) images show that many cristobalite grains show mosaic-like textures. On the other hand, cristobalite grains adjacent to shock-melt veins or melt-pockets show tweed-like textures. We excavated such silica grains having tweed-like textures using a FIB system, and became block pieces. We put the block pieces on a single crystal diamond and scanned them with a synchrotron X-ray at SPring-8 BL-10. We identified a high-pressure polymorph of silica, alpha-PbO_2 type silica (seifertite) based on the X-ray diffraction (XRD) patterns. Seifertite was identified only from shocked Martian meteorites so far [6]. BSE images show that some cristobalite grains in the host-rock of NWA 4734 have lamellae-like textures. Raman spectroscopy analysis and XRD patterns reveal that such silica grains include stishovite along with cristobalite. Nano-sized coesite grain assemblages were also found in silica grains entrained in the shock-melt veins.

Phase equilibrium diagram deduced from static high-temperature and high-pressure synthetic experiments indicate that the stable pressure filed of seifertite is ~100 GPa or more [e.g., Ref. 7]. On the other hand, recent several studies propose that the stable pressure filed of seifertite depends on starting material for a synthetic experiment and impurity (e.g., Al)[8-9]. The original silica in NWA 4734 is cristobalite and contains small amounts of Al (< 0.99 wt% as Al_2O_3). Considering its original material and impurity, shock-pressure condition recorded in NWA 4734 would be ~40 GPa or more.

^{40}Ar-^{39}Ar radio-isotopic age of NWA 4734 is ~2.7 Ga [10], which is the one of the youngest ages among lunar meteorites. ^{40}Ar-^{39}Ar radio-isotopic age is very sensitive to thermal metamorphism. High-pressure polymorphs easily vitrify by heating under ambient pressure condition. NWA 4734 has not suffered from any thermal metamorphism after the dynamic event formed coesite, stishovite and seifertite. The dynamic event formed coesite, stishovite and seifertite would occurred ~2.7 Ga ago. Our finding allows us to infer that intense meteoroid impact had continued on the moon till ~2.7 Ga at least.

References:

[1] Papike J. J. (1998) In *Reviews in Mineralogy and Geochemistry* 36, 7-1–7-11.
[2] Lucey P., et al. (2006) In *Reviews in Mineralogy and Geochemistry* 60, 83-220.
[3] Ohtani E., et al. (2011) *PNAS* 108, 463-466.
[4] Barrat J. A., et al. (2005) *GCA* 69, 5597–5609.
[5] Zhang A. C., et al. (2010) *MAPS* 45, 1929–1947.
[6] El Goresy A., et al. (2008) *Eur. J. Mineral.* 20, 523–528.
[7] Murakami M., et al. (2003) *Geophys. Res. Lett.* 30, 1207.
[8] Dubrovinsky L.S., et al. (2001) *Chem. Phys. Lett.* 333, 264–270.
[9] Lakshtanov D. L., et al. (2007) *PNAS* 104, 13588–13590.
[10] Fernandes V. A., et al. (2009) 40th *Lunar Planet. Sci. Conf.* 1045pdf.

Pyroxene-akimotoite phase transformation in shocked chondrite (NWA 5011)

Sz. Nagy[1](sz.j.nagy@gmail.com), I. Gyollai[2], H. Nishido[3], A. Gucsik[4]

[1]*University of Szeged, Department of Mineralogy, Petrology and Geochemistry, H-6701 Szeged, P.O. Box 651, Hungary.*
[2]*University of Vienna, Department of Lithospheric Research, Althanstrasse 14, 1051-Vienna, Austria.*
[3]*Okayama University of Science, Department of Biosphere-Geosphere Science, 1-1 Ridai-Cho, Okayama, 700-0005, Japan*
[4]*Department of Geology, University of Johannesburg, Johannesburg, 2600 Auckland Park, South Africa*

Introduction: Shock-events by asteroidal collisions may cause the effect of high-pressure metamorphism on the mineral assemblages [1]. The low-Ca pyroxene can transform to its high-pressure phases including the followings of jadeite, majorite-pyrope$_{ss}$, majorite, akimotoite, Mg-perovskite and pyroxene glass depending on the shock-metamorphic conditions. In this study we have examined a new microstructure form of akimotoite in NWA 5011 meteorite to clarify pyroxene-akimotoite phase transformation during shock-metamorphism.

Result and Discussion: The NWA 5011 contains numerous akimotoite-bearing assemblages various in size. These assemblages were well observed as their dark-elongated patterns in the OM images. Probably, these patterns correspond to the cracks enriched in iron, and might be formed by the transformation during shoch metamorphism. The transformation of the pyroxene and akimotoite promotes the volume reduction of ~16%. We have found glassy material around the iron-enriched cracks and occasionally inside of the akimotoite aggregates. The detail observation distinguishes two types of microstructure in the akimotoite. One is so-called intracrystalline lamellar and the other is the polycrystalline granular. In BSE-image, we have recognized cell-like structure in NWA 5011 as reported by Hu et al. [1]. According to Hu et al. [1], cell structure may have formed in the earlier stage of the phase creation of perovskite, but of which structural evidences have not been found. In spite of Hu et al. [1] we suggest that these cells are iron enriched cracks after akimotoite formation. This section is represents the direction of oxygen hcp-layer of akimotoite structure on the grounds of volume decrease by transformation process. The akimotoite was identified by micro-Raman spectroscopy. It coexists with the pyroxene as the type of intracrystalline lamellar. The chemical analysis reveals that akimotoite grains occurred as the type of polycrystalline granular contain less iron than the cracks due to the volume decrease. Furthermore, in the element mapping process calcium mostly associates; suggesting the presence of oldhamite (CaS). A very high melting point (2450 °C) of oldhamite infers its formation as an early nebular condensate. In the shocked chondrites the oldhamite phase has been produced by shock vein formation. The present of the oldhamite is an evidence for the very high-temperature condition during the shock-vein formation rather that supposed in earlier work [2]. A mixed-type pyroxene chondrule (~1 mm in diameter) contains a number of subchondrules observed in the sample. One of the subchondrules exhibits a dense cleavage network, where the angle between two directions of the cleavages is nearly perpendicular (87°) (Fig. 1). Therefore, the zone axis of the cleavages is {110}. The BSE-images reveal that the plain area of the cleveages is riched in Fe showed by microgranular texture. However, this texture is characterized by slightly overhang from the original boundary of the cleavages to the host grain. The thickness of "overhanged" transition area is up to 0.5μm with the direction parallel to the cleavages. Between the space of the separable cleavages we observed incoherent akimotoite transformation. Raman spectral analysis along the cleavage confirms the pyroxene-akimotoite phase transition. The Fe-enrichment along the cleavages happened due to the melting process, and the subsequently diffusion events. Furthermore, the Raman spectra provide main vibrations of ringwoodite and stishovite besides the vibration peaks of akimotoite. This suggests a subsequent evidence for the high P-T regime in shock melt veins, but within a small specific area.

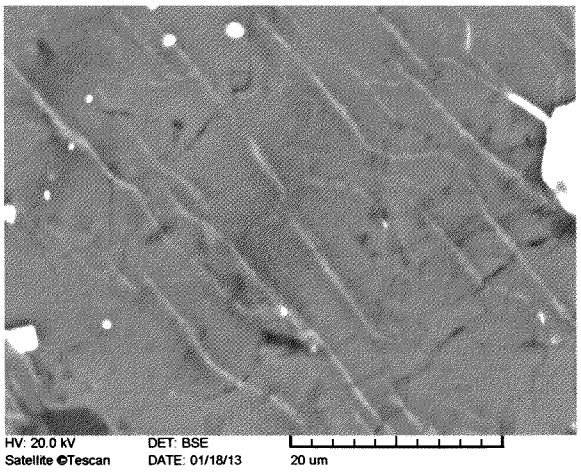

Fig. 1. Along the cleavage plains the pyroxene-akimotoite transformed area is less than few microns.

References: [1] Hue et al. (2012) 43rd LPSC, abstract#2728 [2] Miyahara et al. (2010) EPSL, 295, 321-327

Micro-Raman characterization of cation disordering in ringwoodite

Sz. Nagy[1](sz.j.nagy@gmail.com), E. Pál-Molnár[1,5], H. Nishido[2], K. Fintor[1], I. Gyollai[3], Sz. Bérczi[4] *[1]University of Szeged, Department of Mineralogy, Petrology and Geochemistry, H-6701 Szeged, P.O. Box 651, Hungary. [2]Okayama University of Science, Department of Biosphere-Geosphere Science, 1-1 Ridai-Cho, Okayama, 700-0005, Japan. [3]University of Vienna, Department of Lithospheric Research, Althanstrasse 14, 1051-Vienna, Austria. [4]Eötvös University, Institute of Physics, Department of Material Physics, CMSRG, H-1117 Budapest, Pázmány P. Street 1/A, Hungary. [5]MTA-ELTE Volcanology Research Group, H-1117 Budapest, Pázmány P. Street 1/C, Hungary*

Introduction: Ringwoodite is a high-pressure polymorph of olivine occasionally found from shocked L-type meteorites. In such a case of NWA 5011, the phase transformation is often uncomplete in shock melt veins. A short-period pulse of shock pressure makes an insufficient phase transformation of olivine due to not enough time for the complete cation ordering, suggesting new or metastable phases frequently with structural defects. Previously we found out a new Raman spectral peak at 880 cm^{-1} in NWA 5011 ringwoodite [1], which was also observed in the Taiban chondrite [2]. In this study we have characterized this spectral data to clarify the cation ordering in NWA 5011 ringwoodite.

Result and Discussion: Ringwoodite aggregates with ~150 μm size were selected for micro-Raman measurements. All spectra were collected using a Thermo DXR Micro-Raman microscope under same conditions with the laser at 532 nm during 600 sec on a 1 μm spot. The measured area (Fig. 1) in the same ringwoodite aggregate shows the domain-like texture with colorless and blue in OM-image. In this area we have collected three spectra from the colorless areas, and three ones from the blue-colored areas. From the colorless areas, the spectral peaks were detected at 712, 798, 845, and 918 cm^{-1}. The peaks at 712 and 918 cm^{-1} are probably assigned to wadsleyite, but the others at 798 and 845 cm^{-1} belong to ringwoodite. From the blue-colored areas, the peaks at 798 and 880 cm^{-1} were observed. The chemical investigation reveals neither difference in chemical composition, nor chemical heterogeneity between them. The most characteristic difference is the intensities of the spectral peaks collected from the different-colored areas. Fig. 2 shows the spectra normalized by referring the intensities of colorless and blue-colored areas. It indicates a characteristic peak at 880 cm^{-1} in the spectrum from the blue-colored areas, which has not been assigned to any olivine-related structures. The appearance of 880 cm^{-1} peak may be explained by the reason of partial occupancy in tetrahedral sites of ringwoodite with Fe^{2+} (or oxidized to Fe^{3+}) as an acceptable theory, however which conflicts with the absence of 845 cm^{-1} peak as the main characteristics of SiO_4 antisymmetric stretching vibration in ringwoodite and the very weak one at 798 cm^{-1}peak. This uncertainty could be dissolve if, the structure is beginning to ordering into inverse spinel, and at the moment stage is represent a disordered unrelaxed ringwoodite structure. This possibility should be investigated in details. The spectrum of blue-colored area implies the presence of inverse spinel structure in it, or the presence of an intermediate phase may be a possibility at extreme conditions [3]. We assume that the observed 880 cm^{-1} peak in the Raman spectrum form the blue-colored areas can show the degree of the cation disordering in ringwoodite, resulting in the variaous cooling history even within the same aggregate.

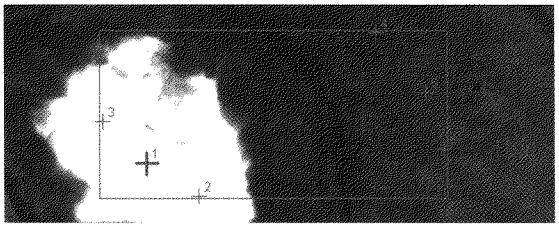

Fig. 1. *Six measured points (signed by red cross) in the selected ringwoodite aggregates from NWA 5011 meteorite. The numbers of 1, 2 and 3 correspond to colorless areas, and the numbers of 4, 5 and 6 to blue-colored areas. The width of picture is 150 μm. OM-image.*

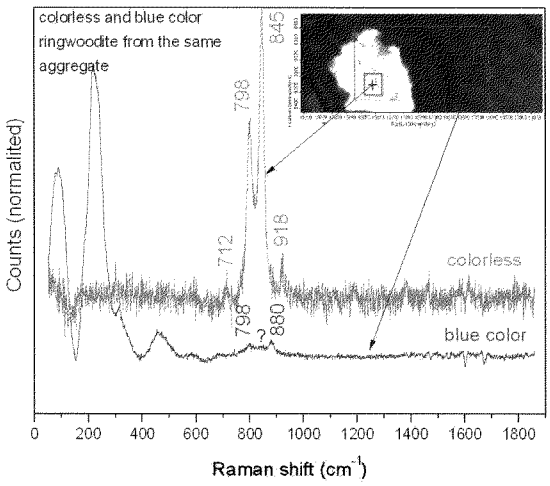

Fig. 2. *Raman spectra normalized by referring the intensities of colorless and blue-colored areas.*

References:

[1] Nagy Sz. et al., (2010) LPSC 41, Abs#1228. [2] Acosta T. E. et al., (2012) LPSC 43, Abs# 2725. [3] Kiefer B. et al., (1999) *Am. Min.*, 84, 288-293.

The morphology, distribution and modal abundance of graphite in monomict ureilites in relation to mg# of olivine core.

Y. Nakamuta[1], [1]Kyushu University Museum, Kyushu University, 6-10-1 Hakozaki, Fukuoka, 812-8581, Japan. (nakamuta@museum.kyushu-u.ac.jp)

Introduction:

Ureilites are ultramafic achondrites composed mostly of olivine and pyroxene with lesser amounts of elemental carbon, sulfide and metal[1,2]. Their high carbon content distinguished ureilites from other achondrites. The carbon occurs mostly as graphite, but shock-produced diamond and lonsdaleite have partly replaced graphite in many ureilites[3,4]. Their olivine compositions show large range of mg# (molar Mg / [Mg + Fe]) values (~ 76 - 92) at essentially constant Mn / Mg, which indicates that they are related to one another principally by various degrees of oxidation or reduction rather than various degrees of melting[5]. This redox relationship can be explained by smelting[6], simply expressed as

$$(Mg, Fe)_2SiO_4 + C = MgSiO_3 + Fe + CO.$$

In this reaction, gas of large molar volume appears only on the right-hand side, the reaction is expected to be strongly pressure sensitive. Smelting is suppressed at elevated pressure and promoted as pressure fall. Then, mg# of olivine is controlled by the depth at which it has been crystallized[5]. One observation which supports the smelting-model is a correlation between mg# and modal abundance of pyroxene in low-Ca pyroxene ureilites[5]. Many authors have sought a relation between carbon content and geochemical parameters and have found no correlation[2].

In this study, the modes of occurrence of carbon minerals in ureilites were observed by an optical microscope with a reflected light and SEM. The morphology, distribution and modal abundance of graphite before shock which have converted a part of graphite crystals into diamond were analyzed.

Results:

Carbon minerals in polished thin sections (PTS) of thirteen Antarctic ureilites, Y-791839, Y-74130, ALH 78019, Y-8448, Asuka 881931, Y-74123, Y-792663, Y-790981, Y-82100, Y-74154, ALH 77257, Y-74659 and Y-791538 were investigated. Micro-photographs of the whole sections of representative ureilites with various mg#s were shown in Fig. 1 and the relationship between mg# of olivine core and modal abundance of carbon was shown in Fig. 2. As shown in Fig. 1, euhedral blade-like shaped graphite crystal occurs preferentially in low-mg# ureilites and amoeboid-shaped interstitial graphite occurs mainly in ureilites showing mg#s higher than 80. The modal abundance of graphite shows the negative correlation with mg# of olivine core, supporting smelting-model of the ureilite asteroid.

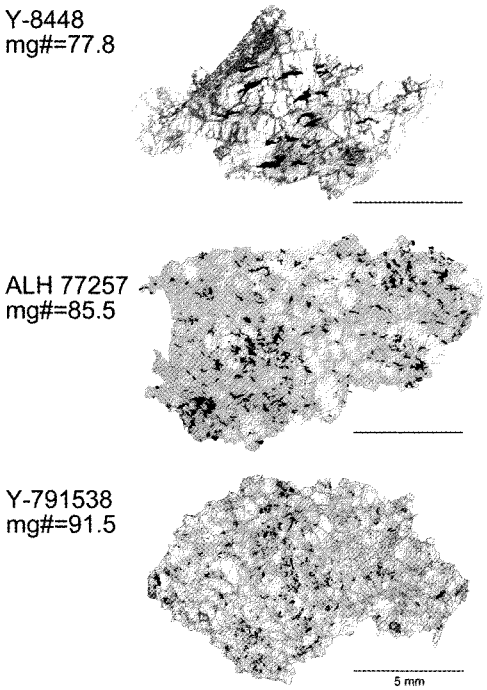

Fig. 1. Micro-photographs of representative ureilites showing morphologies and distributions of graphite (black in color).

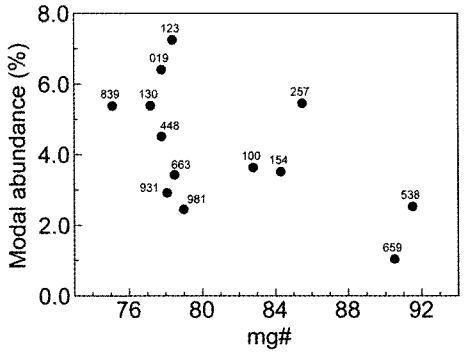

Fig. 2. Relationship between mg# of olivine core and modal abundance of carbon in monomict ureilites. Number of each plot shows last three letters of the name of each meteorite.

References:

[1] Goodrich, C. A. (1992) *Meteoritics, 27*, 327-352. [2] Mittlefehldt, D. W. et al. (1998) In *Planetary Materials* (ed. J.J. Papike), Mineralogical Society of America, *Rev. Mineral., 36*, 195pp. [3] Nakamuta, Y. and Aoki, Y. (2000) *Meteorit. Planet. Sci., 32,* 487-493. [4] Nakamuta, Y. and Toh, S. (2013) *Amer. Mineral., 98*, 574-581. [5] Goodrich, C. A. et al. (2004) Chemie der Erde, 6, 283-327. [6] Singletary, S. J. and Grove, T. L. (2003) *Meteorit. Planet. Sci., 38,* 95-108.

Thermoluminescence Study of Japanese Antarctic Meteorites XV. K. Ninagawa[1], S. Fukuda[1], N. Imae[2], and H. Kojima[2], [1]Okayama University of Science, [2]National Institute of Polar Research.

Induced TL (thermoluminescence), the response of a luminescent phosphor to a laboratory dose of radiation, reflects the mineralogy and structure of the phosphor, and provides valuable information on the metamorphic and thermal history of meteorites. Especially the sensitivity of the induced TL is used to determine petrologic subtype of unequilibrated ordinary chondrites [1]. Natural TL, the luminescence of a sample that has received no irradiation in the laboratory, reflects the thermal history of the meteorite in space and on Earth. Natural TL data thus provide insights into such topics as the orbits of meteoroids, the effects of shock heating, and the terrestrial history of meteorites [2]. Usually natural TL properties are applied to find paired fragments [3-5].

We have measured TLs of 193 Yamato and 136 Asuka unequilibrated ordinary chondrites [6]. This time we measured induced and natural TL properties of twenty-three Yamato unequilibrated ordinary chondrites (LL3: 1, L3: 15, H3: 7) from Japanese Antarctic meteorite collection. Sampling positions of these chondrites were measured by GPS.

As reliable pairing approach, TL properties within large chondrites were analyzed, taking advantage of the fact that serial samples from these meteorites are known to be paired. Then a set of TL pairing criteria: 1) the natural TL peak height ratios, LT/HT, should be within 20%; 2) that ratios of raw natural TL signal (LT) to induced TL signal (TL Sensitivity) should be within 50%; 3) the TL peak temperatures should be within 20℃ and peak widths within 10℃ was proposed [3].

Above pairing criteria were applied to the 23 samples. Figure 1 shows how to search fragments satisfying the pairing criteria 1) and 2). We found 12 TL potential paired fragments. They constructed one H3, and a large chained L3 group.

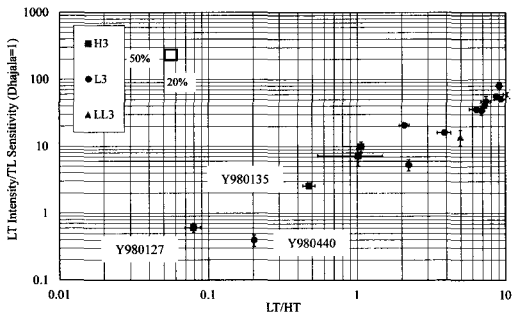

Fig.1. Ratio of LT to TL Sensitivity vs. LT/HT ratio to search fragments satisfying the pairing criteria 1) and 2).

Most of the chondrites had TL sensitivities over 0.1 (Dhajala=1), corresponding to petrologic subtype 3.5-3.9. Two chondrites, Y980465 (H3) and Y980576 (H3), were revealed to be primitive ordinary chondrites, petrologic subtype 3.2 and 3.3, respectively. They are not conflicted to olivine heterogeneity as shown in Fig.2. It is particularly significant in understanding the nature of primitive material in the solar system.

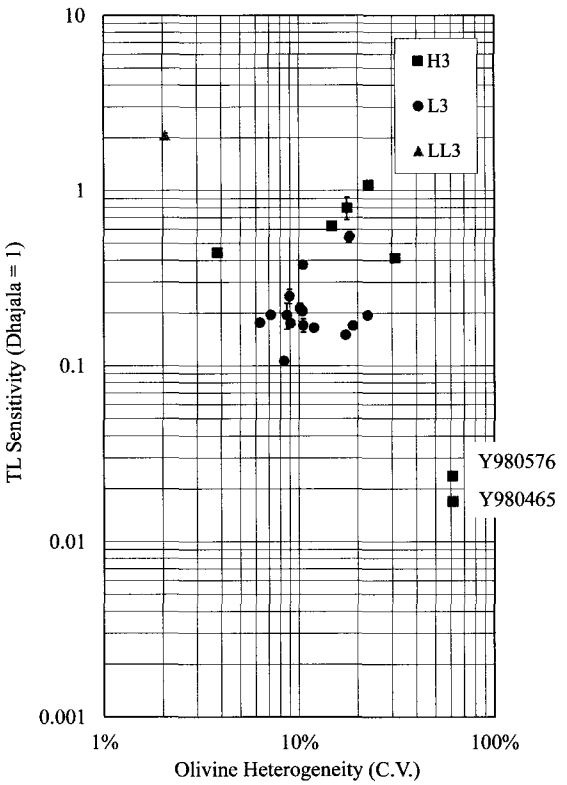

Fig.2. Dhajala-normalized TL sensitivity vs. olivine heterogeneity

References: [1] D. W. G. Sears et al. 1991. Proceedings of Lunar and Planetary Science 21:493-512. [2] P. H. Benoit et al. 1991. Icarus 94: 311-325. [3] K. Ninagawa et al. 1998. Antarctic Meteorite Research 11:1-17. [4] K. Ninagawa et al. 2002. Ant-arctic Meteorite Research 15:114-121. [5] K. Ninagawa et al. 2005. Antarctic Meteorite Research 18:1-16. [6]K. Ninagawa et al., 2012. 35th Symposium on Antarctic Meteorites (NIPR, Tokyo), 114-116.

Table Thermoluminescence data of unequilibrated Japanese ordinary chondrites

Meteorite	Class	Natural TL				Induced TL				LT /TL Sens. (x103)	Low Ca-Py Heterogenity (C.V.)†	Ol Heterogenity (C.V.)‡	Ol Subtype	Recom-mended Subtype	Sampling Location	
		LT/HT	LT (10^3 counts)	LT Peak Temp. (℃)	HT Peak Temp. (℃)	TL Sensitivity (Dhajala=1)	Peak Temp. (℃)	Width (℃)	TL Subtype							
Y980400	L3	6.39 ± 0.70	7.0 ± 0.7	223 ± 3	359 ± 7	0.20 ± 0.01	156 ± 2	145 ± 1	3.5-3.6	36 ± 4	37%	7%	3.9		35.148 E	72.070 S
Y980413	LL3	4.98 ± 0.03	28.6 ± 7.3	221 ± 7	361 ± 10	2.06 ± 0.07	164 ± 4	132 ± 0	3.8-3.9	14 ± 4	20%	2%			34.999 E	72.083 S
Y980422	L3	3.88 ± 0.40	2.7 ± 0.2	219 ± 0	351 ± 0	0.17 ± 0.00	155 ± 1	138 ± 1	3.5	16 ± 1	41%	19%	3.8		35.143 E	72.069 S
Y980423	L3	7.26 ± 0.06	7.0 ± 0.5	213 ± 3	365 ± 1	0.16 ± 0.00	153 ± 3	142 ± 1	3.5	42 ± 3	48%	12%	3.8		35.158 E	72.071 S
Y980439	L3	6.93 ± 0.13	8.8 ± 0.1	219 ± 5	357 ± 4	0.25 ± 0.02	167 ± 2	135 ± 1	3.5-3.6	35 ± 3	45%	9%	3.9		35.110 E	72.068 S
Y980440	L3	0.20 ± 0.00	0.1 ± 0.0	219 ± 11	367 ± 7	0.19 ± 0.03	122 ± 6	180 ± 3	3.5-3.6	0 ± 0	38%	9%	3.9		35.172 E	72.079 S
Y980446	L3	2.23 ± 0.09	1.1 ± 0.2	232 ± 6	363 ± 1	0.21 ± 0.01	139 ± 24	143 ± 2	3.5-3.6	5 ± 1	35%	10%	3.9		35.211 E	72.091 S
Y980448	L3	10.82 ± 0.15	12.6 ± 1.8	205 ± 1	349 ± 0	0.20 ± 0.01	163 ± 4	140 ± 0	3.5-3.6	61 ± 9	39%	10%	3.9		35.350 E	72.066 S
Y980452	L3	6.88 ± 0.10	6.1 ± 1.0	213 ± 5	355 ± 2	0.18 ± 0.01	147 ± 2	150 ± 1	3.5	35 ± 6	28%	6%	3.9		35.135 E	72.071 S
Y980465	H3		0.2 ± 0.0	237 ± 2		0.02 ± 0.00	95 ± 7	79 ± 6	3.2	9 ± 0	72%	61%	≤3.4	3.2	34.987 E	72.098 S
Y980472	H3				376 ± 1	0.44 ± 0.02	155 ± 0	122 ± 2	3.6-3.7		7%	4%			35.024 E	72.077 S
Y980484	L3	8.61 ± 0.31	9.5 ± 0.5	213 ± 1	349 ± 1	0.17 ± 0.02	144 ± 3	144 ± 0	3.5	56 ± 6	27%	11%	3.8		35.142 E	72.071 S
Y980505	L3	8.98 ± 0.06	30.5 ± 3.7	210 ± 1	343 ± 5	0.38 ± 0.01	154 ± 4	151 ± 1	3.6	81 ± 10	55%	11%	3.8		35.152 E	72.092 S
Y980576	H3		0.2 ± 0.0	218 ± 6		0.024 ± 0.000	82 ± 2	75 ± 1	3.3	7 ± 0	83%	61%	≤3.4	3.3	34.926 E	72.050 S
Y980588	L3	9.21 ± 0.86	9.0 ± 0.1	213 ± 1	343 ± 4	0.17 ± 0.00	114 ± 6	144 ± 2	3.5	51 ± 2	46%	9%	3.9		35.122 E	72.079 S
Y980597	L3	7.32 ± 0.54	7.0 ± 1.4	211 ± 4	357 ± 17	0.15 ± 0.00	129 ± 12	142 ± 3	3.5	47 ± 9	38%	17%	3.8		35.163 E	72.077 S
Y980768	L3		0.1 ± 0.0	213 ± 0		0.11 ± 0.00	154 ± 6	149 ± 1	3.5	1 ± 0	35%	8%	3.9		35.243 E	72.084 S
Y980056	H3	1.02 ± 0.47	4.5 ± 1.3	232 ± 2	362 ± 4	0.63 ± 0.03	160 ± 6	134 ± 2	3.7	7 ± 2	19%	15%	3.8		35.337 E	72.153 S
Y980057	H3	1.06 ± 0.02	8.0 ± 0.7	234 ± 4	364 ± 3	0.80 ± 0.12	157 ± 3	132 ± 0	3.7-3.8	10 ± 2	40%	18%	3.8	3.8	35.337 E	72.153 S
Y980127	H3	0.08 ± 0.01	0.7 ± 0.1	235 ± 2	369 ± 2	1.08 ± 0.06	152 ± 3	133 ± 4	3.8	1 ± 0	36%	23%	3.7		35.512 E	72.381 S
Y980135	H3	0.48 ± 0.05	1.1 ± 0.0	266 ± 0	366 ± 7	0.41 ± 0.02	169 ± 7	149 ± 3	3.6-3.7	3 ± 0	41%	31%	3.6	3.6	35.409 E	72.494 S
Y980180	L3	2.08 ± 0.16	11.3 ± 0.3	230 ± 1	346 ± 7	0.54 ± 0.04	157 ± 0	147 ± 3	3.7	21 ± 1	36%	18%	3.8		35.321 E	72.449 S
Y980331	L3	10.21 ± 0.62	11.6 ± 0.8	206 ± 3	337 ± 2	0.19 ± 0.00	165 ± 0	144 ± 2	3.5	60 ± 4	41%	22%	3.7		35.232 E	72.093 S

Mineralogical, Chemical, and Isotopic Heterogeneity in Zagami: Evidence for a Complex Petrogenesis. L. E. Nyquist[1], K. Misawa[2], C-Y. Shih[3], T. Niihara[3,5], J. Park[4,5]. [1]NASA Johnson Space Center, Houston, TX 77058, USA. [2]Natl. Inst. Polar Res., Tachikawa, Tokyo 190-8518, Japan. [3]Jacobs, Houston, TX 77058, USA. [4]Rutgers Univ., Piscataway, NJ 08854, USA. [5]Lunar Planet. Inst., Houston, TX 77058, USA.

Introduction:

Textural variations in the shergottite Zagami were initially interpreted as evidence that it formed in a heterogeneous lava flow [1, 2]. Variations in initial $^{87}Sr/^{86}Sr$ ratios between a Coarse Grained (CG) and a Fine Grained (FG) lithology [3,4] and evidence for more extensive fractionation of the Rb/Sr ratio in a Dark Mottled Lithology (DML) [2, 5] are consistent with such an interpretation. More recently, Niihara et al. [6] and Misawa et al. [7] have reported the mineralogy and Sr-isotopic systematics of an Olivine Rich Lithology (ORL) found in association with the coarse-grained DML lithology in the Kanagawa Zagami specimen [6,7]. Here we call this lithology DML(Ka) to maintain a distinction with DML(USNM) as studied by [2]. An Ar-Ar study by Park et al. [8] of a late stage K-rich melt enriched in K_2O to ~7% and intruded into ORL yielded an Ar-Ar age of 202±7 Ma. The present work extends the study of Kanagawa Zagami to Nd-isotopes.

Alkali (*e.g.*, Rb) and REE (*e.g.*, Sm) abundances:

Distinguishing features of the Kanagawa Zagami lithologies are their enrichments in trace elements compared to so-called Normal Zagami. Even the Dark Mottled Lithology (DML (Ka, 05)) that is host to the volumetrically smaller ORL (~1 cm^3 in ,54) appears to be somewhat enriched in Sm compared to the CG and FG Normal Zagami lithologies and a DML subsample obtained from the US National Museum specimen USNM 6545 (Fig.1).

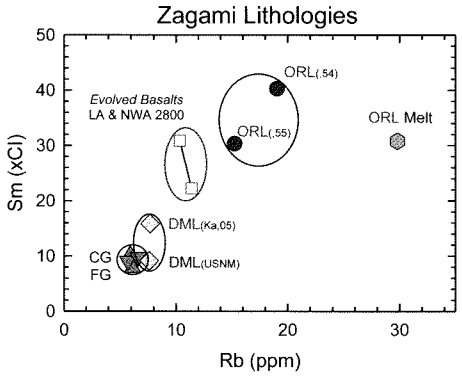

Figure 1. Sm and Rb abundances in Zagami lithologies. CG and FG are Normal Zagami lithologies, DML was obtained from the US National Museum USNM 6545, courtesy of T. McCoy. DML (Ka,05) was sawdust from cutting the DML end of Kanagawa Zagami and contains ~5% admixture of ORL. ORL(,55) was sawdust from cutting ORL, whereas ORL(,54) was a bulk (WR) sample of subsample ,54 used for isotopic studies. ORL Melt was an ~9 mg portion of the dark, late-stage, K-rich melt found in association with ORL.

(Our DML sawdust sample ,05 is estimated to contain ~5% ORL admixture). ORL and "ORL Melt" are enriched in Sm and other REE by about fourfold compared to the Normal Zagami lithologies. The Rb enrichments in ORL are somewhat smaller. ORL Melt found in association with ORL occurs as dark clusters a few mm^3 in volume associated with ORL. Its ~4X enrichment compared to Normal Zagami in the subsample used for isotopic studies is accompanied by an even greater enrichment in K in this lithology. K was found to be heterogeneously distributed in eight subsamples of ~42-315 μg studied for Ar-Ar chronology. The material in those samples had crystallized mostly to pyroxene containing irregular areas of enrichment in K and/or phosphate [8].

Heterogeneity in initial $^{87}Sr/^{86}Sr$:

Studies in 1995 and repeated in 2006 [3,4] showed FG Normal Zagami to have a significantly higher initial $^{87}Sr/^{86}Sr$ ratio than CG Normal Zagami (Fig. 2). A 2010 study of DML from USNM 6545 showed it to have the same initial $^{87}Sr/^{86}Sr$ ratio as CG [5], but the Rb-Sr study of ORL by [7] yielded initial $^{87}Sr/^{86}Sr$ lower than in CG, providing further evidence of heterogeneity in the initial Sr-isotopic composition among different lithologies.

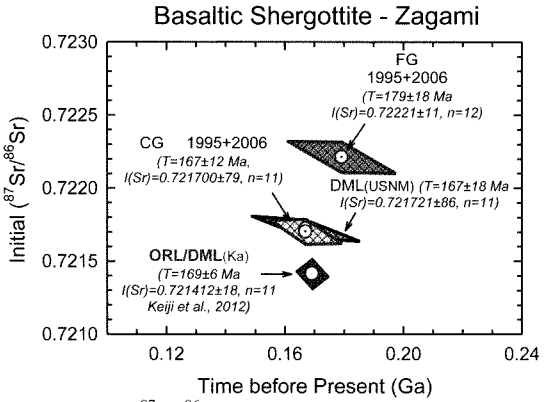

Figure 2. Initial $^{87}Sr/^{86}Sr$ vs. Rb-Sr isochron age for Zagami lithologies.

Heterogeneity in initial $^{143}Nd/^{144}Nd$:

Fig. 3 shows Sm-Nd-isotopic data for ORL(Ka ,55) and DML(Ka ,05) sawdust, ORL Melt, and subsamples of ORL (Ka ,54). The data for the two sawdust samples are nearly identical, consistent with differentiation of ORL from its host DML(Ka), although ORL is greatly enriched in trace elements (Fig. 1). As expected, WR1, a bulk sample of ORL(Ka ,54) also shares very similar Sm-Nd isotopic data. WR2(1), a leachate of a second whole rock (bulk) sample has only a slightly lower $^{147}Sm/^{144}Nd$ ratio, as expected if most of the REE are

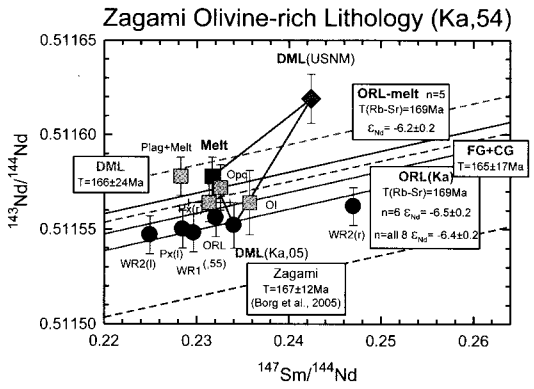

Figure 3. Sm-Nd data for ORL and ORL Melt. Red circles: Bulk samples and leachates, except for WR2(r). Dark blue square: ORL Melt. Light blue squares: density separates. Light green diamond: Bulk analysis of DML(USNM) [5].

in easily leachable phosphate minerals. However, the residue after leaching (WR2(r)) has a lower $^{147}Sm/^{144}Nd$ ratio than expected, suggesting that phosphates were not totally removed in the leaching process. ORL is observed petrographically to contain coarse-grained merrillite, probably the phosphate mineral contributing most REE to the leachates. These data are slightly displaced beneath an 165±17 Ma reference isochron calculated from the combined data for (FG+CG) Normal Zagami (Fig 4).

The data for ORL Melt and mineral separates are displaced towards higher $^{143}Nd/^{144}Nd$ ratios than for the whole rock and leachate samples. Mineral separation was by heavy liquids. (Plag+Melt) of density <2.85 g/cm^3 was observed to contain a significant melt component. "Px" of density 2.85-3.7 g/cm^3 was observed to contain pyroxene, melt, and phosphates. This sample was leached in 2N HCL for 10 min. to generate a leachate "Px(l)" and residue "Px(r)". "Ol" of density 3.7 g/cm^3 was observed to contain olivine and melt. "Opq" was observed to contain opaque minerals like spinel. Of these samples, the Sm-Nd data for the leachate Px(l) plots close to the bulk sample WR1 and the leachate WR2(l). However, Px(r) and Opq have $^{147}Sm/^{144}Nd$ that are very close to that of ORL Melt and much higher REE abundances than expected. Most of the Sm and Nd in these samples came from melt contaminants. Melt was observed in thin section to intrude maskelynite and elsewhere in ORL. The K-rich melt was observed to contain fine-grained phosphates, which would contribute REE to these samples.

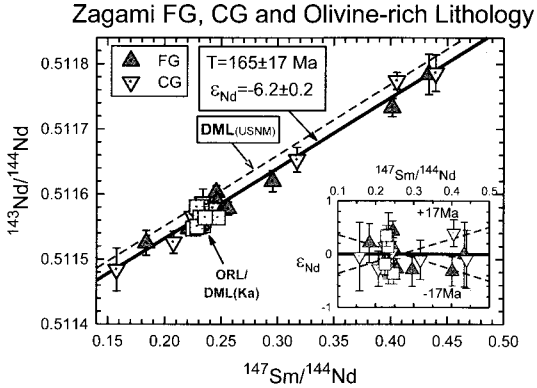

Figure 4. Sm-Nd data for combined CG, FG, ORL, and ORL Melt.

As shown in Fig. 5, in spite of the similarity in initial $^{87}Sr/^{86}Sr$ between DML and CG, initial $^{143}Nd/^{144}Nd$, expressed as ε_{Nd}, was found to be slightly higher in DML than in FG and CG [5]. In this study, we find ε_{Nd} of both DML (Ka) and ORL to be slightly lower than in CG and FG, but perhaps within uncertainty of the value for these Normal Zagami samples. The disagreement between the ε_{Nd} values of DML(USNM) and DML(Ka) is puzzling, but suggests (a) "high" and variable $^{143}Nd/^{144}Nd$ in DML, and (b) some contribution from DML to ORL Melt. Sawdust DML(Ka) has some contribution from DML, also.

Initial $^{87}Sr/^{86}Sr$ more strongly distinguishes among shergottite lithologies than do the ε_{Nd} values, and also distinguishes DML(Ka) from DML(USNM). The high initial $^{87}Sr/^{86}Sr$ in FG normal Zagami is slightly lower than that measured for Shergotty, whereas the lower initial $^{87}Sr/^{86}Sr$ for ORL is slightly greater than that of Los Angeles (Fig. 5).

Conclusions:

Localized differentiation was important in producing the variety of lithologies observable in Zagami. Heterogeneity in initial Sr- and Nd-isotopic compositions and initial trapped $^{40}Ar/^{36}Ar$ ratios close to the Martian atmospheric composition [8] and possibly relict radiogenic ^{40}Ar suggest that complex models are required to understand the petrogenesis of Zagami and other enriched shergottites. Such models may involve magma recharge, magma mixing, and crustal assimilation occurring in an upper crustal magma chamber.

References:[1] McCoy T. J. et al. (1992) GCA, 56, 3571-3582. [2] McCoy T. J. et al. (1995) LPS XXVI, 925–926. [3] Nyquist L. E. et al. (1995) LPS XXVI, 1065–1066. [4] Nyquist L. E. et al. (2006). Meteorit. Planet. Sci., 41, A135. [5] Nyquist L. E. et al. (2010) Meteorit. Planet. Sci., 45, A154. [6] Niihara T. et al. (2012) 75th Ann. Met. Soc. Mtg., Abst #5075. [7] Misawa K. et al. (2012) 75th Ann. Met. Soc. Mtg., Abst #5190. [8] Park J. et al. (2013) *LPS XXXXIV*, abs. 2556.

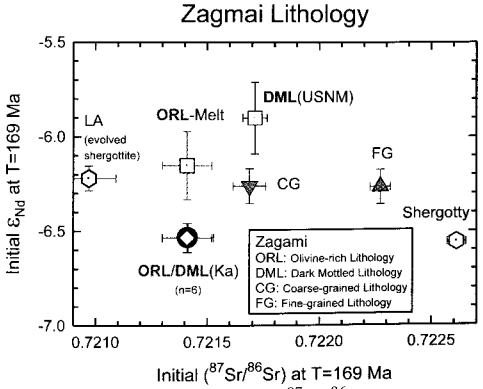

Figure 5. Summary of initial $^{87}Sr/^{86}Sr$ and ε_{Nd} values in Zagami lithologies for an age of 169 Ma.

Impact and igneous processes on a ureilite parent body inferred from Y-983890 polymict ureilite.

S. Ozawa[1, 2], A. Yamaguchi[1] and H. Kojima[1]

[1]National Institute of Polar Research, Japan,
[2]Department of Earth Science, Graduate School of Science, Tohoku University, Japan.

Ureilites are the second most common achondrites. They are largely divided into two types: monomict and polymict. Monomict ureilites are unbrecciated ultramafic rocks mainly composed of coarse-grained olivine and pyroxene with interstitial carbonaceous materials. They are thought to be residues left after partial melting of precursor materials at asteroidal interiors. However, any basaltic counterpart to the ultramafic residues has not been identified as meteorite. On the other hand, polymict ureilites are polymict breccias which consist of lithic clasts and mineral fragments of various lithologies [1]. Among these clasts, feldspathic clasts and chondritic clasts are important to understand igneous and impact processes on ureilite parent bodies, respectively. Feldspathic clasts contain feldspar or feldspathic glass which is basically absent in monomict ureilites. Therefore, feldspathic clasts in polymict ureilites can be fragments of basaltic counterparts to monomict ureilites. Whereas, chondritic clasts are considered to be fragments of impactors collided with the ureilite parent bodies.

In this study, we examined feldspathic and chondritic clasts in Yamato (Y-) 983890 polymict ureilites. Through careful petrographic observations on these clasts, we try to understand impact and igneous processes on a ureilite parent body.

We identified four distinct populations of feldspathic clasts in Y-983890: (a) Albitic clasts, (b) Labradoritic clasts, (c) Anorthitic clasts and (d) Glassy clasts.

Albitic clasts are characterized by albitic plagioclase ($Ab_{76-91}Or_{1-5}$) in association with pigeonite ($En_{70-85}Wo_{7-10}$, mg#=77-92) and/or olivine (Fo_{74-76}) and/or augite ($En_{41-56}Wo_{37-38}$, mg#=65-90). Many fractures are observed inside the plagioclase, which are filled with weathering products (Fe-O-H). The plagioclase, olivine and pyroxenes are similar in grain size (~100 μm in diameter). One albitic clast shows a distinct texture, consisting of large albitic plagioclase ($Ab_{84-89}Or_{2-4}$) and fine-grained intergrowth of albitic plagioclase laths ($Ab_{88-91}Or_{4-7}$), augite ($En_{31-38}Wo_{12-21}$, mg#=35-48) and K-rich mesostasis.

Labradoritic clasts are characterized by labradoritic plagioclase ($Ab_{40-45}Or_0$), orthopyroxene ($En_{78}Wo_5$, mg#=82) and augite ($En_{51-65}Wo_{30-41}$, mg#=84-92). The pyroxenes are subhedral. Fractures filled with Si-rich mesostasis are also observed.

Anorthitic clasts are mainly composed of large (50-500 μm) idiomorphic anorthite ($An_{90-92}Or_0$) with thin augite ($En_{45-56}Wo_{40-43}$, mg#=78-93) lamellae inside the anorthites.

Glassy clasts are composed of albitic glass ($Ab_{74-85}Or_{5-10}$) with idiomorphic pyroxene phenocrysts. The pyroxene phenocrysts are highly magnesian in composition and zoned from enstatite core ($En_{92-99}Wo_1$, mg#=93-100) to augite ($En_{56-62}Wo_{37-46}$, mg#=96-99) rim.

Anorthite contents in plagioclase and Fe/Mg ratios in coexisting pyroxene of these feldspathic clastsare plotted along the fractional crystallization trends by Cohen et al. (2004) [4] except for "Glassy clasts". It suggests that feldspathic clasts in Y-983890 can be formed by fractional crystallization of partial melts derived from the precursor materials proposed in [4]. The residues of the partial melting also correspond to monomic ureilites. Therefore, feldspathic clasts in Y-983890 can be basaltic counterparts to monomict ureilites.

Chondritic clasts include two types. One is dark clasts consisting of fine-grained phyllosilicate-rich matrices with variable amounts of opaque minerals such as magnetite, pyrrhotite and pentlandite. The dark clasts mineralogically resemble the matrices of CI carbonaceous chondrites. Another is a chondrule fragment with a barred olivine chondrule texture. It is composed of olivine (Fo_{81}) with a mesostasis of albitic composition ($Ab_{86-88}Or_{6-7}$). The chemical composition of the olivine suggests that this is a fragment of H chondrite. The CI- and H-chondrite-like materials are considered to be fragments of impactors collided with the parent body of Y-983890.

References:

[1] Goodrich C. A. et al. (2004) Chemie der Erde, 64, 283–327. [2] Yamaguchi A. et al. (2012) Meteorite Newsletter, 21. [3] Goodrich C. A. (1992) Meteoritics, 27, 327–352. [4] Cohen B. A. et al. (2004) GCA, 68, 4249–4266.

Ordinary Chondrite classification by Raman Spectroscopy. L. Pittarello[1,2,3], V. Debaille[2], W. DeVos[3], and Ph. Claeys[1] [1]Earth System Science, Vrije Universiteit Brussel, Brussels, Belgium; [2]Université Libre de Bruxelles, Brussels, Belgium; [3]Royal Belgian Institute of Natural Sciences, Brussels, Belgium.

Introduction:

Antarctic expeditions return more and more meteorites [1], which have to be classified. Statistically most of them are ordinary chondrites [2]. The classification of ordinary chondrites is based on at least two analytical steps: chemical composition and petrography [3]. The composition of olivine and low-Ca pyroxene, especially molar contents of fayalite (Fa) and ferrosilite (Fs), is sufficient to assign them to H, L, or LL grouping. Analysis of these minerals is commonly performed with expensive and time-consuming techniques, such as electron microprobe (EMPA) or quantitative energy-dispersive x-ray spectroscopy (EDX) by scanning electron microscopy (SEM), in comparison with standards and mineral formula recalculation. These analytical techniques require specific sample preparation, which includes fine polishing of the surface and carbon coating, and exceptional operation condition, such as high vacuum. Petrographic observations are made in both reflected and transmitted light on polished thin sections.

In this work, we propose to use Raman spectroscopy for the compositional characterization of ordinary chondrites instead of electron microscopy. Raman spectroscopy has been already used for meteorite characterization, but mostly for possible *in situ* analyses of lunar and martian rocks e.g., [4] and [5]. Here, we present a calibration curve for olivine composition evaluation by Raman spectroscopy for a Type 3 meteorite. The method has been tested on a few meteorites already classified with the usual procedure, and gives consistent results for olivine composition.

Sample description and methods:

A Type 3 ordinary chondrite that provides a wide range of possible olivine composition in meteorites has been chosen for the calibration. Olivine in 16 chondrules was analyzed with at least 3 and 5 point-analyses per chondrule for Raman and EDX respectively (Fig. 1).

For Raman spectroscopy two instruments have been used. The first is a confocal Raman microscope LabRAM HR Evolution (HORIBA Scientific), equipped with a multichannel air-cooled CCD detector (spectral resolution <1cm-1, lateral resolution 0.5µm, axial resolution 2µm), with a solid-state laser corresponding to green light (532nm), at the Vrije Universiteit Brussel (VUB). The second is a SENTERRA Dispersive Raman Microscope (BRUKER), equipped with a thermoelectrically cooled CCD (ANDOR DU420-OE) with a spectral resolution of ~9 cm^{-1} in the 100-4000cm^{-1} range (50x1000µm slit) and a continuous automatic calibration (0.1cm^{-1} accuracy) with a solid-state laser corresponding to green light (532nm) at 2mW for excitation at the Royal Belgian Institute of Natural Sciences (RBINS). The Raman spectra have been processed in Microsoft Excel, filtered for automatic peak detection [6] and for average and standard deviation calculation.

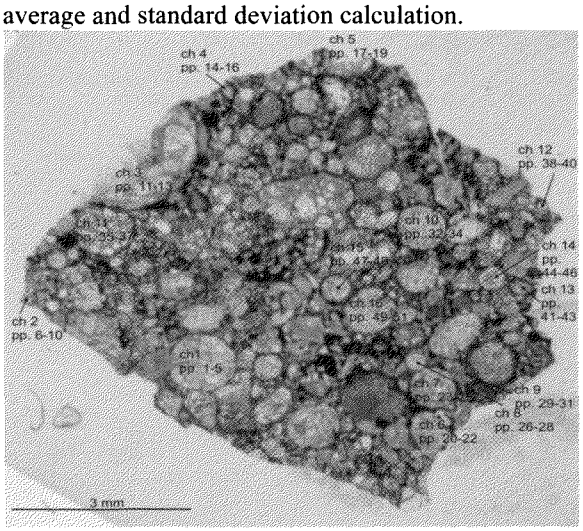

Fig. 1. *Scan of the selected polished thin section used for the Raman calibration. The analyzed chondrules (ch) are marked. The number of points (pp.) refers to Raman spectroscopy.*

The composition of olivine in the selected chondrules was determined with a FEI-Inspect-S SEM at the RBINS, equipped with back-scattered electron and EDX detectors. The quantitative analyses were calibrated by comparison with olivine standards from the series MINM 25-53 of the Astimex Scientific Limited.

Calibration curve for olivine:

The typical Raman spectrum of olivine (Fig. 2) presents two major peaks with Raman shift of ~818 and ~846 cm^{-1} in green light for standard fayalite [7]. Between the olivine end-members fayalite and forsterite, the Raman shift of these two peaks seems to have a linear correlation with the Fa content [5]. We focused on these peaks and evaluated the average Raman shift in each chondrule. The standard deviation of Raman shift in a chondrule (at least 3 measurements) is less than 0.06%. Figure 3 shows the correlation between the average Fa content and the respective Raman shift of the selected peaks in the investigated chondrules. The standard deviation for olivine composition as determined by quantitative EDX analysis on 5 grains per chondrule corresponds to less than 2%. The range of Fa content is limited to 0-50 in the investigated Type 3 chondrite (Fig. 3). Nevertheless, this portion of our correlation curve is consistent with data in literature (e.g., Fig. 8a in [5]).

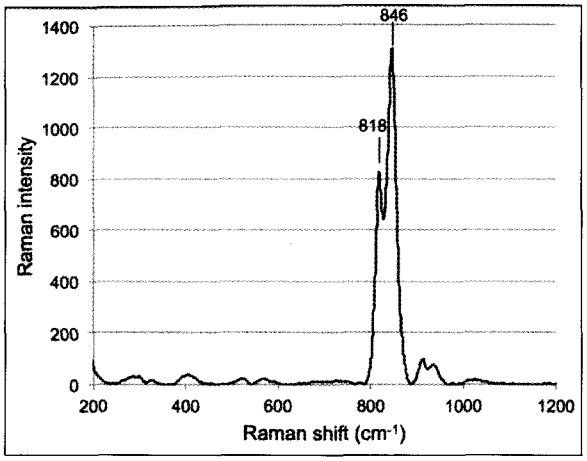

Fig. 2. Raman spectrum for a standard sample of fayalite [7].

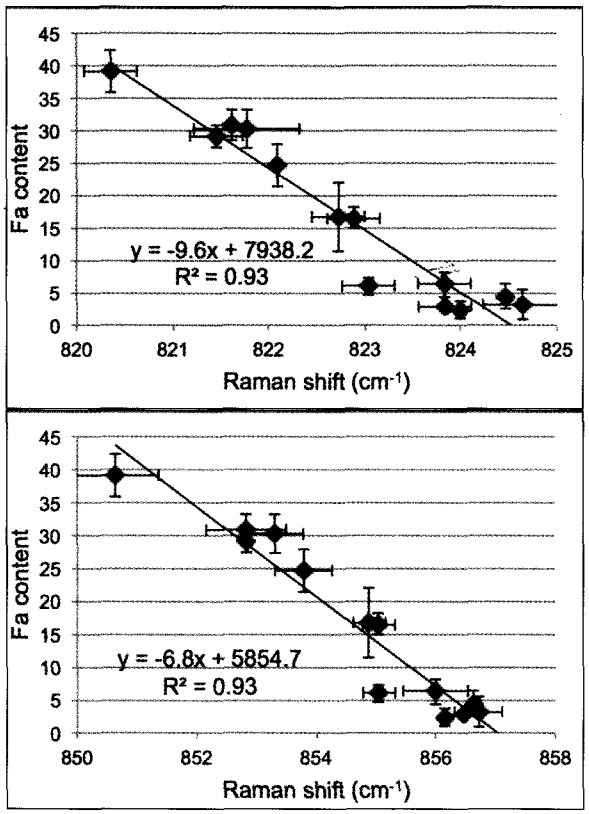

Fig. 3. Correlation between the average Fa content and the wavelength shift of the two major Raman peaks for olivine. The error bars represent the standard deviation between measurements within the same chondrule.

Reliability of the correlation curve:

A preliminary check was performed on highly equilibrated ordinary chondrites, with negligible variation of Fa content in olivine. We compared the Fa content as determined by Raman spectroscopy with that calculated by EDX composition. Although only a few samples have been investigated, the technique has given results consistent with EMPA.

A major concern about the reliability of the correlation curve is the presence of shocked olivine. Shocked olivine exhibits a Raman spectrum with a lower shift of the two characteristic peaks, progressively reaching the typical wavelength shift for ringwoodite, a high-pressure polymorph; e.g., [8] and [9]. In fact, the Raman spectroscopy has been extensively used to constrain shock metamorphism in olivine [10]. Although shocked olivine in our samples is generally localized along shock veins, which can be easily identified with the optical microscope, a check of the composition with electron microscopy might be necessary for shocked meteorites.

Conclusions:

The use of Raman spectroscopy is a promising alternative to electron microscopy for the chemical classification of ordinary chondrites. In particular, a correlation curve between the Raman shift of the two main peaks of Raman spectrum for olivine and the Fa content shows a way forward. This approach will also be applied to low-Ca pyroxene to evaluate the Fs content. Our long-term goal is to classify an ordinary chondrite by the use of Raman and optical microscopy.

This technique does not require carbon coating of the sample, which should be cleaned for the petrographic observations, and in addition, the petrological type can be determined at the microscope at the same time as the chemical grouping, reducing the classification of ordinary chondrite to a single step process.

Acknowledgments:

A special thank to the National Institute of Polar Research in Tokyo (Japan) for loan of a thin section (provisional sample name A09178). Other samples used in this study belong to the RBINS, Brussels, Belgium. Kitty Baert of the VUB and Christian Burlet of the RBINS are thanked for Raman assistance.

References:

[1] Harvey R. (2003) *Chem. Erde-Geochem.*, 63, 93–147. [2] Nagata T. (1982) *Adv. Space Res.*, 2, 3–11. [3] Weisberg, M. K. et al. (2003) in Meteorites and the Early Solar System II, D. S. Lauretta and H. Y. McSween Jr. (eds.), Univ. of Arizona Press, Tucson, 943 pp., p.19-52. [4] Haskin L.A., et al. (1997) *JGR*, 102, 19,293-19,306. [5] Wang A. et al. (2004) *J. Raman Spectrosc.*, 35, 504–514. [6] Copyright (c) 2013, Thomas C. O'Haver (toh@umd.edu). [7] American Museum of Natural History B06-045, RRUFF catalog R100102.2. [8] Miyamoto M. and Ohsumi K. (1995) *Geophys. Res. Lett.*, 22, 437-440. [9] Walton E.L. (2013) *Geochim. Cosmochim. Acta*, 107, 299-315. [10] Farrel-Turner S. et al. (2005) *Meteorit. Planet. Sci.*, 40, 1311-1327.

The Importance and Relevance of Meteorite Collection and Curation to Meteoritic Research – Past, Present and Future. C. L. Smith[1,2,3]. [1]Department of Earth Sciences, The Natural History Museum, Cromwell Road, London, SW7 5BD, United Kingdom. [2]European Space Agency ESTEC, Keplerlaan 1, 2200 AG Noordwijk, The Netherlands. [3]UK Space Agency, Atlas Building, Harwell Science and Innovation Campus, Didcot, Oxfordshire, OX11 0QX, UK.

Introduction:

Meteorites are some of the rarest, most precious and valuable geological materials available for scientific study, thus the curation of these important materials is of critical importance. Meteorite curation covers the care and management of the physical specimen but importantly, also covers the recording and archiving of many types of information related to individual specimens, such as recovery and collection, sub-sampling and use of the specimens and details of results or specific analyses undertaken.

The birth of meteorite curation and research - the 18th and 19th centuries:

Prior to the late 18th century meteorites were considered to be little worthy of scientific study and very few specimens have been preserved. Two notable exceptions are the Nogata meteorite, which fell 19th May, 861 and the Ensisheim meteorite, which fell 7th November, 1492. The recovery and preservation of these samples is very unusual and solely down to the circumstances and locations of their falls; the Nogata meteorite falling close to a Shinto shrine and the Ensisheim meteorite falling at a time of great political turmoil in that region of Europe [1,2]. The modern science of meteoritics and meteorite curation can be considered as beginning in the 1760s with the witnessed fall and recovery of the Albaretto and Lucé meteorites. Lucé is the first meteorite for which detailed eyewitness accounts of the fall were recorded and, importantly, the first sample to be chemically analyzed [3]. However, it was not until the last two decades of the 18th century that meteorites became the subject of sustained and detailed scientific scrutiny and even then their extraterrestrial origin was still doubted by many of the scientific elite of the time.

New opportunities for curation and research – the 20th century:

The 20th century saw tremendous technological advances in a wide variety of analytical techniques used to study meteorites, however the number of meteorites available for study was not increasing at a corresponding rate. Prior to the late 1960s there were approximately 2100 known meteorites curated in museum and university collections around the world and of these, approximately 40% were witnessed falls. The 1960s saw the start of dedicated fireball observation programs. These had the dual aims of gaining a better understanding of fireball phenomena and the potential for recovering meteorites from observed fireballs. Three programs operated in Canada, the United States and Europe with varying degrees of success and of the three the European network is the only one still operating [4-6].

1969 was an extremely important year for meteoritics. A "tantalizing" discovery of nine meteoritic stones in the Yamato Mountains region of Antarctica by the Japanese Antarctic Research Expedition heralded new strategies for meteorite collection and curation [7,8]. This fortuitous discovery led to the realization that Antarctica is an extremely fertile region for meteorite collection, owing to the favourable environmental conditions for sample preservation and concentration [9]. To date, just over 31,000 meteorites have been recovered from the Antarctic continent [10]. The same year, Apollo 11 astronauts returned the first Moon rocks to Earth. These priceless samples were sent to the Lunar Receiving Laboratory in Houston for initial characterization and curation. This laboratory was the first purpose built facility for the analysis and curation of extraterrestrial samples [11].

In the latter part of the 20th century it was recognized that hot desert regions were also favourable meteorite hunting grounds, with the dry environment preserving meteorites and the sparse vegetation aiding visual searching [12]. To date more than 10,000 meteorites have been recovered from hot deserts worldwide [10].

Meteorite curation today and tomorrow – challenges and opportunities:

'The Curator's Dilemma': The ever increasing collection of meteorites and the accompanying scientific study of them have posed some interesting challenges for the scientific curatorial staff that care for and manage collections. There are, perhaps, three major challenges presently faced by meteorite curators: 1) *Maintaining access to the collection whilst preserving material for future generations.* Although modern analytical techniques allow for the analyses of relatively small samples and sub-samples, the major meteorite collections are receiving increasing numbers of requests for material from researchers. Careful consideration of each loan request is a necessity to ensure the most appropriate samples are being allocated for each research project. In some circumstances it is not possible to fulfill requests for samples, which can lead to tensions between curators and researchers. 2) *Protecting the collection from damage/contamination whilst*

maintaining access. Rapidly recovered fall meteorites and those collected in Antarctica are considered to be the least contaminated of all samples and so are most appropriate for the majority of scientific investigations. Storage and handling of samples will always add a risk of contamination, however careful curatorial practice can minimize this risk, through the use of appropriate storage materials and environments and the recording of curatorial actions. 3) *Acquiring new specimens for the collection whilst competing in a commercial market and fulfilling legal/ethical requirements*. Collections that curate non-Antarctic meteorites are dependent on acquiring meteorites through field collecting, exchanging with other institutions or through purchase/exchange with commercial dealers and collectors. Meteorite falls, which are often the most scientifically relevant owing to the lack of contamination, have high monetary values as do rare or particularly unusual meteorite types. With limited resources it may only be possible to acquire very small amounts of particularly interesting specimens, which is problematic as these are the most requested samples. Some countries have laws that prohibit the removal of meteorites without the required permits so ensuring that specimens have not been illegally or illicitly removed is also significant issue for consideration.

Sample return space missions and 'end to end curation': Since the Apollo missions, only three space missions have successfully collected extraterrestrial samples and returned them to Earth – NASA's Genesis mission (solar wind particles) and Stardust mission (cometary and interstellar particles) and JAXA's Hayabusa mission (asteroidal material). Over the coming decades a number of missions are programmed, or are in the planning stages, to visit Solar System bodies and return samples. NASA's OSIRIS-Rex, JAXA's Hayabusa 2 and ESA's MarcoPolo-R are all asteroid sample return missions and there are early-stage proposals for missions to visit Phobos, Mars and the Moon. A major driver for all these sample return missions is to provide the international scientific community with samples that are uncontaminated by terrestrial materials, which otherwise could compromise various science results, for example detection of organic molecules of astrobiological significance.

Whilst it is obvious that samples will need to be curated once they are returned to Earth, curation also plays a critical part in the planning stages of sample return missions. For example, in the same way that meteorite samples are carefully collected during Antarctic field work, samples collected by 'robotic geologists' will also require careful collection and handling to prevent possible contamination and damage to the sample. Similarly, how the samples are stored for return to Earth is also important. Storage vessels need to be designed so that the samples are protected during transit and landing on Earth and made from materials that are inert and un-reactive to the specimens they contain. Once the samples are received in the curation facility the prime concern is to retain their scientific integrity. Thus, they need to be stored under stringent environmental conditions e.g. ultra clean, inert atmosphere or under vacuum, and for Mars samples in a biologically sterile environment. These will be some of the most desirable samples available for study and so the curation facility must also be able to prepare samples for study and then manage and track the movement and use of samples by the scientific community. Thus, curation of sample return samples should be considered as 'end to end' – curation is a critical element from the first stages of mission planning to the long-term care and management of samples for perhaps many decades post-return.

Concluding remarks:

Since the birth of meteoritics as a scientific discipline in the late 18th century, collection, curation and research have progressed hand in hand. The increasing numbers of meteorites collected and the developments in a wide variety of analytical techniques used to study them has necessitated a close, but occasionally tense, relationship between scientific curators and researchers. Meteorite curation and research continue to support each other through a 'virtuous circle' of well-curated and appropriate materials supporting internationally significant research. This in turn supports and justifies both the continuing existence of collections and the enhancement of them though the acquisition of new samples. Technologies developed and experience gained in the curation of meteorites, cosmic dust, Apollo, Genesis, Stardust and Hayabusa samples has provided a solid foundation of knowledge and experience of how to successfully curate some of the rarest specimens on Earth. International teams are applying this curatorial legacy in planning for the next phases of Solar System exploration through sample return space missions.

References:

[1] Shima M. et al. (1983) *Meteorit.*, 18, 87-102. [2] Marvin U. B. (1992) *Meteorit.*, 27, 28-72. [3] Marvin U. B. *in* McCall G. J. H. et al. (2006) *Geol. Soc. London Sp. Pub.*, 256, pp15-71. [4] Oberst J. et al. (1998) *Meteorit. Planet. Sci.*, 33, 49-56. [5] McCrosky R. E. and Boeschenstein H., Jr (1965) *SAO Special Report* #173. [6] Halliday I. et al. (1978) *J. Roy. Astr .Soc. Can.*, 72, 15-39. [7] Shima M. et al. (1973) *EPSL*, 19, 246-249. [9] Nagata T. (1976) *Meteorit.*, 11, 181-184. Harvey R. (2003) *Chemie der Erde*, 63, 93-182. [10] *Meteoritical Bulletin Database*. [11] Mangus S. and Larsen W. (2004) *NASA/CR-2004-208938*. [12] Bevan A. W. R. *in* McCall G. J. H. et al. (2006) *Geol. Soc. London Sp. Pub.*, 256, pp. 325-343.

Surface features of the Chelyabinsk meteorite fragments.

N.Sugiura[1], [1]University of Tokyo.

Introduction:

Fireball explosions are explained as a result of rapid increases in (1) the air density and (2) cross-sectional area of a meteoroid during the descent. The latter is due to disintegration of the meteoroid which occurs when the ram pressure (air density x velocity x velocity) exceeds the material strength. However, the nature of the disintegration is not clear; it could be related to compressive strength or tensile strength. Also, if we consider that smaller rocks are generally stronger than larger rocks, this tends to suppress disintegration of small fragments. Therefore, it is not clear if a fireball explosion is well understood. Surface features of meteorite fragments may afford evidence concerning how and where they separated from the main meteoroid body. They may also tell us physical conditions in a fireball. This is a preliminary study on surface features of the Chelyabinsk meteorite fragments.

Chelyabinsk fireball:

According to [1], the main explosion continued for 1.2 seconds during which the meteor travelled ~23 km. Because of the shallow flight angle (~17 °, [2]) the altitude decreased only by 7 km during the explosion. This corresponds to an increase in the air density by a factor of 2.4 (assuming an exponential atmosphere with a scale height of 8 km). This means (assuming a constant velocity) that every part of the Chelyabinsk meteoroid has material strength within a factor of 2.4. This is a very small range.

Surface morphological features of Chelyabinsk meteorite fragments:

There are many fragments of the Chelyabinsk meteorite. It is to be noted that most of my observations in this study were made by looking at pictures shown on web sites. The fragments are divided into several groups based on the degree of ablation that they experienced.

(1) Small size (peas and buttons):

These are small (< 1g) well ablated fragments. Peas are spheroidal whereas buttons are hemispherical with a flat rear face. Presumably, the buttons formed by breakup of peas. Rollover lips are often observed on peas. This suggests that their flights were not oriented during the early part of their flights resulting in spherical shape. Then, later on, the angular momentum was lost by the ablation and their flights became oriented and formed rollover lips. Since these small meteorites are found in the foreground of the strewn field [3] they are likely to have separated from the main body at a high (~90 km?) altitude.

(2) Intermediate size with smooth surfaces:

There are many smooth-surface sub-rounded fragments which weigh ~10 g and are completely covered with fusion crusts, suggesting un-oriented flight during ablation. The roundness suggests that they experienced considerable ablation, perhaps losing more than ~80% of the initial mass of the fragments at their breakup from the main body. I suggest that they separated from the main body before the main explosion.

(3) Large size and irregular shape:

This group is further divided into three subgroups.

(a) Fully crusted:
This group is distinguished from the intermediate size group by the irregular (non-rounded) shape which indicates that the ablation process removed only a small fraction (less than 50%) of the initial mass of the fragments at their breakup from the main body. Because there are many of such fragments they probably originated in the main explosion. The full coverage by fusion crusts means that the fragments were not oriented during the ablation. The following two subgroups probably formed by subsequent fragmentations of this group.

(b) Partly crusted with a roasted rear face:
There are many fragments whose rear faces are not covered with fusion crusts. (In some cases the judgment of "rear" may be subjective.) In many cases, the rear faces are flat. In other cases, the rear faces are rough with depressions and protrusions. The rear faces are more or less roasted (scorched) and rollover lips are often observed on the edges, showing that the ablation process was continuing after the breakup of the rear faces and the flight is oriented (if rollover lips are present). The roasting is understood as due to the hot air in the wake. A simple minded calculation of adiabatic expansion of hot and dense air (20000 K and ~4×10^7 Pa) in the bow shock to an ambient air pressure (~10^4 Pa) in the wake shows that the temperature in the wake may be ~1860 K. This seems to be just about the right temperature for roasting if one considers that the process continued for only a second or so. Since there are numerous fragments with this feature and since they have to form in a hot environment they probably formed during the main explosion. The often-observed flat rear face is due to failure along pre-existing fractures.

(c) Partly crusted with a fresh rear face:
This is similar to the previous group except for the fresh (un-roasted) rear face. The un-roasted nature indicates that the ambient temperature was low, suggesting formation after the main

explosion. Some of the rear faces may have formed by the impact onto the ground. But since the ground was mostly covered with snow, many of the fragments with fresh rear faces probably formed in the air.

Surface color:

Surface (mostly covered with fusion crust) color of chondrites is usually black, suggesting dominance of magnetite. In the case of Chelyabinsk meteorite fragments of group 3, red color (indicating dominance of hematite) is often observed on flat (or concave) faces. This is not due to terrestrial weathering because it is observed even on fragments recovered soon after the fall [3]. The well molten fusion crust and protruded areas of the same fragment are black. Redox conditions in the wake of a meteor are close to the hematite-magnetite buffer. Assuming the pressure in a wake is the ambient air pressure, at 20 km and 30 km altitudes, hematite is stable at <1270 C and at <1200 C, respectively [4]. Therefore, the red-colored areas were probably formed under these conditions. Fusion crusts on the front (and side) faces (heated by the hot compressed air both due to conduction and irradiation) formed at much higher temperatures where magnetite is stable. These observations are consistent with the interpretation that the group 3 fragments formed in the main explosion.

Discussion:

Based on morphological features, Chelyabinsk meteorite fragments were classified into 5 groups. The interpretations of the features are not particularly new, but the grouping fits nicely with the degree of ablation expected for fragments produced during pre-explosion, explosion and post-explosion phases of the fireball. The observation that red-colored surfaces are not rare among the Chelyabinsk fragments is explained as a result of deep penetration of the meteor and fragmenting at low altitudes. This may be a common feature of meteorites produced by huge meteoroids.

Regarding disintegration processes of meteoroids, an important implication may be obtained from the group 3b fragments. In particular, the presence of fragments with a flat (rear) surface decorated with rollover lips seems important. The flat face is produced by breaking up a pre-existing fracture. We know that fractures produced in chondrites are often parallel to each other. There are actually pieces of parallelepiped and slab shaped Chelyabinsk meteorite fragments which were produced by breaking up of the parallel fractures. Taken together, these observations suggest that the flat rear face of group 3b may be produced by breakup of a slab from the rear face. In such a case, the flight orientation is likely to be kept during the breakup. This reasoning and the presence of rollover lips mean that the flight was already oriented before the breakup. This finally means that the breakup could be due to tensile failure, because not much compressive stress is available near the rear surface. There is a super-sonic air flow near the edge of the rear face along the side faces. This causes a strong tensile stress on the side faces which could cause the tensile failure.

If my reasoning given above is wrong or not applicable to all group 3b fragments, flight of some fragments may be un-oriented before the breakup and became oriented by the change in the fragment shape. The plausibility of such an interpretation depends on the time scale of stopping rotation and the time scale of fusion crust formation. My explanation in the previous paragraph is based on the assumption that fusion crusts form instantaneously if the normal vector of the newly formed surface is momentarily directed forward. Correctness of this explanation hinges on rotation rates and the number of rotation before the flight becomes oriented. This is an important subject of a future study because oriented meteorites provide useful information on fireballs.

If it is agreed that the group 3b fragments with a flat surface decorated with rollover lips were produced by tensile failure, this conclusion may be extended to the case with a rough surface whose edge is decorated by rollover lips. In this case, because the new rough surface has to be created by tearing up grain boundaries, we expect significant interaction between the fractured surfaces which may cause rotational torque. Yet there may be fair chances that such fragments were oriented before the breakup and remained oriented after the breakup, too. I note that rough surfaces are likely to be produced by tensile stresses because compressive failure of rocks usually results in a nearly flat fracture. Shock induced flat fractures (due to compressive failure) are abundantly observed in the Chelyabinsk meteorite. In passing, I suggest that regmaglypt which is the name for depressions on meteorite surfaces may simply be remaining depressions created by tensile failure and remained un-erased by the ablation process.

In conclusion, based on surface features of the Chelyabinsk meteorite fragments, I suggest that tensile failure near rear surfaces is an important disintegration process of meteoroids. If tensile strength of a meteoroid is restricted to a very narrow range, one may conclude that the Chelyabinsk fireball explosion is well understood. Thus, tensile strength measurements of Chelyabinsk meteorite fragments are important.

References:

[1] Emel'yanenko V. V. et al. (2013) Solar System Res., 47, 240-254. [2] Artemieva N. and Shuvalov V. (2013) EPSC abstract, 2013-1039. [3] http://www.meteorite-recon.com/en/Meteorite_Chelyabinsk_1.html. [4] Myers J. and Eugster H.P., (1983) Contri. Min. Petrol., 82, 75-90.

Mineralogy of Y-790782 LL Chondrite and Thermal Processes of the Parent Asteroid.

H. Takeda[1], H. Nagaoka[2], A. Yamaguchi[3], Y. Karouji[4] and Y. Yazawa[5], [1]Univ. of Tokyo, Graduate School of Sci., & Chiba Inst. of Tech. (CIT), Forum Res., [2]Waseda Univ., Res. Inst. for Sci. & Engn., [3]NIPR, [4]JAXA/ISAS, [5]CIT, Dept. of Life & Environm. Sci.

Introduction:

Because of the recent asteroid missions, Hayabusa [1], Dawan [2] etc., we have renewed interests in the asteroid-meteorite connection, in order to better understand the evolutional processes on asteroids. It is generally understood that the chondritic materials preserve the chemical records of primitive solar system materials, because their parent bodies are mostly small. However, the presence of a Vest-like asteroid larger than 500 km in diameter [2], suggests more advanced differentiation on primitive planetary bodies. We recognized melting and metamorphic records in the LL chondrites [3]. We will compare the degree of differentiation of the Vesta-like body with those of the LL chondrite parent body. We already pointed out that zoning profiles of pyroxenes in totally molten LL chondrites including Y-790964 [4] are comparable with one grain in the Itokawa dusts [1]. In this paper, we will report other partly molten LL chondrites, to discuss evolution of the LL body with respect to Vesta-like bodies.

Samples and Methods:

We examined a new PTS (polished thin section) of LL chondrite, prepared at the NIPR. Y-790782,91-2 [5] was observed by a petrographic microscope and was analyzed with a JEOL JXA-8900 EPMA at AORI (Atomosph. Ocean Res. Inst.). Other PTSs previously studied, including Y-981971,51-1, Y-793214,92-1 (LL5), were also reexamined to compare with the new one.

Results:

PTS Y-790782,91-2 (0.9X0.8 mm in size) consists of dark fine-grained mafic silicates (Fig.1). The PTS is characterized by many opaque spherules up to 7 mm in diameter. The presence of Fe and Ni suggests that these spherules are products of partial melting of chondritic metals and sulfides. The opaque spherules distribute throughout the PTS, indicating total melting. The texture is different from that of Y-790964 [6]. A few clasts of crystalline materials are present in the matrices (Fig. 2). This clast shows a granulitic texture with an opaque vein.

The matrix resembles devitrified glass, but enlarged photograph (Fig. 3) shows that they are aggregates of fine fragments of low-Ca pyroxene and olivine. Some fragments are large enough to give single mineral compositions, but fine materials between the fine fragments give compositions intermediate between low-Ca pyroxene and olivine. Among 8 by 8 grid analysis with 20 microns interval, 8 olivine points and 20 low-Ca pyroxene points, and 24 points with mixtures of pyroxene and olivine. The Mg numbers (MgX100/(Mg+Fe) mol %) of the olivine range from 72 to 78. The pyroxene compositions are nearly uniform and range from $Ca_5Mg_{74}Fe_{22}$ to $Ca_8Mg_{68}Fe_{24}$, approximately.

Discussion:

Perspectives of solar system evolution have been obtained by comparisons of spectroscopic studies of materials of asteroids and planets, and mineralogy, petrology and geochemistry of meteorites. Recently, in-situ observation of asteroid Itokawa by Hayabusa Mission and the dusts returned from Itokawa are revealing new data. Dawn mission results provide key insights into the formation and geologic evolution of Vesta and into the processes shaping the asteroid belt over time

Because of the small sizes of most asteroids, the chondritic materials preserve the chemical records of primitive solar system materials [7]. However, we found the presence of the products of partial melting and thermal metamorphism in some chondrite parent bodies. We found the first evidence of a product of partial melting of the chondritic primitive solar system materials with albite and diopside assemblage in Y-74160 [3] and similar materials were recognized in other LL with granulitic texture and in silicate inclusions in some iron meteorite [8]. The facts suggested that even the primitive solar system material, such as chondrites experienced strong thermal events.

The microscopic textures of the LL chondrites, including Y-790964, Y-981971, and Y-793214 suggest extensive processes of possible melting and metamorphism even in a primitive parent body, comparable to some parts of lunar crust. Mineralogy and petrology of Y-790782 in this study revealed that the presence of opaque spherules is the direct evidence of melting in the LL parent body. It is to be noted that the silicate matrices are not molten. The presence of the granulitic clast with spherules suggests that an impact related to the formation of spherules took place after the granulite formation. It is important to recognize that such events took place in a region of the LL chondrite parent body, from where Itokawa and parent asteroids of the Antarctic meteorites were ejected.

Products of high temperature episodes were well known in the differentiated meteorite parent bodies. The mineralogy of Vesta, based on data obtained by the Dawn mission [2], is consistent with HED achondrites [9], and confirmed the presence of the proposed layered crust model [10]. This

second massive asteroid is the largest protoplanet visited to date, and thereby provides a direct link to materials of the smallest terrestrial planet and basic mode of planetary evolution of the solar system [10]. Pyroxene compositions of a variety of lithic clasts and mineral fragments in the HED meteorites reveal the continuum of chemical compositions, which can be explained more readily by fractional crystallization. Crystallization of diogenitic (D) orthopyroxene is followed by low-Ca pigeonite and plagioclase of cumulate eucrites, and then the Ca and Fe contents of pigeonite in ordinary eucrites (E) increase while crystallization proceeds. Pigeonite-eucritic clasts in the Y-7308 howardite (H) show weak clustering around the compositions near the field of ordinary eucrites (like Juvinas) with the peritectic compositions. The variations of Mg numbers of the D-E trend and those of H are much larger than that of the type 6 LL chondrites.

The sampled material of Itokawa was thermally metamorphosed, as is the case for most ordinary chondrites. Peak temperatures in chondrite parent bodies ranged from about 750-950°C for type 6. The onion-shell models [11] of chondrite show that type 6 is produced in the interior of a body nearly 170 km in diameter. The variations of their chemical compositions are relatively small. To be heated sufficiently, the samples must have originated inside a much larger asteroid. The granulitic textures in some lunar samples are widely believed to have formed deep in the lunar crust. The granulitic materials in the LL parent body may also have been formed in some depth of their parent body.

It is to be remembered that chondritic materials keep records of primitive solar system, but some parts are partly melted and heavily metamorphosed.

Acknowledgments:

We thank the NIPR for the samples and PTS preparation. We thank Prof. M. Miyamoto and Dr. T. Mikouchi of Univ. of Tokyo, Graduate School of Sci., and Prof. N. Hasebe of Waseda Univ., Res. Inst. for Sci. & Engn., Prof. T. Nakamura of Tohoku Univ. and Dr. T. Noguchi of Ibaraki Univ. for their discussion and support of our researches. This research was supported in part for the Cooperative Program (No. 108, 2012) of AORI, the Univ. of Tokyo, and for a program of Research Forum of CIT.

References:

[1] Nakamura T. *et al.* (2011) *Science*, 333, 1113-1116. [2] De Sanctis M. C. *et al.* (2012) *Science* 336, 697-700. [3] Takeda H., Huston T. J. and Lipschutz M. E. (1984) *Earth Planet. Sci. Lett.* 71, 329-339. [4] Yamaguchi A. *et al.* (1998) *Antarctic Meteorite Res.*, 11, 18-32. [5] Antarctic Meteorite Data Base (2011) NIPR. [6] Takeda H., Miyamoto M. and Ishii T. (1983) *LPS 14th*, 771-772. [7] Fujiwara A., Kawaguchi J., Sasaki S. (2005) Dust in Planetary Systems: *Workshop Program and Abstracts.* Vol. 1280, pp. 50-51. [8] Takeda H., Hsu W. and Huss Gary R. (2003) *Geochim. Cosmochim. Acta*, 67, 2269-2288. [9] Takeda H. (1997) *Meteorit. Planet. Sci., 32*, 841-853. [10] Takeda H. (1979) *Icarus* 40, 455-470. [11] Miyamoto M., Fujii N., and Takeda H. (1981) *Proc. Lunar Planet. Sci. Conf.* 12*th*, 1145-1152.

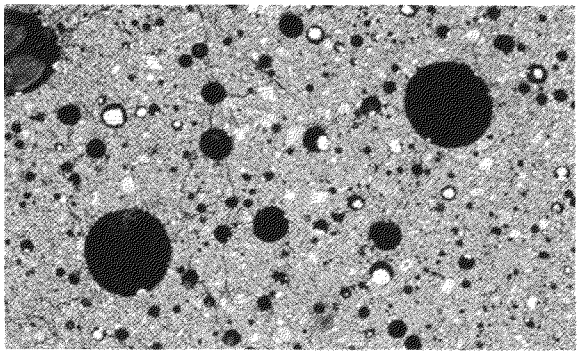

Fig. 1. The PTS view of Y-790782,91-2 LL chondrite (NIPR) with the largest opaque spherules. Open light. Width is 3.3mm.

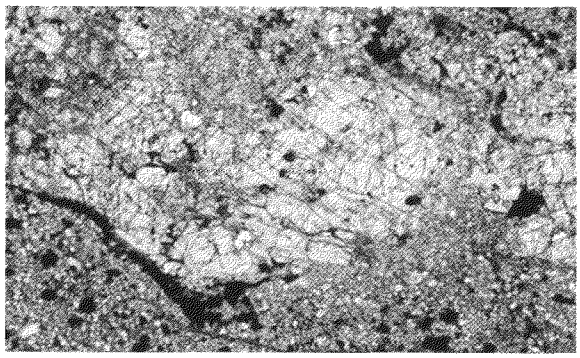

Fig. 2. Photomicrograph of a granulitic clast in Y-790782,91-2. Open light. Width is 1.3 mm.

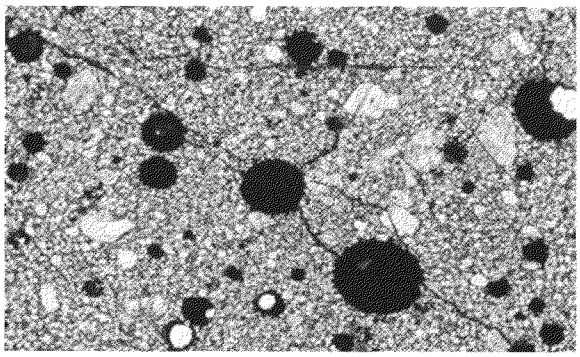

Fig. 3. An enlarged view of Y-790782,91-2 PTS showing matrix textures. Open light. Width is 1.3 mm.

What Are Space Exposure Histories Telling Us about CM Carbonaceous Chondrites? A. Takenouchi[1], M. E. Zolensky[2], K. Nishiizumi[3], M. Caffee[3], M. A. Velbel[4], K. Ross[5], A. Zolensky[6], L. Le[5], N. Imae[7], A. Yamaguchi[7], T. Mikouchi[1], [1]*The University of Tokyo,* [2]*NASA Johnson Space Center, Houston, TX, USA,* [3]*Space Science Laboratory,* [4]*Michigan State University, East Lansing, MI, USA,* [5]*Jacobs Technology, Houston, TX, USA,* [6]*Nashville, TN, USA,* [7]*National Institute of Polar Research.*

Introduction: Chondrites are chemically primitive and carbonaceous (C) chondrites are potentially the most primitive among them because they mostly escaped thermal metamorphism that affected the other chondrite groups. Rratios of their major, non-volatile and most of the volatile elements are similar to those of the Sun. Therefore, C chondrites are expected to retain a good record of the origin and early history of the solar system.

Carbonaceous chondrites are chemically distinguished from other chondrites by their high Mg/Si ratios and refractory elements, and have experienced various degrees of aqueous alteration. They are subdivided into eight subgroups (CI, CM, CO, CV, CK, CR, CB and CH) based on major element and oxygen isotopic ratios. Their elemental ratios vary over a wide range, in contrast to those of ordinary and enstatite chondrites which are relatively uniform. It is critical to know how many separate bodies are represented by the C chondrites.

In this study, CM chondrites, the most abundant carbonaceous chondrites, are examined. They are water-rich, chondrule- and CAI-bearing meteorites and most of them are breccias. High-temperature components such as chondrules, isolated olivine and CAIs in CMs are frequently altered and some of them are replaced by phyllosilicates and surrounded by sulfides whose Fe was derived from mafic silicates. On the basis of degrees of aqueous alteration, CMs have been classified into subtypes from 1 to 2, although Rubin et al. [1] assigned subtype 1 to subtype 2 and subtype 2 to subtype 2.6 using various petrologic properties. The classification is based on petrographic and mineralogic properties. For example, though tochilinite (2[(Fe, Mg, Cu, Ni[])S] 1.57-1.85 [(Mg, Fe, Ni, Al, Ca)$(OH)_2$]) clumps are produced during aqueous alteration, they disappear and sulfide appears with increasing degrees of aqueous alteration.

Cosmic-ray exposure (CRE) age measurements of CM chondrites reveal an unusual feature. Although CRE ages of other chondrite groups range from several Myr to tens of Myr, CMs exposure ages are not longer than 7 Myr with one-third of the CM having less than 1 Myr CRE age. For those CM chondrites that have CRE ages <1 Myr, there are two discernable CRE peaks. Because a CRE age reflects how long a meteorite is present as a separate body in space, the peaks presumably represent collisional events on the parent body (ies) [2].

In this study we defined 4 distinct CRE age groups of CMs and systematically characterized the petrography in each of the 4 CRE age groups to determine whether the groups have significant petrographic differences, with such differences probably reflecting different parent body (asteroid) geological processing, or multiple original bodies.

Samples and Method: We observed thin sections of 125 CM and CM-related chondrites by optical microscopy and scanning electron microscopy (SEM). Moreover, we made whole mosaics of each thin section by reflected light and backscattered electron imaging (Fig. 1). We then grouped the meteorites into several groups based on the following nine petrographic criteria:

1. Abundance of chondrules
2. Abundance and thickness of chondrule rims
3. Chondrule sizes
4. Degrees of chondrule fracturing
5. Degrees of mafic silicate alteration in chondrules
6. Amount of metal iron
7. Amount of CAIs
8. Amount of tochilinite clamps
9. Brecciation

These criteria follow characterizations mentioned in Rubin et al. [1]. Our resultant groupings are performed qualitatively because this is the first attempt to group them with their CRE ages and textures.

Some element maps are also made by SEM and some quantitative analyses were made of matrix by electron microprobe to compare compositions between each CRE age groups.

Result and Discussion: Figure 2 is the CRE age distribution plot of CMs observed in this study [2]. In this plot, the 73 well determined CMs are shown. According to this plot, there are several distinct peaks and the large number of samples permits investigation of each CRE age group. We label the perceptible 3 peaks approximately around 0.2 Myr, 0.6 Myr

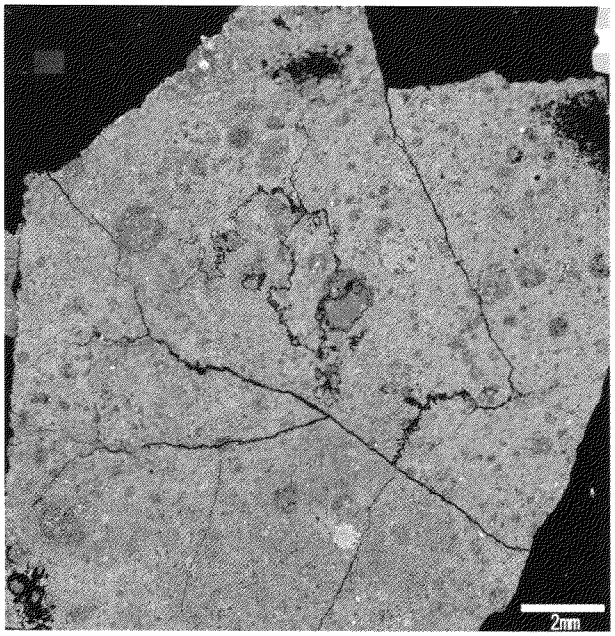

Fig. 1 BSE mosaic of Murchison

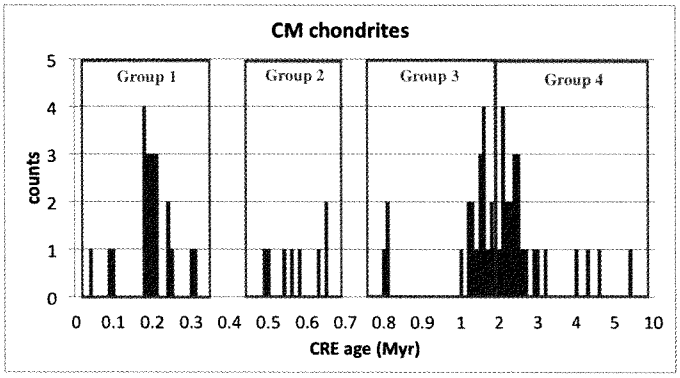

Fig. 2 CRE age distribution plot of observed CMs

and 1.5 Myr as group1, 2 and 3, respectively. Although meteorites whose CRE age is over 2.5 Myr are plotted, their CRE ages are still uncertain because of limitation on measurement, therefore they all are grouped as group 4.

According to our observations, we find that some meteorites in the same CRE age group have the same texture (or the same clast). For example, LON94101, Y-793595 and ALH85007 are belonging to the same group and some rare clasts (compressed tochilinite) similar to the texture in Y-793595 are found in the other meteorites. This is consistent with the hypothesis that they are ejected by the same collisional event and the peak in the CRE age distribution plot represents each collisional event [2].

Then, we compare each meteorite by the criteria and find some trends. Although the average chondrule sizes and rim thicknesses of each group are similar, the degree of alteration and the amount of tochilinite is different. Meteorites in group 1 to 3 tend to be more altered than meteorites in the other groups. The amount of tochilinite tends to decrease from group 1 to group 3 and be constant from group 3 to 4. Therefore, it seems that there are some correlations between the CRE ages and the textures, however this observation is still qualitative and we need to confirm whether these variations are significant.

Figure 3 shows elemental maps of 4 meteorites selected from 3 different CRE age groups and not-measured group. From these images we can find that Mg is abundant in ALH88045 and Cold Bokkeveld, however it is low in Murray and LEW90500, and Al and Ca are more abundant than Mg in LEW90500. As above, we see compositional differences between each meteorite. However, we have only a small amount of compositional data, and it is therefore unclear whether the compositions of meteorites with similar textures are alike or not.

Conclusions: In this study, we sought correlations between the CRE age and textures of CMs for the first time and we found the degree of alteration and the amount of tochilinite vary with the CRE ages. However, this observation is still qualitative, therefore, quantitative observation, for example the compositional analysis by electron microprobe to quantify the degree of alteration is needed.

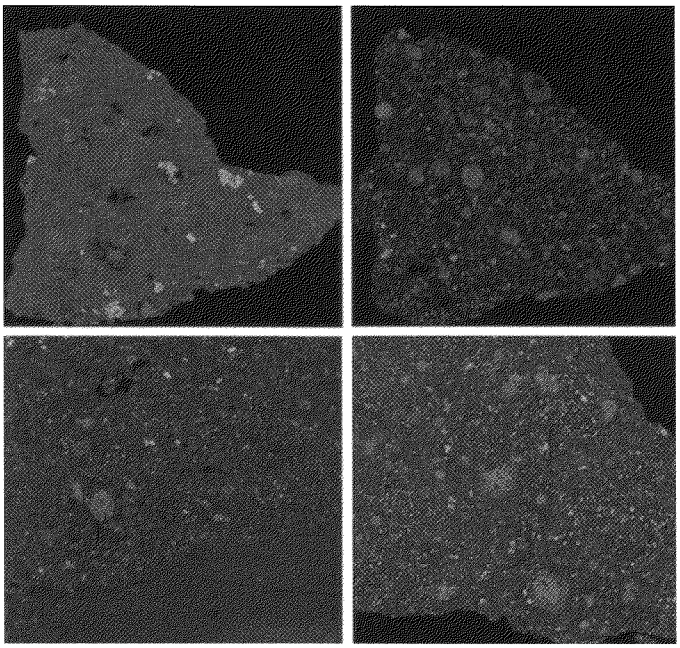

Fig. 3 Composite elemental maps of 4 meteorites
Red, green and blue represent Mg, Ca and Al, respectively. Upper left: ALH88045, Upper right: Murray, Lower left: Cold Bokkeveld, Lower right: LEW90500. Mg, Ca and Al contrast and brightness are adjusted to be the same within each image.

We also found CMs in each CRE age group have many different kinds of textures, some are similar and others are different. This means that meteorites from each group were ejected by the same collisional event and the parent body(ies) of CMs is (are) complex and not uniform.

At this time, although it is not clear that the differences in each group are significant and what they represent. Our preliminary analysis suggests that some CRE age groups are from separate parent bodies. However, further investigation is required to permit selection of the correct situation.

References: [1] Rubin A. E. et al. (2007) *Geochim. Cosmochim. Acta 71. 2361-2382.* [2] Nishiizumi K. and Caffee M. C. (2012) *LPSC XLIII*, abst #2758.

Formation of the Mont Dieu IIE non-magmatic iron meteorite. N. Van Roosbroek[1], V. Debaille[1], S. Goderis[2], J. W. Valley[3], M. J. Spicuzza[3] and Ph. Claeys[2], [1]Laboratoire G-Time, Université Libre de Bruxelles, B-1050 Brussels, Belgium,[2] Earth System Sciences, Vrije Universiteit Brussel, B-1050 Brussels, Belgium, [3]Dept. of Geoscience, Univ. of Wisconsin-Madison, Madison, WI, 53706, USA.

Introduction:

Recently, the Mont Dieu meteorite was confirmed as a fine octahedrite IIE iron meteorite [1, 2, 3]. The original fragments in the collection of the *Musée National d'Histoire Naturelle* in Paris show rust damage. The much better preserved ~450 kg fragment of the IIE non-magmatic iron (NMI) Mont Dieu II meteorite hosted at the Royal Belgian Institute of Natural Sciences, in Brussels, was studied. The metal phase shows a clear widmanstätten texture, composed essentially of kamacite, with fine lines of Ni-rich taenite, and locally troilite associated with schreibersite. The study focuses on the abundant large, angular, brownish silicate inclusions present in Mont Dieu II. These were studied under SEM/EDX, major and trace elements were determined by ICP-OES & ICP-MS, and oxygen isotopes were measured.

Silicate inclusions:

The silicate inclusions are characterized by coarse-grained granular texture, crossed by metal veins ranging from abundant fine veinlets to a few coarse veins of 100-250 μm wide. Round structures (~ 1 mm in diameter) composed of ferromagnesian minerals are spread throughout the silicate inclusions and are interpreted as relict chondrules. The majority of these chondrules have a recrystallized appearance but three well preserved barred olivine chondrules, a feature so far only present in Netschaëvo IIE [4], have been observed. The mineralogy is of chondritic nature. It contains low Ca-pyroxene, olivine, plagioclase, glass, Fe-Ni, troilite, chromite and phophates. Glass is only found within the chondrules and contains up to 4.7 wt% FeO. The composition of this glass can best be compared to chondrule glass.

The Fa and Fs molar contents are defined for three different regions in the silicate inclusions; the well preserved chondrules, the recrystallized chondrules and the matrix. For both chondrule groups, these values fall within the H-range (Fs = 14.9 ± 6.3; Fa = 17.4 ± 5.3 for the original chondrules. Fs = 15.0 ± 2.5; Fa = 16.4 ± 2.7 for the recrystallized chondrules). For the matrix the Fa and Fs molar contents are 14.9 ± 1.5 and 12.9 ± 0.6 respectively, more reduced compared to H-chondrites. Olivine and low-Ca pyroxene show a wide compositional range (2σ) which is decreasing from original chondrules to recrystallized chondrules to matrix.

The major element composition of the silicate phase of Mont Dieu II can best be compared to enstatite and ordinary chondrites. Because barred olivine chondrules do not occur in enstatite chondrites, an enstatite chondrite affinity is excluded. Within the ordinary chondrites, the composition of Mont Dieu II can best be compared to H-chondrites.

The oxygen isotope analyses carried out on Mont Dieu II yield a mean $\Delta^{17}O$ of 0.714±0.024 ‰. In terms of its oxygen signature, Mont Dieu II falls within the range defined for H 3-6 chondrites [5; 6].

The silicate inclusions show similarities with H6 chondrites, where small chondrules have disappeared and the groundmass has coarsened. It is likely that the silicate minerals underwent appreciable metamorphic recrystallization but that melting was very limited. Metal, troilite and phosphates minerals have an irregular and elongated shape, indicating that these minerals were once molten. From these observations, it is clear that Mont Dieu II has been heated.

Precursor material:

Several lines of evidence let us believe that Mont Dieu II originated as an H-chondrite; the preserved chondrules, the chondritic mineralogy, its major element composition and its oxygen isotopic composition. Three other important features indicate that the precursor material could have been an unequilibrated H3 chondrite; (1) The occurrence of chondrule glass in some chondrules, (2) The wide compositional range of the minerals in those chondrules and (3) The oxygen isotopic composition that is situated in the H3 range.

Formation:

An impact formation model is proposed. An H-chondrite parent body was impacted by an Fe-Ni impactor that created a metal-magma pool on the surface of the H-chondrite parent body. The material of the impactor is mixed with the silicate material when sinking towards the bottom of the magma pool. A certain amount of the impactor sinks to the magma pool. The upper part of the magma pool consists of a silicate-metal mixing region. In this environment, Mont Dieu II was formed. A position near the edge and at a shallow depth of the magma pool is favored for Mont Dieu II, because fast cooling is necessary to preserve the chondrules and glass. No strong evidence for shock was observed in the silicate phase, meaning that Mont Dieu II did not form at the surface of the parent body. An H3-chondrite affinity for Mont Dieu II is consistent with the onion shell model, where the least metamorphosed regions are situated at the surface of the H-chondrite body, where the impact took place.

Classification:

To position Mont Dieu II within the IIE group several classification criteria have been evaluated. The occurrence of chondrules in the silicate phase of Mont Dieu II, its major element composition and its chondritic mineralogy place Mont Dieu II on the same level as Netschaëvo. The preservation of chondrule glass and its oxygen isotopic composition favor a more primitive nature for Mont Dieu II and therefore we propose that Mont Dieu makes up a new, the most primitive subgroup, within the IIE classification.

References:

[1] Grossman J. N. (1997) *Meteoritics & Planetary Science, Supp. 31,* A159-166. [2] Desrousseaux A. et al. (1996) *Meteoritics & Planetary Science, 31,* A36. [3] Van Den Borre N. et al. (2007) *Meteoritics & Planetary Science*, *42*:A153. [4] Olsen E. and Jarosewich E. (1971) *Science, 174*, 583-585. [5] Clayton R.N. and Mayeda T.K. (1996) *Geochemica and Cosmochimica Acta 60*, 1999-2017. [6] Folco L. et al., (2004) *Geochemica and Cosmochimica Acta 68*, 2379-2397. [7] Franchi I.A. (2008) *Reviews in Mineralogy and Cosmochemistry*, *68*, 345-397.

Present status of international announcement of opportunity and consortium studies for Hayabusa-returned samples. T. Yada[1], M. Abe[1,2], T. Okada[1,2], M. Uesugi[1], Y. Karouji[1], Y. Ishibashi[1], and M. Fujimoto[1,2,3], [1]Inst. Space Astronaut. Sci. and [2]Lunar Planet. Explor. Program Group, Japan Aerosp. Explor. Agency, JAPAN, [3] Earth-Life Sci. Inst., Tokyo Inst. Technol., JAPAN.

Introduction:

The Hayabusa spacecraft accomplished touchdowns onto a S-type asteroid Itokawa twice and returned its reentry capsule to the Earth in June 2010 [1]. After it was recovered in the Australian desert and sent back to Japan, it was treated in clean rooms of the extraterrestrial sample curation center (ESCUC) of JAXA and finally returned samples were recovered from a sample catcher, as described in [2]. Here we report the present status of the sample recovery, the international announcement of opportunity (AO), and consortium studies conducted by JAXA.

Present status of the sample recovery:

The Hayabusa's sample catcher is composed of room A and B and a rotational cylinder, and samples by the first touchdown was recovered in the catcher room B whereas those by the second one in the room A, through the rotational cylinder. JAXA extraterrestrial sample curation team (ESCUTE) has recovered particles from the sample catcher by the following two ways. One is from quartz glass disks which had been attached to the openings of the catcher room A and B, and received particles fell down from its inside by tapping it. The other is from a cover of the catcher room B. Particles on the disks and the cover are handpicked one by one with an electrostatically controlled micromanipulator in a clean chamber filled with N_2. Then they are set in a special sample holder for transportation to the SEM without exposing to air and then analyzed by the SEM. After the SEM observation, they are sent back to the clean chamber, placed on gridded quartz glass slides, given own their IDs and preserved in the chamber with N_2 condition. So far, 430 particles have been recovered and described, and almost 80% of them are mainly composed of silicates, supposed to originate from Itokawa. However, sample recovery from the catcher is still under on the way.

Now we ESCUTE start observing the surface of the cover of the catcher room B directly by SEM, expecting more particles overlooked by optical microscope observation might be recognized with this method. And we are planning to recover particles on metal disks to be observed directly by SEM to increase the working efficiency.

Memorandum of understanding between JAXA and NASA:

Before the launch of the Hayabusa, JAXA published memorandum of understanding (MOU) between JAXA and NASA. It includes that 15% of samples recovered from Itokawa will be allocated to preliminary examination, 15% to international AO, 15% to JAXA, 10% to NASA, and rest 45% is preserved for future. Based on the MOU, ESCUTE distributed samples to preliminary examination, whose results have been already published in elsewhere [3-10].

International AO:

Based on the MOU, JAXA started international AO of the Hayabusa-returned samples in 2012. In the first international AO held in 2012, 17 research proposals were approved for sample distributions, and more than 60 particles were distributed to the selected researchers. Most of their results have been presented in "Hayabusa 2013: symposium of solar system materials" held in Oct. 2013. In 2013, the second international AO was published, and 16 proposals were approved for the sample distributions. So far, 44 particles have been distributed to the approved researchers. The third international AO will be published in the beginning of 2014.

Consortium studies:

There exist particles which have rare features and should not be allocated to one research proposal. Utilizing the fraction assigned to JAXA based on the MOU, JAXA started consortium studies such rare particles in 2013. So far, four consortium studies are undertaken. The first one is the largest particle recovered so far. It must be for analyses which need large volume of samples. The second is a particle bearing NaCl. It is the only silicate one including NaCl so far. The key for this consortium is to prove its extraterrestrial origin. The third are ones which are mainly composed of Fe-Ni metal and iron sulfide. They must be analyzed for siderophile elements abundances and solar wind components. The forth are ones including phosphate. They should be analyzed for U-Pb dating and REE abundances. All the consortium studies are accepting proposals from researchers until the end of this Oct., and then their analysis schemes will be discussed with the researchers to maximize their scientific gains.

References:

[1] Abe M. et al. (2011) *LPS XXXXII*, #1638. [2] Yada T. et al. (2013) *Meteoritics Planet. Sci.*, early online view. [3] Nakamura T. et al. (2011) *Science* 333, 1113. [4] Yurimoto Y. et al. (2011) *Science* 333, 1116. [5] Ebihara M. et al. (2011) *Science* 333, 1119. [6] Noguchi T. et al. (2011) *Science* 333, 1121. [7] Tsuchiyama A. et al. (2011) *Science* 333, 1125. [8] Nagao K. et al. (2011) *Science* 333, 1128. [9] Naraoka H. et al. (2012) *Geochem. J.* 46, 61. [10] Nakamura E. et al. (2012) *PNAS* 109, E624.

Petrology and geochemistry of NWA 5480 diogenite and evidence for a basin forming event on Vesta. A. Yamaguchi[1], J.A. Barrat[2], N. Shirai[3], M. Ebihara[3], [1]National Institute of Polar Research, Tachikawa, Tokyo 190-8518, [2]Université Européenne de Bretagne, U.B.O.-I.U.E.M., CNRS UMR 6538, Place Nicolas 20 Copernic, 29280 Plouzané Cedex, France, [3]Graduate School of Science, Tokyo Metropolitan University, Hachioji, Tokyo 192-0397.

Introduction:

Vesta is the only protoplanet that has survived intact and constitutes the parent body of HED (Howardite, Eucrite, Diogenite) meteorites [e.g., 1,2]. In 2011 DAWN provided compositional information of Vesta that matched with HED meteorites [e.g., 3]. Eucrites are basalts or gabbros that formed the outer crust of Vesta crystallized from a magma ocean [e.g., 4]. Diogenites are orthopyroxene-rich cumulates that located in a deep crust (upper mantle) or intrusions into the eucritic crust formed by secondary volcanism after magma ocean crystallization [5-7]. Howardites are mainly mechanical mixtures of eucrites and diogenites produced by impact events. Petrologic and geochemical study of HED meteorites as well as remote sensing observations of Vesta provide important clues for understanding igneous, metamorphic, and impact history of protoplanets.

Samples and Analytical techniques:

We performed a petrological and geochemical study of NWA 5480 and other olivine-bearing diogenites for comparison. Polished thin sections (PTSs) of NWA 5480 were examined optically and with an EPMA and SEM at NIPR. Platinum group elements (PGEs) were determined by ICP-MS at TMU. The ICP-MS procedure was described in Shirai et al. [8].

Results and Discussion:

NWA 5480 is an unbrecciated diogenite with heterogeneous textures. PTSs of NWA 5480 show large, irregular olivine grains (typically, ~0.1 mm, up to ~1 cm) set in a microporphyritic groundmass composed of pyroxene pepped with small droplets of olivine (30-50 μm in size) (Fig. 1). Fine granules of olivine are attached to the edges of the olivine grains. Chromite occurs as large irregular grains as well as very fine strings or lines (a few μm thick) interstitially between pyroxene and olivine. Large chromite grains contain thin irregular veins of pyroxene filled with fine euhedral chromite (10-50 μm in size). These textures indicate that the large olivine and chromite grains were relicts of resorption. These features are unlike igneous cumulate rocks, but similar to impact melt rocks, for example as observed in ordinary chondrites [9].

Compositions of pyroxene ($Wo_{1.-2}En_{74-75}$) and olivine (Fo_{71-72}) of NWA 5480 are within the range of normal diogenites [7]. However, major minerals show a number of disequilibrium features that are not observed in most diogenites. Olivine relicts have chemical zoning of CaO near the rims (from 0.04-0.08 wt% to 0.10-0.12 wt%). The CaO contents of olivine in the matrix (0.04-0.08 wt%) are less than those of the relict grains (0.06-0.12 wt%). Furthermore, relict chromite grains show chemical zoning. These disequilibrium features argue against a deep mantle origin for this meteorite. Pyroxene in the matrix shows normal igneous zoning (MgO/FeO, CaO, Al_2O_3, TiO_2), indicating that NWA 5480 cooled rapidly at several tens °C/year [10].

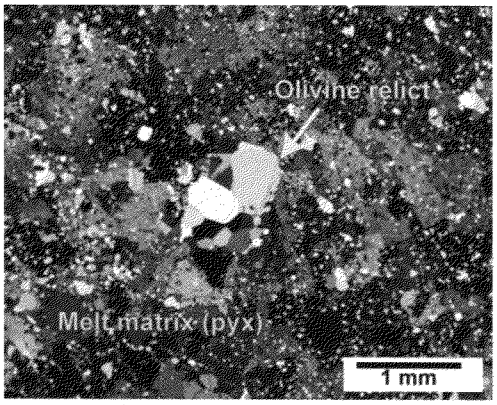

Fig. 1. Photomicrograph of NWA 5480 (crossed-polarized light). Olivine relict is set in a pyroxene matrix.

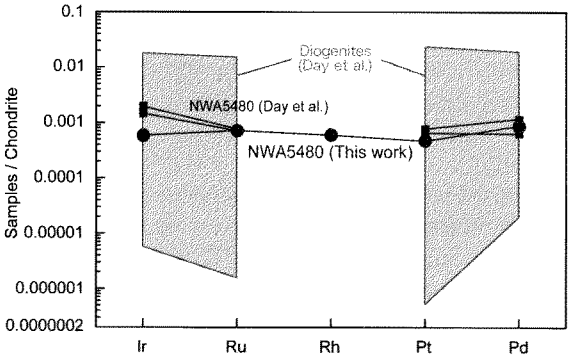

Fig. 2. Chondrite-normalized PGE patterns [this work and 11] of NWA 5480 and other diogenites [11].

NWA 5480 contains a significant amount of PGEs [11, this work] (Fig. 2). The PGE pattern is unfractionated and point to a contamination of ca. 0.1 wt% chondritic materials.

The petrological and geochemical evidence strongly supports that NWA 5480 is an impact melt rock. Our conclusion contradicts with the idea that NWA 5480 has evidence for mantle shear [12]. This point will be discussed in the presentation. NWA 5480 displays heavy REE enrichment indicating the remelting of older mafic cumulates [6]. We suggest that NWA 5480 was derived from impact melts from a large basin of Vesta. One of the best candidates is the Rheasilvia basin (~500 km in diameter), where orthopyroxene-rich materials were observed in the crater floor [3]. Petrological and geochemical evidence from NWA 5480 provides clues to the early intense bombardment history of the parent body, Vesta.

References:

[1] McCord T. et al. (1970) Science 168, 1445-1447. [2] Binzel R.P. and Xu S. (1993) Science 260, 186-191. [3] McSween H. et al. (2013) J. Geophys. Res. 118, 335-346. [4] Righter K. and Drake M.J. (1997) MAPS 32, 929-944. [5] Barrat J.A. et al. (2008) MAPS 43, 1759-1775. [6] Barrat J.A. et al. (2010) GCA 74, 6218-6231. [7] Yamaguchi A. et al. (2011) JGR 116, E08009, doi:10.1029/2010JE003753. [8] Shirai N. et al. (2003) Geochem. Jour. 37, 531-536. [9] Yamaguchi A. et al. (1998) Antarct. Meteorite Res. 11, 18-31. [10] Miyamoto M. (1997) JGR 102, 21613-21618. [11] Day J.M.D. et al. (2012) Nature Geoscience 5, 614-617. [12] Tkalcec B.J. et al. (2013) Nature Geoscience 6, 93-97.

Preliminary analysis of soluble organic compounds in the Murchison meteorite by liquid chromatography/high-resolution mass spectrometry. Y. Yamashita[1] and H. Naraoka[1], [1]Dept. Earth & Planet. Sci., Kyushu Univ., Fukuoka 812-8581 JAPAN.

Introduction:

Various organic matters have been found in carbonaceous chondrites, in which water-soluble bio-related organic compounds such as amino acids and carboxylic acids are fully identified mainly because of their great interests to origins of life in the universe and standards available for analyses. The concentrations of these acids increase significantly after acid hydrolysis of the water extract. The chemical structures of the precursors, however, remain unclear. Aqueous activity on the parent body could affect the alteration of meteoritic organic matter [1]. In contrast to the water extract, less polar methanol extract of chondrites has not been characterized well in spite of relatively high content of organic matter with the D- and ^{15}N enrichment. Recently, ultrahigh-resolution molecular analysis on various solvent extracts of the Murchison meteorite (CM2) was performed by electrosplay ionization (ESI) Fourier transform ion cyclotron resonance/ mass spectrometry (FTICR/MS) to reveal significant chemical diversity to tens of thousands of different molecular compositions having CHO, CHOS, CHNO and CHNOS formulae [2]. With the assumption for molecular formulae calculation and no chromatographic separation, however, chemical structures of the compounds and their isotopic compositions cannot be determined. In this study, we performed a preliminary analysis of soluble organic compounds in the Murchison meteorite by high-performance liquid chromatography-mass spectrometry (HPLC-MS).

Sample and analytical methods:

The Murchison powder was sequentially extracted with hexane (Hex), dichloromethane (DCM), methanol (MeOH) and water by sonication, followed by hot water in a closed condition. After evaporation of solvent, each extract was analyzed using an elemental analyzer (or pyrolysis)-isotope ratio mass spectrometer (EA- or Pyrolysis-IRMS) to determine the CHNO concentrations and their stable isotopic compositions ($\delta^{13}C$, δD, $\delta^{15}N$ and $\delta^{18}O$). Each extract was also analyzed by HPLC-MS (Shimadzu LCMS-8030, Shimadzu LCMS-IT-TOF and ThermoScientific LTQ Orbitrap XL) to identify compound structures with several LC stationary phases including reverse mode (ODS and phenyl) as well as hydrophilic interaction chromatography (HILIC) mode (diol and amide).

Results and Discussion:

The carbon concentration and $\delta^{13}C$ value (relative to PDB) of each fraction are following: Hot water extract (927ppm, 5.4‰) > MeOH extract (304ppm, 5.8‰) > Water extract (169ppm, -0.4‰) > DCM extract (141ppm, 0.0‰) > Hex extract (28ppm, -10.0‰), suggesting that most carbon consist of polar organic components soluble in water and MeOH with ^{13}C-enrichment. In addition, the DCM and MeOH extracts are more enriched in D (+665 to +680‰ vs. SMOW) and ^{15}N (+50 to +98‰ vs. Air) relative to the water extract, which is the similar isotope signature as reported by Krishnamurthy et al (1992). Considering from the heavy-isotope distribution, the MeOH extract may be a main carrier of more primitive organic compounds than the other extracts.

A relatively good separation and MS intensity with the ESI was obtained using a HILIC amide column with an acetonitrile/ammonium formate buffer. Two homologues of N-containing compounds were dominant in positive ions from m/z 100 to 350 (Fig. 1) in the MeOH and DCM extracts. Currently, these compound series are assigned as $C_nH_{2n-4}N$ and $C_nH_{2n-4}N$, which could be produced by aldehydes and NH_3. No oxygen was incorporated into these homologues compounds, suggesting a minimum aqueous alteration on the meteorite parent body. Further compound identification and simulation experiments are needed for the better understanding of formation mechanisms and alteration history of primitive organic compounds in molecular clouds and primitive solar nebulae.

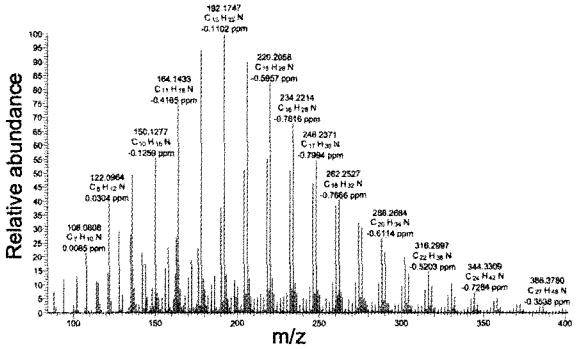

Fig. 1 High-resolution mass spectrum of dominant organic compounds in the MeOH extract of the Murchison meteorite.

Acknowledgements:

We are grateful to Mr. T. Akasaka of Kyushu Univ. and Ms. M. Yamaguchi of ThermoScientific for HPLC-MS analyses.

References:

[1] Oba Y. and Naraoka (2009) *Meteorit. Planet. Sci., 44,* 943–953. [2] Schmitt-Kopplin P. et al. (2010) *Proc. Natl. Acad. Sci., 107,* 2763-2768. [3] Krishnamurthy R. V. et al (1992) *Geochim. Cosmochim. Acta, 56,* 4045–4058.

K–Ca ISOTOPIC SYSTEMATICS OF ALKALI-RICH FRAGMENTS IN THE YAMATO–74442 LL–CHONDRITIC BRECCIA.

T. Yokoyama[1], K. Misawa[2], O. Okano[3], C.-Y. Shih[4], L. E. Nyquist[5], J. I. Simon[5], M. J. Tappa[4], S. Yoneda[1]. [1]Natl Museum Nature and Sci., Tsukuba, Ibaraki 305–0005, Japan. E-mail: yokoyama.tatsunori@gmail.com. [2]Natl Inst. Polar Res., [3]Okayama Univ., [4]JETS/Jacobs., [5]NASA-JSC.

Introduction:

Alkali-rich rock fragments were reported in LL- and H-chondritic breccias, Krähenberg (LL5), Bhola (LL3-6), Yamato (Y)-74442 (LL4), Siena (LL5) and Acfer 111 (H3-6) [1,2,3,4,5]. Previous studies revealed that alkali and alkaline elements in Krähenberg, Bhola, Y-74442 and Acfer 111 rock fragments are fractionated relative to CI-chondrites with heavier alkalis in general being progressively more enriched while their sodium abundances are sub-chondritic ($Cs_{CI\text{-}norm}$ > $Rb_{CI\text{-}norm}$ > $K_{CI\text{-}norm}$ > $Na_{CI\text{-}norm}$) [1,2,3,5].

Highly enriched rubidium in Krähenberg and Y-74442 enable Rb-Sr isotope dating and determination of isotopic constraints on the chemical characteristics of their source materials [1]. We recently reported a new Rb-Sr crystallization age of 4.429 ± 0.054 Ga for Y-74442 fragments [5]. The results suggested that the source material of Y-74442 fragments could have formed from mixtures of an alkali-rich component from an alkali-rich planetesimal or early nebular condensates and a chondritic component that was flash heated during an impact on the LL-chondritic parent body ~4.4 Ga ago. Further enrichments of rubidium relative to strontium as well as a progressive enrichment of the heavier alkalis could have occurred during the final melt differentiation event on the parent body [5].

Because the alkali-rich rock fragments in Y-74442 and Bhola also show relatively high potassium abundances, up to 20 x CI-chondrites and highly radiogenic $^{87}Sr/^{86}Sr$ ratios up to ~5 [5], we have undertaken K–Ca isotopic analyses of the samples previously analyzed for Rb–Sr isotopes. We also report a refinement of our Rb-Sr isochron by including Rb-Sr measurements for an additional nine Y-74442 fragments.

Marshall and DePaolo (1982, 1989) [6,7] demonstrated that the ^{40}K–^{40}Ca decay system could be used as chronometer as well as a useful radiogenic tracer for studies of terrestrial rocks. Shih et al. (1993, 1994) [8,9] determined K–Ca ages of lunar granitic rock fragments, and showed the application of the K–Ca chronometer to K-rich planetary materials. Recently, Kreissig and Elliott (2005) [10], Simon et al. (2009) [11] and Caro et al. (2010) [12] performed high precision calcium isotope measurements using new generation thermal ionization mass spectrometers, enabling studies of fractionation processes of alkali-rich planetary materials using K–Ca isotope systematics.

Results:

Over time, the enrichments of potassium in alkali-rich fragments from Y-74442 and Bhola result in comparatively large enrichments in ^{40}Ca relative to other planetary materials. Measured values $\varepsilon^{40}Ca$ range from 1.5 to 7, where $\varepsilon^{40}Ca = (^{40}Ca/^{44}Ca)_{sample} / 47.1583 - 1) \times 10^4$. Here 47.1583 is the mantle $^{40}Ca/^{44}Ca$ value of Caro et al. (2010) [12] re-normalized on the basis of the measured value from SRM 915a of 47.1487 reported by Marshall and DePaolo (1989). The average of 15 analyses of NIST SRM 915a standard during the course of this study was $(^{40}Ca/^{44}Ca)_{915aNMNS} = 47.16408 \pm 0.0040$ ($2\sigma_p$ error). Potassium-calcium data for sixteen alkali-rich fragments of Y-74442 and one alkali-rich fragment of Bhola were obtained. The $\varepsilon^{40}Ca$ values are shown in Fig.1. Also shown in Fig. 1 are the variations in $\varepsilon^{40}Ca$ of other planetary materials reported by [11,12] on a scale where Earth's mantle is $\varepsilon^{40}Ca_{mantle} = 0$. The K–Ca data of the Y-74442 fragments yield an age of 4.40 ± 0.36 Ga (2σ error, n = 13) for $\lambda(^{40}K) = 0.5543$ Ga^{-1} [13] with an initial $^{40}Ca/^{44}Ca = 47.1602 \pm 0.0039$ (2σ) using the Isoplot/Ex program [14] (Fig. 2). We excluded three data points (,121-5 ,130-7 and ,130-11) from the age calculation of Y-74442 fragments since they appear to contain some amount of host material and showed large scatter. A data point of the Bhola fragment deviates downward by −1.5 ε-units from the Y-74442 isochron, and apparently reflects a later event on the LL parent body.

A similar but more precise age of 4.420 ± 0.031 Ga for $\lambda(^{87}Rb) = 0.01402$ Ga^{-1} with an initial ratio of $^{87}Sr/^{86}Sr = 0.7203 \pm 0.0044$ was determined after combining the Rb-Sr results from nine additional Y-74442 fragments to the nine previously reported data [5].

Discussion:

A refined value for the $^{40}Ca/^{44}Ca$ ratio of the alkali-rich source can be obtained using the more precise Rb–Sr age of 4.420 Ga. With this age, a model initial $^{40}Ca/^{44}Ca$ ratio of 47.1597 is determined from the present-day $^{40}Ca/^{44}Ca$ values of the fragments. Then, using the initial $^{40}Ca/^{44}Ca$ value of bulk silicate earth at 4.568 Ga ($^{40}Ca/^{44}Ca_{BSE@4.568}$), a source K/Ca value of 0.27 for the Y-74442 fragments can be obtained, although the associated error (± 0.19, $2\sigma_m$) is large due to the narrow range of $^{40}K/^{44}Ca$ ratios. If we adopt this value as the source K/Ca value for the Y-74442 alkali-rich fragments, it is four

times larger than that of the LL-chondrite parent body (K/Ca = 0.061, [15]). These results are generally consistent with the Rb–Sr systematics of the fragments, and suggest that the potassium enrichment may have also occurred in the early Solar System. If the parent melt had calcium and strontium abundances at 4.420 Ga that were chondritic, a K/Rb ratio of the precursor material is calculated to be ~100, which is less than forty percent of the LL-chondrite [$(K/Rb)_{LL\text{-}chondrites}$ = 255, [15]] or CI [$(K/Rb)_{CI}$ = 235] value. This result indicates that mutual fractionations (i.e. an enrichment of heavier alkalis) could have occurred during the formation of an alkali-rich component from an alkali-rich planetesimal or early nebular condensates, [5]).

Abundance ratios of potassium and rubidium for the Y-74442 fragments are fairly constant (K/Rb = 41–79, except for fragment ,130-7), suggesting that further enrichments of rubidium (and possibly cesium) over potassium could have occurred in a completely different way. Potassium and rubidium were selectively added to individual fragments without significant change in the calcium and strontium abundances. This possibility could have happened during a final melting event that produced a vapor cloud enriched in potassium and rubidium ($Na_{CI\text{-}norm}$ < $K_{CI\text{-}norm}$ <$Rb_{CI\text{-}norm}$ <$Cs_{CI\text{-}norm}$), which condensed into a melt (later glass) phase.

The K–Ca systematics of the Bhola fragment seems to be somewhat different from the Y-74442 fragments, suggesting that a formation process of alkali-rich fragments in the two chondrites might be similar but represent different fractionation events. Assuming an Earth's mantle initial $^{40}Ca/^{44}Ca$ of 47.1583 [12] and an initial $^{87}Sr/^{86}Sr$ of 0.69889 (Allende initial, [16]), K–Ca and Rb–Sr model ages for Bhola ,1806-2 are calculated to be 4.19 and 4.33 Ga, respectively. Bhola ,1806-2 also is different from the Y-74442 fragments in terms of its strontium content (Sr = 4.09 ppm and thus Rb/Sr = 22), implying that the Bohla fragment could have formed at a different time and/or have been derived from a precursor with different proportions of alkali and chondritic components compared to those of Y-74442 fragments. Nevertheless, fractionation processes and precursor components of the Bhola fragment are considered to be almost identical to those of the Y-74442 fragments.

References:

[1] Kempe W. & Müller O. (1969) *Meteorite Res.*, pp. 418. [2] Wlotzka F. *et al.* (1983) *GCA* **47**, 743. [3] Wlotzka F. *et al.*, (1992) *Meteoritics* **27**, 308. [4] Fodor R.V. & Keil K. (1978) Catalog of lithic fragments in LL-chondrites, *Inst. Meteoritics Spec. Publ.* **19**, pp. 38, Univ. New Mexico, Albuquerque. [5] Yokoyama T. *et al.* (2013) *EPSL* **366**, 38. [6] Marshall B.D. & DePaolo D.J. (1982) *GCA* **46**, 2537. [7] Marshall B.D. & DePaolo D.J. (1989) *GCA* **53**, 917. [8] Shih C.-Y. *et al.* (1993) *GCA* **57**, 4827. [9] Shih C.-Y. *et al.* (1994) *GCA* **58**, 3101. [10] Kreissig K. & Elliott T. (2005) *GCA* **69**, 165. [11] Simon J.I. *et al.* (2009) *ApJ* **702**, 1, 707. [12] Caro G. *et al.* (2010) *EPSL* **296**, 1–2, 124. [13] Steiger R.H. & Jäger E. (1977) *EPSL* **36**, 359. [14] Ludwig K.R. (2009) *Spec. Publ.*, vol. 2, Berkeley Geochronol. Cent., Berkley, Calif. [15] Wasson J.T. & Kallemeyn G.W. (1988) *Phil. Trans. R. Soc. Lond.* A **325**, p. 535. [16] Gray C.M. *et al.* (1973) *Icarus* **20**, 213.

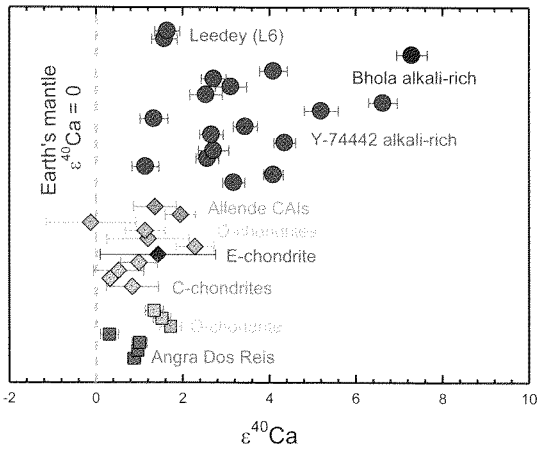

Fig.1 Variation in ^{40}Ca for a range of meteoritic samples and alkali-rich fragments in Y-74442 and Bhola. The data are from (Caro et al., 2010 [12]; squares) and (Simon et al., 2009 [11]; diamonds). $\varepsilon^{40}Ca$ shows the deviation from the Earth's initial composition [($^{40}Ca/^{44}Ca_{sample}$ / $^{40}Ca/^{44}Ca_{mantle}$ – 1) x 10^4], where the $^{40}Ca/^{44}Ca_{mantle}$ = 47.1487 from Marshall and DePaolo (1982) [6] was normalized to NIST SRM 915a $^{40}Ca/^{44}Ca$ = 47.1526 [11], and then all data were normalized to SRM 915a $^{40}Ca/^{44}Ca$ = 47.16223 [12]. Well-defined excesses of ^{40}Ca, with regard to the initial Solar System value are observed in the alkali-rich fragments.

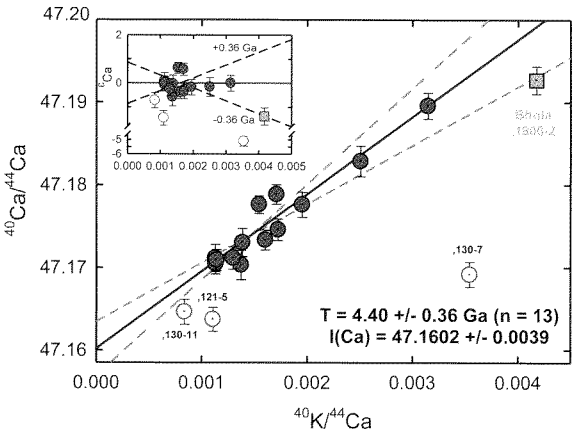

Fig.2 Potassium–calcium isochron diagram for alkali-rich igneous rock fragments inY-74442. Thirteen data points define a linear array corresponding to a K-Ca age of 4.40 ± 0.36 Ga (2σ error, MSWD = 7.6) for $\lambda(^{40}K)$ = 0.5543 Ga^{-1} [14] with an initial ratio of $^{40}Ca/^{44}Ca$ = 47.1602 ± 0.0039 (2σ error) using the Isoplot/Ex program (Model 1 solution, [15]). The inset shows deviations of $^{40}Ca/^{44}Ca$ in parts in 10^4 (ε-units) for Y-74442 alkali-rich fragments relative to the best-fit line. Bhola (LL3-6) fragment ,1806-2 (solid square, blue) is plotted for comparison.

AUTHOR INDEX